GLOSSARY

1. Nominal Compositions of commercial aluminium alloys studied.

(a)	N.3	Al - $1\frac{1}{4}$% Mn.
(b)	N.4	Al - $2\frac{1}{4}$% Mg.
(c)	H.15	Al - 4.4% Cu 0.6% Mg 0.7% Si 0.6% Mn
(d)	DTD.683	Al - 5.3% Zn 2.7% Mg 0.4% Cu 0.5% Mn

2. D.C. Casting - Direct Chill semi-continuous casting

SOME FACTORS AFFECTING THE HOT WORKING OF COMMERCIAL ALUMINIUM ALLOYS

by

B A HUMPHREYS B.Sc., M.Sc.

A Thesis submitted for the degree of Doctor of Philosophy at the University of Aston in Birmingham

September 1969

"Research is to see what everybody else has seen, and think what nobody has thought."

Dr Albert Szent-Gyorgyi.

LIST OF CONTENTS

LIST OF TABLES

LIST OF FIGURES

1. SYNOPSIS

This project was concerned with some of the aspects of the hot working of commercial aluminium alloys. The topic was approached broadly from the three following areas of interest.

i) An investigation of the temperature variation of a rolling slab as it passed through its rolling schedule was made. The investigation was tackled by a mathematical approach and the model formulated compared against experimentally determined cooling curves for commercially rolled slabs.

ii) Rolling schedules were simulated using the hot compression test, and the structures produced were compared with those produced by industrial hot rolling. The simulation also allowed an investigation of structure changes early in the rolling schedule which is not usually possible in industrial rolling.

iii) An investigation of some of the properties of a number of intermetallic phases found in commercial aluminium alloys helped in understanding how the hot rolled structures are formed. Also with the aid of energy curves it was possible to find a criterion which allows the division of commercial aluminium alloys into

two groups. These two groups are usually called "soft" and "strong" by mill operatives depending upon their rolling characteristics. The shape of a plot of the slope of the energy curve for an alloy was found to be a good grouping criterion. The new grouping does not separate alloys purely on resistance to deformation during hot rolling but on a characteristic CHANGE in the resistance to deformation at some stage of the schedule.

2. LITERATURE SURVEY

2.1.1 Some factors affecting the hot working of metals

Two properties which have a strong influence on the fabricating characteristics of materials are -

i) Resistance to flow (strength)

ii) Ductility

These two properties are strongly affected by temperature and the "hot-working" temperature for a material is often defined as the ratio $\frac{T}{T_m} = 0.7$ where T is the working temperature and T_m is the melting temperature, both expressed in degrees absolute.

The important distinction between hot and cold working is that hot working is not accompanied by any strain hardening because dynamic softening processes operate fast enough to balance work hardening processes.

2.1.1.1 The effect of temperature and strain rate on strength and ductility

a) Hot strength

In general strength decreases and ductility increases with temperature rise. This can be modified by precipitation processes during hot working. Also an increase in strain rate will produce an increase in resistance to deformation. A number of equations have been proposed to show a relationship between temperature, strength and strain rate, these usually being of the form shown below.[1.]

$$\mathring{\varepsilon} = A(\sinh \alpha \sigma)^{n'} \quad \exp\left(-\frac{Q}{RT}\right)$$

b) Hot ductility

Up to the present time, no successful correlation has been found between temperature and strain rate with ductility. This is because ductility can be defined in a number of ways and because ductility measured in one stress system may not be related to ductility measured in another system or even to the ductility in the same stress system with a different sized specimen. Because of the effect of stress system on ductility no one laboratory test can satisfactorily describe the behaviour of materials in different working processes. Certain tests for certain materials can give good correlation between say forgeability and ductility measurements as in the case of axi-symmetric compression.

The hot torsion test has received a lot of attention in recent years and the work of Rossard and Blain[2] is of some interest in this connection, as an extensive study was undertaken to apply the hot torsion test as a laboratory simulation of hot working. These workers were able to reproduce very similar structures using the hot torsion test to those developed in reversing, continuous and planetary mill rolling of killed open hearth, rimming open hearth, and basic bessemer steels, by simulation of the rolling schedules.

Two very important factors which influence ductility are strain rate and temperature. The influence of strain rate on ductility is not clear but in the hot torsion test, the adiabatic temperature rise complicates observations and workers report a marked rise in ductility with increase in strain rate. Due to this effect, which is aggravated by the exceedingly large amount of deformation exhibited in hot torsion by ductile materials, it appears that ductility measured in the hot torsion test is sometimes less suitable for correlation with hot working practice than say ductility measured in compression, but the flexibility of the test with respect to strain rate and temperature has led to its use in the study of the relationships between structure and deformation conditions.

The effect of temperature on ductility is less complicated. For pure metals, a high level of ductility is retained up to the melting point, whereas alloys show a decrease below the melting point (hot shortness) which sets a limit to the re-heating temperature that can be used. For example, the temperature range between maximum ductility and zero ductility for steels is about 25-100°C.

2.1.1.2 The effect of homogenization on strength and ductility.

In single phase metals and alloys where temperature control is not too critical the time of reheating is unimportant as long as oxidation and grain growth are restricted and heating is uniform.

In complex materials especially castings (because of segregation and micro-segregation) the temperature and time of reheating can have a marked effect on ductility and strength. The complex high strength aluminium alloys are usually given homogenization treatments to improve ductility in hot rolling and in some alloys these may have to be for extended periods and at temperatures well above the hot rolling temperature range. This is necessary in alloys containing elements with a low diffusion rate such as manganese or zinc. Homogenization of these alloys often leads to coalescence of intermetallics e.g. Al_6MnFe in aluminium $1\frac{1}{4}\%$ manganese. This process can have a significant influence on ductility. Homogenization can also cause one intermetallic (a metastable phase formed during casting) to transform to another, generally with a desirable effect on properties.

2.1.1.3 The effect of reheating temperature on resultant properties.

The final properties of a material are dependent on grain, sub-grain or precipitation effects occurring in the material. Therefore, the properties can depend upon solution temperature, amount of deformation, deformation schedule, cooling rate during working, finishing temperature, and cooling rate after working. The starting condition before hot working is always the condition after reheating, and therefore this must have an important effect on the final structure and properties.

Because of the importance of such variables as reheating temperature, degree of deformation, rate of deformation etc. on the final properties of a material, great interest has been shown in recent years in developing laboratory tests that will simulate the structures, loads etc., developed in industrial fabricating processes, amongst these are -

i) Hot torsion testing[3-22]

ii) Hot tensile testing[23-26]

iii) Hot compression testing[27-30]

2.1.2 Tests for simulating hot working

A hot workability test should be capable of predicting the following data -

i) Hot strength, from these values estimates of mill powers can be made.

ii) Hot ductility, this data gives information about the tendency of a material to crack.

iii) Structural changes, the test should give information about structural changes that occur during the test which can be used to interpret changes that take place in production processes.

In recent years the hot torsion test has been popular amongst workers interested in hot deformation.[3-22] The reasons cited for the selection of this test are -

a) The test can be extended to a high state of deformation.

b) The strain to fracture can be measured.

c) The test apparatus is capable of covering the full range of temperatures met with in practice.

d) The test can cover the full range of strain rates met with in practical deformation processes. Strain rates as high as 1000/sec. are known to occur and therefore the test should be able to supply data at these strain rates at the temperature of interest.

Disadvantages of the test are however that the torque/twist curves when converted to "equivalent tensile" curves do not always coincide with true tensile curves quite as well as curves converted from plane strain compression.[31] It has been shown that even when results obtained from different tests are analysed to provide stress/strain data in terms of "tensile equivalents" such results do not necessarily coincide. Thus if information is required for a given fabrication process it is important that the deformation occurring during the test should closely simulate that which occurs in the process. The deformation occurring during several fabrication processes including rolling is most closely approached by the plane-strain compression test.[32] The plane strain compression test has the added advantage compared with axi-symmetric compression that stress values at high strains can be obtained without a serious increase in the load required for deformation.[33]

Because of experimental convenience axi-symmetric compression (i.e. the compression of cylindrical specimens with equal extension in all directions perpendicular to the compressive stress) is often employed. Using this laboratory test, values of hot strength can be obtained from the flow curve,[34] which is calculated from the stress/strain curve after correction for the increase in diameter produced by deformation.

Serious errors can arise due to the effects of friction between the ends of the specimen and the compression platens which not only cause an increase in load but also cause barrelling. These effects are most undesirable and are difficult to correct for, so that efforts are made to reduce friction. For temperatures up to about 350°C. lubrication with polytetrafluorethylene in the form of thin sheets placed between the compression platens and the ends of the specimen is most effective.[35] Above this temperature the lubricating properties of P.T.F.E. are reduced (also the vapour given off is toxic) and lubrication with low melting point glass and preparations of colloidal graphite are necessary. With sufficient care most of the effects of friction can be suppressed, and with correct proportioning of the specimen geometry, other possible effects such as buckling and rhomboidal distortion can be prevented.

Hot ductility in axi-symmetric compression is usually defined as the greatest single reduction at a given temperature that will produce the first visible crack. This criterion has been used to determine the optimum working temperature in forging for a number of materials.

Axi-symmetric compression has also been used in the past for the determination of stress/strain curves from which values of flow stress for use in rolling load calculations were calculated.[36-39] However less interest seems to have been paid to the possibility of using the test to simulate hot worked structures.

2.1.3 The effect of hot working on the structure of aluminium

Although some interest has been shown in the strength levels of certain aluminium alloys at elevated temperatures for the purpose of calculating hot rolling loads, the structural changes that occur in hot rolling have received little attention. Recently a number of workers have reported the influence of hot working on the sub-structure of aluminium, mainly of high purity. The observations listed below are common to a number of investigations of sub-structure formation in hot worked aluminium.[40, 43-46]

i) Hot deformation results in the formation of a sub-structure in the grains.

ii) The size of the sub-grains is a systematic function of temperature and rate of deformation.

iii) The sub-grain size largely determines the mechanical strength exhibited by the metal during deformation.

iv) The size of the sub-structure is related to the initial temperature and rate of deformation rather than to the temperature of subsequent heating. From these observations, it has been possible to postulate what processes occur during hot working to produce these structures.

During high temperature deformation ($T > 0.55T_m$) the stress/strain curves of many polycrystalline metals show a maximum at about 100% strain and then reach a steady or constant value.[41, 42] In this region which can be called "steady-state" hot working, the flow stress, strain rate, and temperature remain constant, and the phenomonon is similar in many respects to steady state creep,[43] although the strain rates are several orders of magnitude higher.

In metals of medium to high stacking fault energy, extensive dynamic recovery during hot deformation leads to the establishment of a well developed sub-structure, which remains relatively unchanged throughout steady state deformation.[44, 45] Because of the higher strain rates compared with steady state creep, the hot worked structures are finer and thus not observed as frequently.[46]

The sub-structures seen in aluminium extrusions are similar to those formed during creep and indicate that considerable dynamic recovery occurs by cross slip and climb. Dynamic recovery leads to an equilibrium between the rate of dislocation generation and the rate of internal annihilation, so that a stable dislocation density is maintained during steady state deformation which accounts for the constancy of the temperature, strain rate and flow stress. Since the sub-grain size has been observed to remain constant during steady state deformation both in hot working[47] and in creep[48] it follows that the sub-grain misorientation should remain constant to preserve a constant dislocation density. When either the imposed temperature is raised or the imposed strain rate is decreased the enhanced mobility of the dislocations leads to a greater rate of annihilation, a lower equilibrium density, and therefore a larger sub-grain size.

In high stacking fault energy metals such as aluminium, recrystallisation rarely takes place during hot working but usually occurs afterwards during cooling. Recrystallisation is replaced by recovery of which there are two forms -

a) Dynamic recovery, which is manifest by polyganisation during deformation and is driven by external and internal stresses aided by thermal activation energy.

b) Static recovery, which is driven by internal stresses (dislocation arrays) and also aided by thermal activation energy. During hot working, dynamic recovery is accepted as being the predominant recovery process.

During deformation it is observed that after an initial quantity of strain a steady state condition is attained (as described above) during which the flow stress does not alter. In aluminium the structures consist of sub-grains whose size remains constant throughout steady state deformation. The sub-grain size increases as the temperature increases or as the strain rate decreases and depends inversely on the stress. For fixed working conditions the sub-grain size is independent of the initial grain size and in aluminium generally decreases slightly as impurities increase. If after the steady state condition has been achieved the temperature or the strain rate are altered then the stress and sub-structure change to become similar to those in specimens deformed solely at the second temperature and strain rate. This change is not instantaneous because it takes time for deformation to rearrange the dislocations. The dislocation density under steady state hot working conditions reaches a constant value due to the dynamic equilibrium which is established between the dislocation generation and annihilation. An increase in the hot working temperature leads to an increase in the size and perfection of the sub-grains. As the room temperature hardness and U.T.S. vary inversely with the square root of the sub-grain size it follows that the strength of polygonized extrusions decreases as the extrusion temperature increases.

Similar observations made by Vaughan[49] on the structures of hot rolled aluminium plates showed that the structures consisted of deformed grains existing as lamellae running in the rolling direction with little optical evidence of recrystallisation. There was a tendency for the size of this lamellar structure to decrease near each surface of the plates. In specimens where there was evidence of recrystallisation it was usually most distinct at the surface of the plates. Detailed examination of the plate structures suggested that there was a continuous cycle of structural change occurring during rolling. The as cast grains after heating for hot rolling are free from the sub-grains which form during deformation to produce a series of parallel sided lamellae in each grain. In the absence of recrystallisation the structure develops on further deformation into long thin parallel grains aligned in the rolling direction. When conditions allow recrystallisation, the new grains form at the interfaces of the lamellar grains. In the absence of further deformation these are themselves free of lamellar sub-structure. If further deformation takes place it causes these new grains in turn to exhibit the lamellar sub-structure. Thus Vaughan was able to draw the following conclusions from his observations on sub-structure formation. The actual structure obtained in a plate at the end of the rolling schedule depends upon the residual stored energy at the end of the last pass, the slab temperature at the end of the last pass, and also on the structure itself which can govern subsequent recovery and recrystallisation kinetics. Thus for large total reductions involving a large number of passes the linear grain structure predominates since there will have been little chance for recrystallisation to occur during the last few passes due to a low rolling temperature.

Although this aspect of hot working has been investigated, complex alloys have received far less attention in spite of the fact that they are of significant commercial importance, furthermore the role of second phase particles in hot working appears from the literature to have been almost completely neglected.

2.1.4. The effect of non-metallic particles on properties

The type and dispersion of non-metallic inclusions in wrought products are known to have usually detrimental effects on mechanical properties. Of these the fatigue properties, transverse ductility, and impact behaviour are often the most sensitive to the presence of non-metallic inclusions.

2.1.4.1 The influence of second phases on the strength and ductility of alloys.

Where a second phase increases the yield stress of the host phase, the increase is a function of the mean free path (not the volume fraction or mean particle spacing between the second phase particles). Ductility is decreased by a second phase and is independent of the type of inclusion, (i.e. holes and hard particles both reduce ductility) and is a function of volume fraction. It may appear tempting to explain the embrittling effect of a second phase on the premise that the particles are inert and do not participate in the deformation process so that ductility of the aggregate is reduced in direct proportion to the participating matrix. This explanation is compatible with the statement that ductility depends upon the volume fraction of the second phase alone and is not dependent upon the particle size, but that the embrittlement is independent of the nature of the second phase (as long as it is harder than the matrix).

However, this explanation does not predict the correct shape for the ductility/volume fraction curve. It is well known that a notch or other discontinuity in an otherwise uniform plastic mass is a stress concentrator. For example in an ideal rigid plastic mass the mathematical theory of plasticity predicts that strain will be concentrated along definite lines when a notched bar is pulled in plane strain. Real metals do not behave quite so ideally, and strain will spread out from the ideal predicted lines but the strain is still heavily concentrated. Metals with a low strain hardening coefficient should approach ideal behaviour while those with a high strain hardening coefficient will show less strain concentration for a given notch geometry. Hence, it is suggested that the role of uniformly distributed random second phase particles is to concentrate strain within or near some skeletal pattern and that this concentration of strain causes the metal to reach its fracture strain locally within the skeletal pattern at a lower external strain.

The theory of geometric similarity would suggest that if the entire skeletal pattern corresponding to a given dispersion of second phase were to be enlarged the strain pattern would merely be enlarged proportionately. The strain concentration pattern would remain the same; so would the volume fraction of the second phase even though each particle is larger. This illustrates why embrittlement by a second phase is independent of particle size and depends only on the volume fraction. This is supported by the fact that the ductility vs. volume fraction curve for two phase alloys is about the same as ductility vs. notch depth. Similarly, the closer holes of a given size get to each other, the greater will be the concentration of strain and the consequent embrittlement. This would account for the decrease in ductility as the volume fraction of second phase increases. Although the skeletal pattern varies in detail for soft particles (holes) and hard ones the patterns must be similar and this is reflected in the fact that a number of dispersions in a matrix all lower ductility and all fit the same volume fraction/ductility curve.[50] Regarding the influence of second phase particles on strength, it is observed that only phases that are wetted by the host matrix cause an increase in strength, which must therefore depend upon the bond strength with the matrix. When strengthening does occur it is proportional to the mean free path between particles. Although little appears in the literature concerning the influence of second phase particles on the hot working of aluminium alloys, it is worthwhile listing a number of the conclusions made by Edelson and Baldwin[50] from their study of the effects of second phase particles on the room temperature properties of copper. These conclusions have more widespread application to other materials, and have some value in explaining the effects of second phase particles on deformation at elevated temperature.

i) Only certain phases strengthen their alloys.

ii) In order for particle strengthening to occur, firm particle - matrix bonding is required.

iii) When strengthening occurs the yield stress depends upon the mean free path between particles.

iv) The yield stress varies linearly with the logarithm of the mean free path. This holds true for those alloys in which strengthening occurs only within a limited range. For each particle size a minimum free path for strengthening is reached after which the yield stress decreases.

v) All second phase particles as well as voids embrittle their alloys.

vi) Ductility depends upon volume fraction alone and is independent of particle size, shape, or composition.

vii) The volume fractions of several second phases in the same alloy are additive in determining ductility.

The conclusions of Chao and Vlack[51] agree well with those of Edelson and Baldwin above in that they also found that two phases within a material will not behave identically when they are deformed simultaneously. Even if the phases have the same crystal structure, differences in crystal orientation and critical resolved shear stress cause the two phases to deform unequally. The differences become severe when one of the phases is non-metallic and the other metallic. In the extreme case, a small hard non-metallic inclusion resists all deformation as the second phase (the matrix) undergoes some deformation, also the matrix will not be perfectly ductile particularly if there is an opportunity for strain hardening. These conditions provide sites for the initiation of fracture within the material. In alloys where the second phase is softer than the matrix the second phase undergoes more deformation than the specimen as a whole[52] whereas hard particles deform less than the specimen. In aluminium-copper and aluminium-silicon alloys at low temperatures the hard particles of $CuAl_2$ and silicon do not show any signs of deformation[53,54] but often fracture especially if they are angular. There is also a tendency for deformation to become more homogeneous in the matrix and particle as the amount of deformation increases.

Gurland[55] strengthened silver by the addition of tungsten, molybdenum and tungsten carbide, and came to the conclusion that the type of second phase particle was not important as long as it did not deform during the deformation of the alloy. This is true while the volume fraction of hard particles is low, but when the volume fraction becomes very large the hard particles become the load bearer and fracture takes place by cleavage of the brittle hard phase or cleavage of the brittle phase with subsequent transfer of load to the soft matrix which then fails by shear rupture.

The thermal and elastic properties of a second phase usually differ from those of the matrix. This leads to the important consequence that particles can act as dislocation sources when the alloy is cooled or deformed. As a result the substructure around the particles can be modified. In two phase materials containing particles harder than the matrix the first signs of plastic deformation occur at stresses below the general flow stress of the matrix owing to the stress concentration that exists around the particles. The general flow stress of the composite is considerably greater than the matrix and this is attributed to the constraint exerted on the matrix by the rigid second phase. When hard second phase particles remain rigid as a composite deforms the matrix can fail by strain concentration before the flow stress of the particles is reached. In this situation the composite strength is independent of the form of the second phase constituent.

The most significant role of the hard particles is to reduce the ductility of the host material by failure at the weakest interface. This leads to void formation and accelerated ductile fracture.

The nature of the interface between two phases is of considerable importance to the mechanical properties of two phase alloys. With few exceptions it is observed that the transition which occurs when passing through a particle of one phase into an adjoining particle of another phase is extremely sharp and confined to a thin boundary layer. The condition for the co-existence of phases is that the free energy of the system as a function of some variable should possess more than one minimum. On the grounds of continuity, it is expected that material in the interface between two such phases will form a boundary layer intermediate in structure and composition between those of the adjoining phases. This means that its free energy must be high since the free energy climbs to high values in the regions between the minima associated with the phases. To reduce the amount of such material, the system reduces the boundary layers until they are as thin as possible, generally down to atomic dimensions in the case of interfaces between alloy phases. Further reductions can be achieved by altering the shapes of the particles so as to minimise the area of high energy surfaces in contact.

The boundary between two phases in an alloy may either be of the coherent type across which it is possible to trace a continuity of lattice structure from one phase to the other and which has a small surface energy, or of the incoherent type across which there is no continuity of lattice, and which has a large surface energy. The surface energies of incoherent boundaries play an important part in determining the distribution of the phases in phase mixtures. Small amounts of a second phase in an otherwise homogeneous polycrystalline alloy have a tendency to form at the grain boundary of the latter since an economy in the total boundary area can be achieved in this way, part of the large angle boundary between the grains becoming the incoherent boundary of the second phase. The magnitude of the surface energy is about the same in both cases, and it has been shown[96] that surface tension analogies are applicable to both, the interface energy being calculated from the balance of surface tension forces at the junction of a grain boundary and the two phase boundaries.

The ability therefore, of the matrix to form a low energy interface with second phase particles is of prime importance. If bonding is weak, then failure by de-cohesion results at the interface. Firm bonding allows the full toughness of the interface to be realised.

Rigid particles in the form of plates or needles act as strong barriers to matrix slip and result in high stress concentrations that can produce cracks in the second phase.

2.1.5 Factors affecting the dispersion of inclusions in wrought products

Observations made on iron-oxygen alloys deoxidised with manganese, silicon, and aluminium, show that the controlling factors governing the dispersion of the inclusions throughout the steel are the temperature and degree of hot working.[56] The dispersion of inclusions throughout a wrought product will result from repeated deformation and fracture, leading to a fine dissemination of inclusions. These observations agree well with the work of Unckel[57] one of whose conclusions was that hard inclusions deform less than the host matrix and soft inclusions deform more.

The deformation of inclusions during hot working is probably due to the forces operating at the inclusion - metal interface. Such forces will probably increase with both decreasing rolling temperature and increasing reductions in cross-section. Alternatively, as the temperature decreases the inclusions may become less plastic so that deformation will be less probable and the inclusions will be more liable to fracture. Also the less plastic the metal the greater the differential forces at the interface during deformation so that a shearing action is eventually set up which breaks the inclusion. In a complex inclusion forces at the inclusion-metal interface can separate harder particles from the main inclusion and so lead to dissemination of these particles throughout the steel.

If fracture occurs early in the deformation process individual fractured blocks behave as separate inclusions and can experience further deformation and even a second fracturing process. Fracturing which occurs later in the deformation process produces the "fish-tail" effect which is believed to be due to the large forces at the metal-inclusion interface causing only the outside layers of the inclusion to be deformed after fracture. Tilting of fractured blocks of inclusion is also observed and is probably due to the flow of the metal around the inclusion turning it so as to produce less resistance to the flow of the metal. If fracture is delayed to the end of the deformation process, clean fracture surfaces are seen and it is sometimes observed that the metal has not filled in the space between the fractured blocks. In duplex inclusions fracture at the interface between the two phases is common, leading to good dispersion.

At low temperatures included particles may become fractured, sheared and chipped, the particles and debris being drawn out to form a stringer. Small particles deform less than large ones and sometimes only deform at low temperatures and high reductions when the forces on them (at the interface) are large. It would be desirable from the standpoint of property development for large inclusions to be broken down early in the deformation process. If say a slab were given a low temperature reduction the extensive fracturing of particles which might be expected may result in undesirable features which would act as stress raisers. However these effects could be overcome by a further high temperature reduction to fill the fractures by flow of the soft matrix. Hence an understanding of the properties of inclusions may provide modifications to current rolling practices to improve quality. A practical difficulty may arise with such fabrication techniques, since it has been shown[97] that when aluminium and its alloys are re-heated in gas and electric furnaces, it is possible to pick up hydrogen to a considerable extent, even if the material already contains hydrogen above the solid solubility limit before re-heating. This may lead to blistering if the hydrogen is rejected from solution into the cracks in the intermetallics.

Although the foregoing applies largely to observations of inclusions contained in steel, much of the information is useful in understanding the behaviour of intermetallics in aluminium alloys. A small amount of work has been reported in connection with the properties of the intermetallic phases found in aluminium alloys particularly in consideration of their effects on the hot workability of commercial or even experimental alloys.

2.1.6 The influence of intermetallics on the fracture of aluminium

a) Aluminium-iron alloys

In tensile tests conducted over a range of temperatures from room temperature to 500°C. a linear relationship between the logarithm of maximum tensile load and temperature exists[58] in contrast with aluminium copper alloys where there is a distinct inflexion, the significance of which will be dealt with later. (Section 2.1.8)

Two alloys, containing 1.9% and 10% respectively of iron both exhibit this linear relationship which is consistent with the hardness-temperature relationship for $FeAl_3$, the intermetallic contained by these alloys, which shows no inflexion below 500°C. It therefore seems likely that the hot deformation characteristics of these alloys are governed by the properties of the intermetallic phase contained by them. In hot rolling experiments with these alloys it was observed that the needles of $FeAl_3$ fractured at all temperatures up to 500°C.

On solidification of aluminium-iron alloys, the $FeAl_3$ forms with a needle like morphology and during deformation these needles tend to align themselves in the direction of working. The extent of break up (which decreases with rise in temperature) is thought to be due to the shape of the needles and the softness of the matrix. This is illustrated by the fact that the matrix flows into the cracks in the needles filling them at all temperatures above 150°C.; below this temperature many of the cracks remain open. When the particles are short and stiff they have less tendency to crack.

b) Aluminium-manganese alloys

An alloy containing 5% manganese in which the intermetallic phase is $MnAl_6$ behaves in a similar manner to the aluminium-iron alloys but above 530°C. the needles of intermetallic show no signs of cracking by metallographic observations. No plastic deformation can be observed either, probably due to the great difference in strength between the particles and the matrix at this high temperature, the respective hardness numbers being 200 vpn and 3vpn[58].

c) Aluminium-copper alloys

A plot of the logarithm of maximum tensile load against temperature for a series of alloys containing various proportions of $CuAl_2$ all fall near an inflected straight line[58], which indicates that in this range composition has little effect on strength. The temperature at which the inflexion occurs is about 300°C. which is the same temperature at which inflexion occurs in the hardness-temperature relation for pure $CuAl_2$. The inflexion temperature is said to mark the transition from ductile to brittle fracture. Above the inflexion temperature the intermetallic shows no fracturing and below this temperature fracturing is always evident. This suggests that the $CuAl_2$ controls the behaviour of alloys containing large amounts of it which in turn supports the hypothesis that the inflexion temperature marks the point where the intermetallic becomes plastic.

The conclusions to be drawn from these observations are that in alloys containing intermetallic phases the deformation structures depend to a great extent on the inflexion temperatures of the hardness-temperature curve for the phases contained by the alloys. The inflexion point represents the temperature below which brittle fracture will always occur and above which the compound starts to deform in a plastic manner. The size and distribution of intermetallic phases in a deformed alloy will therefore depend largely on the deformation temperature relative to the inflexion temperatures of the phases contained in the alloy. The size and shape of the phase are also important. Long needles or plates will tend to align themselves in the direction of matrix flow, giving rise to poor short transverse properties.

A dispersion of intermetallic particles with a high inflexion temperature and a low solubility in the matrix ought to provide the strongest alloys for elevated temperature applications. When deformed at temperatures well above the inflexion temperature however the particles will tend to elongate and again give a lowering of short transverse properties. There should therefore be an optimum temperature range for an alloy in processes like forging and rolling. Alternatively pre-forging below the inflexion temperature followed by rolling above the inflexion temperature should produce a fine dispersion with cracks in the particles of intermetallic filled by the matrix. The deformation structure depends not only on the size and shape of the phase but also possibly on the amount present. Small rounded particles such as occur in dilute alloys may exhibit less cracking on deformation.

2.1.7 Some properties of intermetallic phases

Unlike ionic compounds the chemical compounds of metals are characterised by the predominance of metallic binding between the different atoms and consequently possess metallic properties (metallic lustre, electronic conductance, thermal conductance, and under certain conditions mechanical workability).[59] Chemical compounds are formed mainly by those components which differ basically in their atomic structure i.e. they stand far apart in the periodic table, have greatly differing atomic volume (or lattice parameter) and different crystal structure. There are over 4,000 intermetallic phases with metallic properties.

These phases fall into two basic groups -

a) Those with a fixed composition

b) Those with a variable composition

Intermetallic phases also have their own electrochemical potential, possess high hardness and are often refractory. Of the 4,000 known intermetallics a very small proportion have been investigated and for many not even their crystal structures have been determined.

2.1.7.1 The influence of temperature on the plasticity of intermetallic compounds.

Due to the complexity of the crystal structure of almost all the intermetallic compounds they are best known for their extreme brittleness at ordinary temperatures. However many intermetallics are sensitive to softening with increase in temperature as shown below.[59]

Phase	Hardness VPN 25°C.	Hardness VPN 350°C.
$MgZn_5$	146	6

Intermetallic phases of variable composition seem to be more susceptible to an increase in plasticity than those of a fixed composition. A consideration of the Hume-Rothery rules for intermediate phase formation for some simple binary intermetallics helps to explain this behaviour. The Hume-Rothery rules provide an explanation for the formation of intermediate phases, classifying them into three main groups.

i) Electrochemical compounds, such as Mg_2Si which obey the valency laws of chemistry, forming compounds with a small composition range, and high melting points. With the exception of this group, Cottrell[98] regards it as preferable to consider intermediate phases not as chemical compounds, but as structures rather similar to primary solid solutions, in which the atoms are held together by an essentially metallic bond.

ii) Size factor compounds are those phases which form when one atom is very much smaller than the other (interstitial compounds, which are not important in aluminium technology) and those where the difference in atomic diameter is 20-30%. These second group of phases include the Laves phases (eg. $MgZn_2$, $CuAl_2$) where the phases have crystal structures of high co-ordination which are entirely consistent with metallic bonding, but not ionic or homopolar bonding.

iii) Electron compounds, which are phases that form with a small composition range about an exact ratio, and include $CrAl_7$, $MnAl_6$, Co_2Al_9, $FeAl_3$ and $NiAl_3$.

The size factor and electron compounds in that order are the groups with the greatest composition range and are the phases with strong metallic bonding. These groups of phases are the ones which are most sensitive to an increase in plasticity with rise in temperature. The electrochemical phases on the other hand, are those phases which show strong ionic bonding and do not become plastic with temperature rise to the same degree as size factor and electron compounds. Hence the development of plasticity at elevated temperatures is determined by the binding forces between the atoms in the phase, metallic binding forces being necessary if plasticity is to be exhibited. Some of the phases that have been deformed plastically in pure form are MgZn, $MgZn_2$, $MgZn_5$, $CuAl_2$ and the beta and gamma phases of the aluminium-magnesium system. Under the correct conditions some of these phases have been deformed by as much as 80-90% reduction in area by hot extrusion. This deformation refines the grain size which makes the phase more ductile in subsequent deformation. Since high rates of strain tend to produce fracture in these phases (consistent with all materials with a tendency to be brittle) extrusion is an obvious choice since both the stress system and strain rates operative in the process are favourable in developing ductile behaviour. The temperature at which ductility is exhibited is usually in the range $0.7 - 0.9\ T_m$ (T_m is the absolute melting point of the phase).

2.1.7.2 The influence of temperature on the mechanical strength of intermetallic compounds.

Apart from the increase in plasticity just described there is also an increase in the strength of some intermetallics when heated to a certain temperature. In this way intermetallics behave quite unlike metals. This can be seen in Fig. 1 (Ref. 59) which illustrates how a metal looses strength progressively with temperature whereas the intermetallic first gains strength and then weakens with temperature in a similar manner to metals. The brittleness at or below room temperature is associated with the complex crystalline structure of intermetallics, the presence of co-valent and ionic bonding, and with poor grain boundary cohesion and also the particular sensitivity of these materials to stress concentration. At low temperatures the phase is only capable of elastic deformation. When heated these phases are capable of withstanding some plastic deformation. As some plasticity is required to allow strength to be maximised it follows that with heating the strength of the brittle phase will also grow and reach a peak at a certain value of plasticity. The plasticity seems to dissipate the concentration of stress to allow the material to reveal its full strength. After the peak has been reached (due to the growth of plasticity) the strength falls in an exponential manner similar to metals. Pure intermetallics and alloys containing large volume fractions of intermetallic can both show this strengthening phenomonon. The mechanisms by which these hard phases deform are not as fully understood as those processes operating in metals, but it is thought that the processes of recovery and recrystallisation may have an important bearing.[60]

A comparison of some of the observations made on the slip mechanisms in simple metal crystals and crystals of the NaCl and CsCl types shows some similarities. In intermetallics as in metals the slip direction is more critical than the slip plane. Thus it is frequently observed that the slip plane may vary with temperature in a given compound or from one individual to another in a group of isomorphous compounds. Ordering has a great effect, intermetallic phases of the CsCl type with weak ordering behave like a normal metal (low values of ordering energy give $\langle 111 \rangle$ slip) or strong enough to act similarly to an ionic compound (high ordering energy gives $\langle 100 \rangle$ slip). In crystals where slip is possible the direction of slip is practically always a close packed lattice vector, e.g. $[110]$ in face centered cubic metals, $[111]$ in body centered cubic metals, and $[2\bar{1}\bar{1}0]$ in hexagonal metals. In ionic crystals the slip direction is always along a line of similar charges e.g. $[110]$ in NaCl, $[100]$ in crystals with the CsCl structure. In intermetallic compounds where the ionic character of the bond is weak, this rule is sometimes obeyed and sometimes not.[99]

The plane of slip is often but not always a closed packed plane, eg. (111) in face centered cubic metals, (0001) in hexagonal metals. Body centered cubic metals do not slip on a clearly defined crystallographic plane, and (110) (112) and (123) planes have been reported in their slip surfaces. NaCl slips on (110) and crystals with the CsCl structure slip on (110) usually.

Deformation bands appear in intermetallics in a similar manner to metals, following an initial period of simple slip, but it is thought that it may set in at an earlier stage of deformation than with metals.[100] The incidence and spacing of deformation bands is a function of both temperature and mode of deformation.

Twinning is not a common mode of deformation in intermetallic phases.

Generalising on the plastic properties of some intermetallics commonly found in aluminium alloys and their behaviour under hot working conditions it appears that the phases can be divided into two broad groups depending upon their hot deformation characteristics. Phases like $CuAl_2$ and Mg_5Al_8 have fairly low hardness values and also low inflexion temperatures which usually indicate a somewhat increased ductility and softer plastic state in the region of 400°C. These phases would therefore be expected to give rise to an easily hot worked alloy but one in which there might be a tendency to produce elongated particles of the phase. Both phases are extremely brittle below the inflexion temperature.

The phases $CrAl_7$ and $MnAl_6$ have hardnesses slightly higher than $CuAl_2$ at room temperature but retain the hardness to the inflexion temperature of 400-500°C. and therefore can be expected to be brittle under most hot working conditions. The phases $FeAl_3$ and $MnAl_4$ are very hard and have inflexions above 450°C. Hence these phases also will behave in a brittle manner during hot working.

2.1.8 The significance of the inflexion temperature in pure metals and some binary intermetallic compounds found in aluminium

Pure metals show an inflexion in the plot of the logarithm of hardness vs. temperature at about 0.5 T_m but for intermetallics the temperature varies and lies in the range 0.5 - 0.75 T_m (where T_m is the absolute melting temperature). In pure metals it is known that different mechanisms of deformation are operative above and below the inflexion temperature T_i. Below T_i

slip processes predominate while above T_i diffusion controlled processes such as dislocation climb and grain boundary sliding prevail.

The intermetallics which occur in commercial aluminium alloys are brittle at room temperature but behave in different ways when their temperature is raised. Some like $CuAl_2$ and Mg_5Al_8 have fairly low hardness values and low inflexion temperatures. Hence these would be expected to give rise to an easily hot worked alloy. Both these phases are extremely brittle at room temperature and at all temperatures up to T_i so that break-up of the constitutent is expected on deformation below 300°C., with particles shearing away from the aluminium interface. Compounds like $CrAl_7$ and $MnAl_6$ have hardness values only slightly higher than that of $CuAl_2$ at room temperature but retain these values up to an inflexion temperature of between 400°C. and 500°C. Brittleness of these constituents would be expected under most hot working conditions. The compound $NiAl_3$ has an initially high hardness but begins to soften rapidly above about 300°C. There is an indication of initial hardening at elevated temperatures which is also apparent for $MnAl_6$. From the literature it would appear that compounds like $FeAl_3$, $NiAl_3$, Co_2Al_9, $CrAl_7$ and $MnAl_6$ would also confer high temperature stability on an alloy especially as all the transition metals are very insoluble in aluminium in the region of 300°C. and would remain as second phase particles. Both $CuAl_2$ and Mg_5Al_8 would be soft above 300°C. and also quite soluble so that strengthening by these phases would be greatly reduced above this temperature. The hardness and inflexion temperatures for some binary intermetallics are shown below in Table I.

Phase	V.P.N. Hardness 25°C.	Inflexion Temp.	T_h	Micro-hardness 25°C.
$CuAl_2$	400	300°C.	0.66	400
$FeAl_3$	730	460 "	0.51	650-800
Mg_5Al_8	200	300 "	0.78	230
$NiAl_3$	720	290 "	0.50	580
$MnAl_6$	540	400 "	0.685	-

Table I - Illustrating the hardness and inflexion temperatures (in degrees Centigrade and as a proportion of the absolute melting temperature (T_h)) for various binary intermetallics of aluminium.[79]

2.2.1 The use of energy curves in hot workability studies

In the calculation of loads and powers for hot mills the variable which introduces the greatest inaccuracy is the temperature of the rolled material at each pass, the determination of which is by no means simple. Some success has been achieved in calculating the temperature distribution in plate rolling by computerising published equations[61] relating to the cooling of a plate by radiation. Reasonable approximations may also be made for pass temperatures when products of large cross sectional area such as slabs and blooms are rolled. Hence it is possible to neglect heat lost by the rolled material to the rolls and cooling water, also the heat gained by the materials from the energy of deformation is small under such conditions. Semi-empirical methods have been proposed[62] for calculating the temperatures of strip rolled in a tandem finishing mill where in addition to radiation losses which cool the material the energy of deformation materially increases the temperature while the water used for roll cooling decreases it. The obvious difficulty in applying any equation for the rolling of strip or plate to load and torque calculations is that the two effects are interdependent. The reduction that can safely be taken in a mill depends critically on the material temperature while the temperature itself depends on the changes in thickness at each pass and in the case of materials rolled to thin gauges on rolling power transmitted to the metal by the rolls.

Load and torque calculations based on empirical methods using energy curves are dependent on both temperature and pass reduction. The energy method of calculating torques (and from them rolling loads) is based on the assumption that the total energy required to deform metal in a mill is independent of the increments of strain, i.e. if the total energy per unit mass for a given reduction is E, then

$$E = Ek + Ef$$

for all rolling schedules to a close approximation[63] where Ek is the pure work of deformation and Ef is the work required to overcome friction. This has been shown to be inaccurate[63]. The energy method of calculating the power and rolling loads[64] for a new mill on data taken on a mill in production will only give acceptably accurate results if the following conditions are satisfied:

a) The geometry of the mill for which the calculations are made does not differ greatly from that of the mill on which the measurements were taken.

b) The rolling schedules for the two mills are nearly identical and the corresponding pass temperatures are within ± 10°C of each other at all times.

The use of energy curves for calculating mill powers may be suspect but they are useful where no computer is available for the utilisation of iterative routines. Although limited for the calculation of rolling schedules energy curves are a useful way of comparing the hot working characteristics of various alloys, the shape of the curves and their position relative to each other when plotted to the same scale giving a visual contrast.

It has been observed that certain "strong" commercial aluminium alloys exhibit a different shaped energy curve from the softer alloys.[65] This can be seen in Fig. 2. No explanation has yet appeared to show why there is a difference in the shape of the energy curve for the two types of alloy.

2.3.1 The determination of the cooling rate of hot rolling slabs during the commercial hot rolling of aluminium alloys

A knowledge of the temperature variation of a rolling slab during the hot rolling process is essential for the calculation of efficient rolling schedules and is also useful in understanding the deformation mechanics occurring during the fabrication process. Reasonable results have already been achieved on reversing mills producing steel plate by considering the radiation heat losses only. Russian workers have also claimed good results by considering heat loss due to radiation and heat input due to the energy dissipated in deformation,[66] but their results are hardly applicable to modern rolling mills and contained very little practical verification. In calculations based on the heat loss due to radiation and heat input due to deformation for steel strip mills the temperatures predicted are usually much higher than measured values. This is due to the neglect of a very important factor (under these conditions) which is the heat conducted to the rolls and the heat lost to the roll coolant. A detailed analysis of this factor is not possible as little is known about the temperature distribution in the roll gap due to the difficulty of determining such variables as roll temperature, coolant temperature and coolant flow rates.

Apart from the theoretical difficulties involved in trying to incorporate all the sources of heat loss and generation into equations for calculating slab temperature there is also the difficulty of measuring the temperature of the slab experimentally during rolling so that the performance of any equations can be checked. The temperature measuring technique must be rapid so that production is not interfered with as any departure from normal rolling practice may result in the recording of artificial slab temperatures. This last factor becomes important with thin gauges, where cooling is rapid. In measuring the temperature of continuously rolled steel strip photographic methods have been used[67] where colour photographs were taken of the hot steel and compared using an optical pyrometer with a photograph of a steel wedge with a known temperature gradient. These methods are not satisfactory as the accuracy is only about ± 20°C. More success has been achieved using radiation pyrometers, but in the case of hot rolling aluminium alloys these methods of temperature measurement are not possible and contact pyrometers have to be used.

The method of developing equations for calculating the temperature at any stage during the rolling programme therefore begins with the use of relatively simple equations to include each element of temperature increase or decrease and then modifying these equations in the light of information gained by comparing predicted temperatures with measured temperatures. This approach is partly empirical but until heat theory is able to deal with the complex and variable conditions encountered in hot rolling this is the most satisfactory method available. In the only reported case where a similar analysis has been done (for the continuous rolling of steel strip) the method gave extremely good results.[62]

2.3.2 Sources of heat transfer during hot rolling

The major sources of heat loss and generation are as follows -

i) Radiation heat loss

ii) Convective heat loss

iii) Heat conducted into the work rolls

iv) Heat lost to the roll coolant

v) Heat gained from energy of deformation.

Each of these will be dealt with individually below.

2.3.2.1 Radiation heat losses from the rolling slab

Calculations of heat lost by radiation are based on the Stefan-Boltzmann law. From this the following simple law is derived -

Heat lost = $H = E\sigma T^4$ cals/sec/sq.cm. where

E = Emissivity-dimensionless

σ = Stefan Boltzmann constant = 1.36×10^{-12} cals/cm^2/sec/$^\circ$K

T = Temperature of the radiating body in degrees Kelvin

The emissive power for aluminium may be taken from published values.[68]

An allowance for the effect of ambient temperature can be made in the equation which may be necessary for fairly low temperatures as in the rolling of aluminium but can be safely neglected in the case of hot rolling steel.

2.3.2.2 Convective heat losses from the rolling slab

A number of equations have been developed for calculating heat loss due to convection under various conditions, the equations themselves having been determined from relationships found to exist between the variables in carefully controlled laboratory experiments conducted into the theory of fluid flow and convection. The equation shown below has been derived from such relationships (its derivation will be shown later) and is applicable under turbulent conditions of flow.

$$H_t = 2.57 \times 10^{-5} \; \theta^{1.33}$$

where H_t = heat loss cals./sq.cm./sec.

θ = mean temperature difference between the surface and convective fluid (air) °C.

Various corrections can be applied (again determined from experimental measurements) to compensate for the position of the surface relative to the convective flow because heat loss due to convection will be different from the top surface of a slab (horizontal surface) to the heat lost from the sides (vertical surfaces).[69] Also the heat loss from the underside of the slab will be different from the upperside. The degree of sophistication achieved using all these corrections is impressive and complicating but their usefulness is debatable. Another correction which may also need to be made is for forced convection. This is necessary because of the movement of the slab through the air between passes and during passes. Once again reference can be made to published data in the form of both equations and graphs.[70]

2.3.2.3 Heat lost from the rolling slab due to conduction to the work rolls.

In the work of Lee et al[62] a purely empirical allowance was made for the heat lost from the slab to the work rolls because of the complexity of the boundary conditions between the slab and the work rolls and the lack of any satisfactory solution. However, there do exist a number of solutions to hypothetical cases[71] such as the rate of heat loss from a plate at temperature Ti in intimate contact with a semi-infinite plate at a lower temperature Tii. Hence if the slab is assumed to be plate 1 at temperature Ti and the work rolls are assumed to be plate 2 at temperature Tii then it is possible to calculate a value for the heat loss from plate 1 to plate 2 or H the "heat transfer coefficient". Using this value which is likely to contain some element of error the heat loss from the slab to the rolls should be calculable if the slab temperature and roll temperature are known.

2.3.2.4 Heat lost from the slab due to conduction to the roll coolant.

For an accurate calculation of this heat loss it is necessary to know the following factors -

i) The temperature of the coolant

ii) The flow rate of the coolant, which may vary considerably from one pass to the next.

iii) The boundary conditions between a layer of coolant supported by a layer of steam between the coolant and the hot slab formed when coolant falls from the rolls onto the slab.

iv) The proportion of the slab surface area covered by coolant at any one time.

v) The length of time that this area is covered by coolant.

vi) The temperature of the coolant after it leaves the slab surface.

vii) The amount of water lost from the coolant in the form of steam.

An analysis of a complex situation like this is very difficult, if not impossible, and so some kind of empiric or assumed allowance must be made to compensate for this heat loss.

2.3.2.5 Heat gained by the slab due to the dissipation of pure energy of deformation in the slab

It has been shown that the amount of energy of deformation transformed into heat is about 95%[72] of the energy expended within the metal. Hence if the energy of deformation is known, its heating effect can be calculated. If it is assumed that a fixed proportion of the power consumed by the mill motor in each pass is used to overcome friction in the roll bearings etc. the remainder is then used as pure energy of deformation. Since the voltage across the mill motor can be measured and the current drawn at each pass also measured with suitable instrumentation, the energy of deformation can thus be calculated, a simple equation of the following form being used -

$$E_r = \frac{F \times 550 \times E \times I}{746 \times Q} \quad \text{ft. lbs/lb.}$$

Where

E_r = The energy of rolling per unit mass

F = The proportion of power supplied to the mill motor used for deformation

E = The voltage across the mill motor

I = The current drawn by the motor at each pass

Q = The rolling throughput lbs/sec.

2.4.1 The production of sound castings in long freezing range aluminium alloys

The desired starting material for this research project was a supply of 1" diameter cast bars (initially of H.S.15) which as far as possible were to be similar structurally to industrial D. C. castings. It was therefore necessary to investigate the factors affecting the soundness of castings in such alloys, to ensure a good simulation.

Porosity due to dissolved hydrogen in aluminium alloys can be overcome fairly easily by adequate degassing of the melt prior to casting with chlorine or nitrogen-chlorine mixtures. However porosity due to shrinkage effects is far more difficult to control. Alloys with a long freezing range are often said to be of the pasty type, and are well known to foundrymen as being extremely difficult materials in which to make completely sound castings. These alloys contain dispersed porosity (micro-porosity) and the tendency to produce this increases with the size of the casting. Normal feeding methods do not seem to have much effect on this form of porosity.

For the greater part of the freezing period the casting consists of a mass of growing crystallites suspended in liquid metal. During solidification all the growing crystallites compete against each other for the residual liquid metal in the interdendritic spaces. Towards the end of the freezing the interdendritic spaces become so narrow that passage of the liquid (feeding) becomes extremely difficult and slow. Hence even if a reservoir of liquid metal is available it becomes isolated from the freezing casting and no further feeding can take place. Therefore porosity is dispersed in a random manner as the last drops of liquid freeze on to the crystallites, but there is a tendency for porosity to be concentrated at the heat centre of the casting. Some evidence has been produced to show that micro-porosity decreases as the amount of liquid at the end of the freezing range i.e. the amount of eutectic present. Solidification in this type of alloy produces shrinkage which is compensated for by "mass-feeding" i.e. a process whereby the pasty liquid-solid mixture settles under the influence of gravity and atmospheric pressure. Later in the freezing process when the crystallites begin to cohere to form a rigid interlocking network (for aluminium alloys this occurs at about 70% solid) mass feeding becomes increasingly difficult, eventually ceasing completely. It is likely that short range movement of liquid metal takes place after mass feeding has completely ceased and that the final soundness of the casting may be significantly influenced by the extent of this liquid movement in the final stages of solidification. The extent to which dispersed porosity occurs in a casting depends upon various factors including

i) Grain size

ii) Rate of solidification

iii) Steepness of temperature gradients

iv) Constitution and freezing range of the alloy

A small grain size promotes mass feeding and is one of the most important factors influencing the occurance of dispersed porosity[73]. The slow pouring of vertical bars in sand moulds for melt test pieces has been found to aid soundness. The slow pouring helps to maintain a vertical temperature gradient through the casting so assisting mass feeding. There is also a lot of evidence to show that the widespread porosity is reduced when the temperature gradients during freezing besides being directional towards the feeder are also steep. This generally implies that the rate of freezing is high. It has been shown in aluminium 4.5% copper alloy that the soundness of cast bars is proportional to the mean longitudinal temperature gradient during the solidification period. Similar observations have been made for magnesium alloys. When the temperature gradients during solidification are steep the beginning and end of freeze waves will be close together (for a pure metal they will coincide) and the interdendritic channels will be short and steeply tapered. Under these conditions it is likely that feeding by the flow of liquid through the interdendritic spaces can take place.

Where the mould extracts heat so rapidly that the casting is solid before the feeder has time to set up favourable heat gradients, solidification can be delayed by heating the mould. With metal chill moulds the decrease in thermal conductivity with heating and the increase in mould-casting interface temperature, means that the casting cools more slowly, so that time will be available for setting up favourable temperature gradients before the casting freezes. It is also reported that low pouring temperatures increase the temperature gradients set up and so helps to increase soundness. Super heat should be avoided as evidence points to the fact that it produces coarsening of the grain size even though the final casting temperature is low. In addition, slow pouring will produce favourable temperature gradients and it is recommended to pour in the thinnest stream possible without break up of the stream.

3. EXPERIMENTAL

3.1 Casting trials

Since in the hot rolling of commercial aluminium alloys the starting material is a pre-heated cast slab it was necessary to produce a cast structure which was similar to that of a commercial D.C. casting. The grain size and intermetallic distribution were replicated without much difficulty by grain refining with the addition of 0.1% titanium and casting into a 1" diameter steel chill mould. However, the problem of achieving a satisfactorily sound casting was more difficult to solve. X-ray radiography proved unsuccessful as a means of measuring the reduction in porosity by improvement in casting technique. This was because the porosity was too fine to resolve, and randomly dispersed. Since the porosity was due to shrinkage effects and not dissolved hydrogen, steps were taken to reduce the porosity by adjusting the variables that control shrinkage porosity, measuring the effectiveness of these alterations by means of a dye penetrant test applied to a smoothly ground surface produced by sectioning the casting along its centre line (i.e. along its heat centre).

Having established the best conditions for producing sound castings a number of bars of 1" diameter were cast in the alloys to be investigated which were H.15, N.4 and D.T.D.683. From these bars hot torsion test pieces were machined and hot torsion tests carried out, but this series of experiments was soon abandoned due to a lack of ductility exhibited by the specimens under the imposed stress system of the test. The major reason for abandoning the hot torsion test was that the equipment available at the time was not sophisticated enough to enable reduction schedules of about 17 passes to be simulated within one revolution of the test piece, after which the specimen fractured (for cast H15). Hot torsion testing was later replaced by hot compression testing which proved to be more suitable to the design of the project.

3.2 Hot Compression Testing

For the intended simulation of hot rolling structures using the hot compression test, a die set was specifically designed and is illustrated in Fig. 3a. The side legs and die holder plates were all machined from $\frac{3}{4}$" bright drawn mild steel which was nickel plated before assembly to prevent excessive oxidation at the test temperatures to be used. The top and bottom die holders were also machined from mild steel (nickel plated) and housed the die plattens which were made from Electron No. 5 die steel. These plattens were easily removed from the holder blocks for re-grinding and were polished to a minimum of 6 micro-inch finish using diamond paste. The die holder blocks were free moving in the vertical plane, reductions being achieved by sliding cold rolled steel shims (whose thickness was equal to the reduction desired) between the base of the press and the bottom die holder block. This action raised the bottom die holder, specimen and top die holder by the reduction desired so that when the top of the press hammer was released it descended (always to the same point relative to the base of the press), pushed the top die down by the amount required thus transmitting the desired reduction to the specimen. When the hammer returned to its raised position another reduction could be achieved by inserting a second shim between the base of the press and the bottom die holder, and then releasing the hammer. In this way a reduction schedule could be built up merely by continuing to add a series of shims thus producing a series of accurately known reductions in the compression sample.

The initial starting temperature of the specimen was achieved by heating the specimen and the die set separately to the desired temperatures, and then inserting the specimen between the platens and returning the die set to the furnace for a long enough period to allow temperature distributions to even out. The whole die set was then transferred to the press where it was accurately located on slides attached to the base of the press ready for the first reduction, as shown in Fig. 3b. Excessive heat loss from the bottom die holder to the base of the press was prevented by inserting an insulating layer between the die holder and the shims, this layer being constructed from several thin sheets of asbestos, held together by a thin sheet steel container. The rather robust nature of the die set was deliberate inasmuch as it was necessary not just for withstanding stresses during compression but also for desired thermal characteristics. Preliminary experiments using pieces of heated steel plate and steel bars sandwiching test pieces of the size to be used, to which were attached thermocouples, helped in designing a die set that would give a certain cooling rate in a certain temperature range. The die set as used is shown in Fig. 3a except that during a reduction schedule, small steel windows were fitted to fill the open spaces at the front and back of the die holder frame. This arrangement gave a cooling curve for the die set which was very similar to that for a slab cooling from its hot rolling temperature during the commercial rolling for H.15. Also, cooling curves plotted for three thermocouples mounted along the centre line of a compression sample (one inch long), one being mounted just below the surface in contact with the top die, one below the surface in contact with the bottom die, and one in the centre of the specimen showed that when the die set was mounted on the press the maximum temperature variation in the compression slug during cooling was never more than 10°C.

Having constructed a die set with the required thermal characteristics it was necessary to find a lubricant that would reduce friction as far as possible. A number of preparations were tried containing molybdenum disulphide, colloidal graphite etc., which were applied to specimens subsequently compressed at 450°C. Evidence of frictional effects was observed not only in the form of barrelling but macroscopically in the form of uneven grain flow. Although friction was never completely removed at reductions over 50% the methods described above allowed the lubricant with the best performance to be selected. The press used to effect the compression schedule is shown in Fig. 3b with the die set located by means of the slides fixed to the base plate of the press. The press was a single action hammer in which the tup was driven down at a constant speed of 9"/sec. by the momentum of a large electrically driven fly-wheel.

3.3 The measurement of hot rolling variables

So that a simulation of commercial hot rolling could be made in the laboratory using the hot compression test, a certain amount of data had to be collected from a mill rolling commercial alloys. An outline of this is given below.

3.3.1 The variation in temperature of a rolling slab during rolling

The temperature drop of a rolling slab during the rolling operation was measured for a number of slabs weighing approximately 4,500 lbs. Since it was necessary to measure temperature quickly to prevent the results differing from those under normal rolling conditions and also to prevent interference with production, contact pyrometers were used. Contact pyrometers are not noted for their accuracy and so the instruments used were carefully calibrated and checked against a known e.m.f. supplied by a potentiometer before use. Two instruments had to be used since the temperature was measured after every pass and since the mill was a reversing mill this meant that there had to be a temperature measuring station on each side of the mill. Adjustments were made until the two instruments recorded the same temperature from the same area of a heated block. It was necessary to measure the temperature of the slab in the same place after every pass since the temperature distribution along the length of the slab varied due to thermal gradients in the soaking pits. Hence the point where the first temperature reading was taken was marked and all other values were recorded from the same place.

The time between passes for different slabs tended to vary but this had little effect on temperature from one slab to the next. At convenient stages of the rolling of later slabs, where the cumulative delay of shearing and temperature measurement would not seriously affect production, samples were cut from the rolling blank. Because of power limitations in the shear, these samples had to be taken after the blank had been rolled to $4\frac{1}{4}$" thick, or less. These samples were later used for metallographic examination.

Other information required from the rolling mill was concerned with the calculation of energy curves. Details of the mill motor were obtained from a recorder chart (see Fig. 4) which was serviced every day and run continuously as a safeguard to the correct functioning and condition of the motor. The motor speed and also the electrical characteristics could be read from the chart. Motor current could be read to an accuracy of ± 100 amps. and voltage to an accuracy of ± 10 volts. Information concerning the weight and dimensions of the rolling slabs was obtained from mill-cards (used for progressing and scheduling) and data concerning the physical parameters of the mill such as gear box ratios and roll dimensions were obtained from records kept by the engineering staff.

3.4 Compression testing used for simulating hot rolling structures

With sufficient data collected on the hot rolling variables and with a die set able to simulate the thermal conditions of hot rolling, schedules were simulated and the structures produced by hot compression were compared with those produced by the commercial hot rolling of H.15 and N.4. Normal metallographic methods were used for the comparison.

3.4.1 Lubrication trials

For the lubricant with the best overall performance, the following method of application was adopted.

The compression samples (0.7" dia. by 1.0" tall) were heated to 140°C. and then dipped into the lubricant. After allowing the excess to drain off the specimens were returned to the furnace to dry and cure. The composition of the lubricant is shown below.[74]

100 c.c.s. DAG extrusion product 1599* (colloidal graphite)

200 c.c.s. Distilled water

12 gms. Cadmium oxide

---

* Acheson Colloids Co. Ltd.

3.4.2 The hot compression of H.15

Since difficulty had been experienced with ageing affects if the samples were lubricated after homogenisation, the samples were given a double heat treatment. They were first heated for 16 hours at 450°C. and then water quenched before machining the 1" dia. bars to 0.7" dia. by 1" long compression slugs. The slugs were then coated in lubricant and reheated for 16 hours at 480-490°C. The specimens were then furnace cooled to 450°C., held for one hour and compressed. Commercial homogenisation would involve heating for 6/12 hours at 480-490°C. and then reheating for say 4/6 hours at the rolling temperature which would be 450-470°C. However the time taken to heat a large rolling slab to its hot working temperature is so long that the total time the slab is in the furnace may be of the order of 24 hours.[75] Hence the protracted preheats given to the compression samples were justified and necessary. Oxidation of the lubricant and loss of lubricating properties was not found to be a problem as the coating was fairly thick. The compression structures of N.4 and D.T.D. 683 were also examined, the preheats for these alloys being described below.

3.4.3 The hot compression of N.4

In commercial practice no homogenisation is given to N.4, the slab being heated to 480-505°C. and then held at that temperature for a minimum of one hour.[75] Again, to simulate a long heating up time the specimens were given 16 hours in a furnace at 490°C. before compression.

3.4.4 The hot compression of D.T.D.683

Commercial practice is to homogenise for 15 hours at 480-500°C., followed by a preheat to 400-420°C. and holding at this temperature for a one hour minimum before rolling.[75] The compression samples were homogenised for 16 hours at 490°C. before machining and lubricating followed by a preheat at 410°C. for 16 hours. A thorough metallographic examination was made of the hot compressed structures for all three alloys, and a similar examination was undertaken for the hot rolled structures of H.15 and N.4 on samples cut from the commercial rolling blanks.

3.5 Metallographic examination

Apart from the examination of the hot worked structures an examination of the cast structures was also made to clearly identify all the phases present. The examination was conducted as follows.

3.5.1 Optical metallography

Identification of the intermetallic phases can be carried out by observing the effect of certain etching solutions on the phases. This method of identification is based on the work of a number of people including Gosta Phragmen.[76] Carefully prepared etchants were used under equally carefully controlled conditions and the distinct colour changes and preferential etching that they produced enabled quite accurate identification to be made.

3.5.2 X-ray diffraction

Particles were extracted by various chemical and electrochemical methods from the host matrix and the diffraction patterns produced in a Debye-Scherrer X-ray camera were analysed.

3.5.3 Electron beam probe analysis

Samples were prepared and inserted into an electron micro beam probe analyser and individual particles of intermetallic were analysed.

3.5.4 Micro hardness testing

Micro hardness tests were conducted on particles contained in the micro structures of the alloys. Where the particles were not large enough for micro hardness testing they were grown by remelting the alloy and slowly cooling it through the liquid range.

3.6 Compression testing with load measurement

Preliminary compression testing was conducted on apparatus which was not equipped for load measurement, and indeed it was not necessary for the early experiments which were designed to investigate structure changes only. However, it became necessary to measure load in later experiments, and the equipment shown in Fig. 5 was used. The equipment (built by Mand Precision Instruments Ltd) consists of two variable speed electric motors capable of producing a wide range of strain rates on a "hard beam" tensile machine. The load is measured electronically from strain gauges fitted to a steel proving ring situated in the head of the machine. The load can be shown continuously on a digital voltmeter, printed out at fixed intervals of time on a teleprinter, or plotted directly on an X-Y recorder as a function of load against time. A jig has been constructed to enable the machine to be used for compression testing as shown in Fig. 6 . The jig is made entirely from high temperature Nimonic alloys and is capable of sustaining loads up to 25,000 lbs. at temperatures up to 900°C.

The whole of the jig assembly can be enclosed in a three zone furnace and temperature control of less than ± 2°C. can be achieved.

Samples of aluminium 8% copper in which the size and distribution of the $CuAl_2$ was varied were compressed in the jig. Also samples of pure intermetallic compounds were deformed and alloys containing large proportions of intermetallic phases. Load-time relationships were plotted on the X-Y recorder for all these samples. Since the samples of intermetallic were extremely brittle, they could not be lubricated by hot dipping, as were the alloys since the quenching stresses would have caused excessive cracking, and so the lubricant was applied cold and the samples were air dried.

3.7 The preparation of pure intermetallic phases

The hot deformation characteristics of certain intermetallics were of interest and so pure samples of some of these were made. The details of the compositions and methods of production are as follows.

3.7.1 The preparation of pure $CuAl_2$

An alloy containing 53.5% copper and 46.5% aluminium was melted in a recrystallised alumina crucible in a tungsten wound vacuum furnace shown in Fig. 7. The furnace was pumped down to about one micron mercury pressure and then argon was admitted to the furnace chamber until a partial pressure of about 100mm. mercury was obtained; this was sufficient to prevent excessive vapourisation of aluminium by boiling during melting. When the aluminium and copper were completely melted they were cast under partial vacuum into a copper chill mould. Since this intermetallic is too brittle to machine it was remelted and cast into a round mould whose diameter was that of the desired sample size. The phase cannot be melted in a silica tube or an evacuated silica envelope as the aluminium reduces the silica producing needles of silicon in the cast bar and also causing a loss in aluminium which results in the formation of a small amount of another aluminium copper intermetallic, CuAl. Therefore tubes of graphite were machined with a $\frac{1}{2}$" internal diameter which were then heated to 900°C. before use to dry them and to drive off any volatile impurities.

The cast bar from the vacuum furnace was crushed in a jaw-crusher to disperse any segregation (stirring was not possible in the vacuum furnace) and the particles put inside the graphite tube. The graphite tube was then placed inside the boro-silicate tube as shown in Fig. 8 and sealed at the top. The tube was then flushed with either argon or nitrogen (both effective) for several minutes before inserting into a furnace set at 700°C., which is 110°C. above the melting point of $CuAl_2$. After 15 minutes the furnace was switched off and the bar was allowed to cool slowly to room temperature. The slow cooling was necessary to reduce cracking due to thermal stresses which result if cooling is too rapid. Cracking due to thermal stresses can be seen in Fig. 9. When cool, the bar of $CuAl_2$ was removed from the graphite tube and test pieces $\frac{1}{2}$" tall were cut from the areas of the bar that appeared to be free from cracks on visual examination. This selection sometimes yielded only two test pieces from a fourinch bar. Since the material is so brittle cutting has to be done by electric spark discharge machining and even with this precaution, the power of the spark has to be limited to prevent cracking of the cut surface. Because neither aluminium or copper vapourises easily and because of the limit on spark power, the time taken for a 0.015" thick steel electrode to pass through the $\frac{1}{2}$" bar was about 3 hours.

After grinding the spark cut surfaces (silicon carbide papers coarser than 400 grade could not be used as they caused cracking) and the outside surface of the bar the samples were radiographed. None of the samples showed any signs of defects so they were lubricated and hot compressed.

3.7.2 The preparation of pure $MgZn_2$

Due to the volatile nature of the components of this phase especially zinc, vacuum melting could not be used, so granulated zinc and magnesium were put directly into a graphite tube and melted in an inert atmosphere of nitrogen in the same apparatus used for $CuAl_2$. Again spark machining was used for the cutting operation but the cutting time for this phase was only about 20 minutes using the same conditions as for $CuAl_2$. Final preparation of the samples was as for $CuAl_2$.

3.7.3 The preparation of pure Al(Mn, Fe)Si

When an alloy containing 61.4% Al, 15.7% Mn., 16.1% Fe and 6.8% Si[76] was melted under partial vacuum and chill cast, the structure revealed that the Al(Mn, Fe)Si present had formed by an uncompleted peritectic reaction. Therefore a number of protracted heat treatments were carried out in an attempt to drive the reaction towards completion. None of these were successful and so an attempt was made to produce the phase by powder metallurgical techniques. Aluminium, iron, manganese and silicon powders were mixed and compacted at a pressure of 50 t.s.i. and the resultant compacts sintered in a vacuum.

3.8 The preparation of alloys containing a large volume fraction of intermetallic

Due to the experimental difficulty in producing pure samples of intermetallic and the difficulties in machining and handling them, alloys containing a large volume fraction of intermetallic were made in which many of these difficulties did not arise.

3.8.1 The preparation of an aluminium copper alloy containing approximately 80% by weight of $CuAl_2$

An alloy containing 40% by weight of copper was melted in air (small losses are less significant than with pure $CuAl_2$) and cast into a preheated graphite mould. Due to the presence of some soft aluminium in the form of an aluminium-$CuAl_2$ eutectic, thermal stresses could be relieved so that cracking of this alloy was no problem. Cutting could be done by conventional means and again ½" tall specimens were produced for compression in the Mand testing machine.

3.8.2 The preparation of an aluminium iron alloy containing approximately 80% by weight of $FeAl_3$

An alloy containing 32% by weight of iron in the form of carbonyl powder was melted under a partial atmosphere of argon and chill cast. The alloy was then re-melted in a furnace set at 1275°C. as quickly as possible to prevent excessive oxidation and cast into a preheated graphite mould. Final preparation of the specimens was as for the aluminium 40% copper alloy.

4. RESULTS

4.1 Casting trials

The casting procedure found to give the soundest bars was as follows -

i) The aluminium addition to the charge was melted in a clean plumbago crucible in an electric furnace under a dry flux cover.

ii) When the aluminium was molten the alloy additions were added in the form of hardeners through the flux cover.

iii) When the charge was thoroughly melted and reached a temperature of 720°C., it was removed from the furnace and degassed with hexachloroethane pellets.

iv) The crucible was allowed to stand quietly for 20 minutes in the furnace at 690°C.

v) The crucible was removed from the furnace and the dross and dry flux were skimmed off.

vi) The melt was gently stirred and poured as slowly as possible in a continuous unbroken stream into a warmed dry mould. The best results were achieved if the mould is tilted towards the crucible.

The results shown in Fig. 10 illustrate the improvement achieved by following this procedure the micro porosity being shown by dye penetrant testing.

4.2 Observations of commercial hot rolling

4.2.1 Survey of temperature variation of rolling slabs during hot rolling

The results of the thermal survey are shown in Tables 2-7 below.

Thickness after pass ins.	Temperature after pass °C.
10.0	423
6.7	421
5.5	415
4.0	420
3.75	420
2.5	410
1.75	398
1.1	390
0.57	370

Table 2

Slab No. 1, alloy - H.15.
Measured slab temperature variation during hot rolling

Thickness after pass ins.	Temperature after pass °C.
10.0	425
6.6	418
5.5	420
4.0	418
3.25	422
2.5	402
1.75	394
1.1	385
0.58	375

Table 3

Slab No. 2, alloy - H.15
Measured slab temperature variation during hot rolling

Thickness after pass ins.	Temperature after pass °C.
10.0	425
6.5	415
5.25	420
4.0	410
3.25	420
2.5	403
1.75	403
1.1	395
0.58	371

Table 4

Slab No. 3, alloy - H.15
Measured slab temperature variation during hot rolling.

Thickness after pass ins.	Temperature after pass °C.
10.0	440
6.5	430
5.25	432
4.0	420
3.25	423
2.5	405
1.75	403
1.1	398
0.58	382

Table 5

Slab No. 4, alloy - H.15
Measured slab temperature variation during hot rolling

Thickness after pass ins.	Temperature after pass °C.
10.0	420
6.5	410
5.25	414
4.0	405
3.25	410
2.5	400
1.75	395
1.1	385
0.58	370

Table 6

Slab No. 5, alloy - H.15
Measured slab temperature variation during hot rolling

Thickness after pass ins.	Temperature after pass °C.
10.0	478
9.0	478
8.0	477
7.0	476
6.0	475
5.0	474
4.0	472
3.0	469
2.0	464
1.0	450
0.7	434

Table 7

Slab No. 6, alloy N.4
Measured slab temperature variation during hot rolling.

The results shown in the previous tables were plotted as temperature vs. thickness curves and can be seen in Fig. 11.

4.2.2 Time elements of pass schedules

The times taken for the rolling of slabs 3 and 4 are shown below in tables 8 and 9. The times for the other slabs are not listed as certain difficulties in the operation of the mill lead to delays which increased the rolling time from the normal 10 minutes to about 13 minutes. These delays however had no significant effect on the temperature of the slabs.

Thickness after pass inss.	Time to complete pass mins.
10.0	0
6.5	2.08
5.25	3.13
4.0	4.16
3.25	5.00
2.5	7.50
1.75	8.25
1.1	9.00
0.58	10.25

Table 8

Slab No. 3, alloy H.15
Measured time intervals in a commercial rolling schedule

Thickness after pass ins.	Time to complete pass mins.
10.0	0
6.5	2.16
5.25	3.25
4.0	4.16
3.25	5.08
2.5	7.75
1.75	8.66
1.1	9.00
0.58	10.66

Table 9

Slab No. 4, alloy H.15
Measured time intervals in a commercial rolling schedule.

The results shown in the tables above are plotted as time vs. temperature in Fig. 12 for slabs 3 and 4.

Operation	Pass No.	Mean I amps	Mean V volts	Length ft.	Thickness ins.	Mean HP	R.P.M	Speed f.p.m	Pass Time mins.	Output tons/hr	HP hrs/ton	Cum.
Seal	1	1,760	600	10.05	9.8	1,415	270	154.3	0.0648	1,852	0.76	0.76
Seal	2	2,640	600	10.15	9.6	2,122	380	217.1	0.0461	2,603	0.82	1.58
Seal	3	2,360	600	10.30	9.5	1,897	390	222.9	0.0448	2,679	0.71	2.29
Seal	4	2,640	600	10.50	9.25	2,122	380	217.1	0.0480	2,500	0.85	3.14
Broadside	5	1,760	600	3.76	8.8	1,415	350	200	0.019	6,316	0.22	3.36
Broadside	6	3,440	520	3.99	8.3	2,397	160	91.4	0.044	2,727	0.88	4.24
Broadside	7	3,480	600	4.25	7.8	2,798	190	108.6	0.059	3,077	0.91	5.15
Broadside	8	3,240	560	4.48	7.4	2,430	290	165.7	0.027	4,444	0.55	5.70
Broadside	9	2,960	600	4.73	7.0	2,379	300	171.4	0.0276	4,347	0.55	6.25
Broadside	10	3,240	560	4.79	6.6	2,430	310	177.2	0.027	4,444	0.55	6,80
Straightway	11	3,920	600	12.58	5.5	3,152	310	177.2	0.071	1,690	1.87	8.67
Straightway	12	4,200	480	17.30	4.0	2,700	230	131.4	0.131	916	2.95	11.62
Straightway	13	3,000	600	21.29	3.25	2,412	340	194.3	0.11	1,091	2.37	13.39
Straightway	14	3,000	580	27.7	2.5	2,310	350	200	0.139	863	2.68	16.67
Straightway	15	3,800	600	39.5	1.75	3,055	340	194.3	0.203	591	5.17	21.84
Straightway	16	3,040	540	62.9	1.1	2,189	340	194.3	0.324	370	5.92	27.76
Straightway	17	3,080	600	119.3	0.58	2,476	300	171.4	0.696	172.4	14.36	42.12

Slab No. 2 10" x 43" x 120" Weight = 4,480 lbs.

Alloy - H.S.15

Table 10 - Showing the elements of power consumption and the cumulative energy requirements through the rolling schedule

Operation	Pass No.	Mean I amps.	Mean V volts	Length ft.	Thick-ness ins.	Mean HP	R. P. M	Speed f. p. m	Pass Time mins.	Output tons/hr	HP hrs/ton	Cum.
Seal	1	1,760	600	10.05	9.8	1,415	340	193	0.0565	2,124	0.67	0.67
Seal	2	2,160	600	10.15	9.6	1,737	400	224	0.0437	2,537	0.68	1.35
Seal	3	2,160	600	10.3	9.5	1,737	400	224	0.050	2,400	0.72	2.07
Seal	4	2,640	600	10.5	9.25	2,123	410	233	0.0497	2,414	0.88	2.95
Broadside	5	1,760	600	3.86	8.6	1,415	370	210	0.0218	5,505	0.26	3.21
Broadside	6	3,440	510	3.99	8.3	2,353	260	149	0.032	3,750	0.63	3.84
Broadside	7	3,440	600	4.25	7.8	2,766	210	119	0.0372	3,226	0.86	4.70
Broadside	8	3,120	510	4.48	7.4	2,215	260	149	0.032	4,000	0.55	5.25
Broadside	9	3,360	600	4.65	7.0	2,701	210	119	0.0428	2,804	0.96	6.21
Broadside	10	3,520	500	4.83	6.5	2,358	270	153	0.0368	3,261	0.72	6.93
Straightway	11	4,160	600	12.95	5.25	3,345	190	107	0.078	1,538	2.17	9.10
Straightway	12	3,640	540	17.0	4.0	2,635	210	119	0.119	1,008	2.61	11.71
Straightway	13	3,760	600	20.9	3.25	3,023	310	175	0.105	1,143	2.64	14.35
Straightway	14	3,240	560	27.3	2.5	2,433	330	186	0.133	903	2.69	17.04
Straightway	15	3,960	600	39.0	1.75	3,184	310	175	0.207	579	5.50	22.54
Straightway	16	4,040	530	61.9	1.1	2,868	310	175	0.31	387	7.41	29.95
Straightway	17	2,960	600	117.5	0.58	2,379	290	163	0.664	181	13.14	43.09

Slab No. 3 10" x 43" x 120" Weight = 4,484 lbs.

Alloy - H.S. 15

Table 11 - Showing the elements of energy consumption and the cumulative energy requirements through the rolling schedule

Operation	Pass No.	Mean I amps.	Mean V volts	Length ft.	Thickness ins.	Mean HP	R.P.M	Speed f.p.m	Pass Time mins.	Output tons/hr	HP hrs/ton	Cum.
Seal	1	1,800	600	10.05	9.8	1,447	320	181	0.0565	2,124	0.68	0.68
Seal	2	2,600	600	10.15	9.6	2·090	410	232	0.046	2,609	0.80	1.48
Seal	3	2,520	600	10.3	9.5	2,026	420	238	0.0417	2,878	0.70	2.18
Seal	4	2,800	600	10.5	9.25	2,251	410	232	0.0497	2,415	0.93	3.11
Broadside	5	1,800	600	3.76	8.8	1,447	410	232	0.0161	7,453	0.19	3.30
Broadside	6	3,200	570	3.99	8.3	2,445	260	149	0.0291	4,124	0.59	3.89
Broadside	7	2,600	600	4.25	7.8	2,090	350	198	0.0225	5,333	0.39	4.28
Broadside	8	3,000	570	4.48	7.4	2,292	280	159	0.0302	3,974	0.58	4.86
Broadside	9	3,320	600	4.65	7.0	2,669	230	131	0.0339	3,540	0.75	5.61
Broadside	10	3,280	530	4.83	6.5	2,329	280	159	0.0302	3.974	0.59	6.20
Straightway	11	4,000	600	12.95	5.25	3,216	210	119	0.0667	1,799	1.79	7.99
Straightway	12	4,200	480	17.0	4.0	2,700	200	113	0.106	1,132	2.39	10.38
Straightway	13	3,600	590	20.9	3.25	2,894	330	186	0.0938	1,279	2.26	12.64
Straightway	14	3,200	580	27.3	2.50	2,486	340	193	0.1448	829	2.99	15.63
Straightway	15	4,120	600	39.0	1.75	3,313	330	186	0.1797	668	4.96	20.59
Straightway	16	4,000	520	61.9	1.1	2,788	320	181	0.361	332	8.40	28.99
Straightway	17	3,000	600	117.5	0.58	2,412	300	170	0.642	187	12.89	41.88

Slab No. 4 10" x 12" x 120" Weight = 4,484 lbs.

Alloy - H.S.15

Table 12 - Showing the elements of energy consumption and the cumulative energy requirements through the rolling schedule

Operation	Pass No.	Mean I amps.	Mean V volts	Length ft.	Thickness ins.	Mean HP	R.P.M	Speed f.p.m	Pass Time mins.	Output tons/hr	HP hrs/ton	Cum.
Level	1	-	-	7.5	12.0	-	-	-	-	-	-	-
Level	2	-	-	7.5	12.0	-	-	-	-	-	-	-
Broadside	3	1,400	600	3.13	12.0	1,125	400	229	0.0137	7,700	0.15	0.15
Broadside	4	1,600	600	3.25	11.5	1,287	460	263	0.0123	8,550	0.15	0.30
Broadside	5	1,300	600	3.41	11.0	1,045	340	194	0.0176	6,000	0.18	0.48
Broadside	6	3,000	600	3.57	10.5	2,420	280	160	0.0223	4,700	0.52	1.0
Straightway	7	2,900	600	8.1	9.75	2,320	230	131	0.062	1,700	1.36	2.36
Straightway	8	3,000	600	8.75	9.0	2,420	460	263	0.0333	3,160	0.77	3.13
Straightway	9	2,400	600	9.82	8.0	1,930	410	240	0.041	2,560	0.75	3.88
Straightway	10	2,700	600	11.25	7.0	2,170	410	240	0.048	2,200	0.99	4.87
Straightway	11	2,500	600	13.1	6.0	2,010	360	206	0.0636	1,660	1.21	6.08
Straightway	12	3,200	560	15.75	5.0	2,400	400	229	0.068	1,550	1.55	7.63
Straightway	13	2,300	600	19.65	4.0	1,850	440	252	0.078	1,350	1.37	9.00
Straightway	14	2,800	600	26.3	3.0	2,250	430	236	0.102	980	2.3	11.3
Straightway	15	2,500	600	35.7	2.2	2,010	380	217	0.165	637	3.16	14.46
Straightway	16	2,900	600	56.25	1.4	2,340	430	236	0.229	460	5.1	19.56
Straightway	17	3,200	600	112.5	0.7	2,580	340	194	0.58	181	14.2	33.76

Slab No. 6   36" x 12" x 90"   Weight = 3,920 lbs.

Alloy - N.S.4

Table 13 - Showing the elements of energy consumption and the cumulative energy requirements through the rolling schedule.

Operation	Pass No.	Mean I amps.	Mean V volts	Length ft.	Thickness ins.	Mean HP	R.P.M	Speed f.p.m	Pass Time mins.	Output tons/hr	HP hrs/ton	Cum.
Level	1	1,400	600	9.17	12.5	1,125	160	91	0.10	1,745	0.65	0.65
Broadside	2	2,680	600	3.92	12.02	2,160	240	137	0.0286	6,110	0.35	1.0
Broadside	3	3,640	500	4.16	11.5	2,440	190	109	0.0382	4,570	0.53	1.53
Broadside	4	3,520	600	4.37	10.96	2,830	150	86	0.0508	3,440	0.82	2.35
Broadside	5	3,760	500	4.55	10.5	2,530	190	109	0.0418	4,170	0.61	2.96
Broadside	6	3,400	600	4.79	10.0	2,740	160	91	0.0526	3,320	0.83	3.79
Broadside	7	2,520	600	4.88	9.8	2,030	340	194	0.0251	6,950	0.29	4.08
Straightway	8	1,600	600	9.5	9.5	1,285	380	217	0.0437	4,000	0.32	4.40
Straightway	9	3,440	600	10.0	9.0	2,770	200	114	0.0878	1,980	1.4	5.80
Straightway	10	3,520	500	11.4	7.89	2,360	200	114	0.10	1,745	1.35	7.15
Straightway	11	3,000	600	12.8	7.0	2,410	200	114	0.112	1,560	1.54	8.69
Straightway	12	2,160	600	14.0	6.47	1,735	240	137	0.102	1,710	1.01	9.70
Straightway	13	2,080	600	15.0	6.00	1,675	210	120	0.125	1,395	1.20	10.90
Straightway	14	3,440	550	17.9	5.02	2,540	240	137	0.130	1,340	1.90	12.80
Straightway	15	3,400	600	20.0	4.50	2,730	240	137	0.146	1,195	2.28	15.08
Straightway	16	3,480	500	24.0	3.75	2,330	340	194	0.123	1,420	1.64	16.72
Straightway	17	3,000	600	27.8	3.24	2,410	320	183	0.152	1,150	2.10	18.82

Slab size = 46" x 12" x 110". Weight = 6,520 lbs. Alloy Dural Lp. (D.T.D. 683)

Table 14 - Showing the elements of energy consumption and the cumulative energy requirements through the rolling schedule.

Operation	Pass No.	Mean I amps.	Mean V volts	Length ft.	thickness ins.	Mean HP	R.P.M	Speed f.p.m	Pass Time mins.	Output tons/hr	HP hrs/ton	Cum.
Level	1	-	-	7.5	12.0	-	-	-	-	-	-	-
Straightway	2	2,200	600	7.53	11.96	1,595	370	211	0.0356	3,960	0.403	0.403
Straightway	3	3,720	500	8.19	11.0	2,490	300	171	0.0478	2,950	0.845	1.3
Straightway	4	3,200	600	8.59	10.49	2,570	280	160	0.0536	2,460	0.974	2.3
Straightway	5	3,880	500	9.51	9.5	2,600	350	200	0.0467	2,970	0.876	3.2
Straightway	6	3,000	600	10.0	8.98	2,410	250	143	0.0699	2,020	1.18	4.4
Straightway	7	3,720	520	12.0	7.5	2,590	200	114	0.105	1,340	2.46	6.9
Straightway	8	3,000	600	12,85	7.0	2,410	260	148	0.0868	1,620	1.49	8.4
Straightway	9	3,040	600	15.1	5.98	2,450	270	154	0.098	1,440	1.70	10.1
Straightway	10	1,920	600	16.5	5.46	1,545	240	137	0.120	1,170	1.32	11.4
Straightway	11	1,280	600	18.35	4.91	1,030	150	85	0.216	653	1.58	13.0
Straightway	12	1,800	600	22.5	4.00	1,445	250	143	0.157	899	1.61	14.6
Straightway	13	1,600	600	25.2	3.58	1,285	350	200	0.126	1,120	1.15	15.8

Slab size = 46" x 12" x 90". Weight = 5,260 lbs.

Alloy = Dural Ld. (D.T.D. 683)

Table 15 - Showing the elements of energy consumption and the cumulative energy requirements through the rolling schedule.

Operation	Pass No.	Entry thickness ins.	Exit thickness ins.	Output tons/hr	Mean I amps.	Mean V volts.	Mean H.P	HP hrs/ton	Cum.
Straightway	1	12.75	11.25	3,640	1,900	500	1,260	0.371	0.371
Straightway	2	11.25	9.75	3,180	2,500	490	1,625	0.512	0.883
Straightway	3	9.75	8.25	2,670	2,800	450	1,680	0.628	1.511
Straightway	4	8.25	6.75	2,180	2,900	490	1,900	0.871	2.382
Straightway	5	6.75	5.25	1,700	2,700	490	1,755	1.03	3.412
Straightway	6	5.25	4.00	1,300	3.000	470	1.885	1.45	4.862
Straightway	7	4.00	3.00	975	3,300	500	1,950	2.00	6.862
Straightway	8	3.00	1.7	550	4,100	550	2,820	5.13	11.992
Straightway	9	1.7	0.9	292	2,900	490	1,910	6.66	18.542

Alloy - 99% aluminium

Table 16 - Showing the elements of energy consumption and the cumulative energy requirements through the rolling schedule.

Operation	Pass No.	Entry thickness ins.	Exit thickness ins.	Output tons/hr	Mean V volts.	Mean I amps.	Mean H.P	HP hrs/ton	Cum.
Straightway	1	12.25	11.0	3,560	480	4,000	2,540	0.713	0.713
Straightway	2	11.0	9.86	3,210	490	2,800	1,825	0.568	1.281
Straightway	3	9.86	9.00	2,915	480	3,900	2,500	0.857	2.138
Straightway	4	9.00	8.01	2,580	490	4,200	2,770	1.072	3.21
Straightway	5	8.01	7.00	2,275	450	3,500	2,110	0.928	4.138
Straightway	6	7.00	5.99	1,940	500	3,400	1,810	0.933	5.071
Straightway	7	5.99	5.00	1,625	490	3,000	1,940	1.195	6.266
Straightway	8	5.00	4.00	1,300	490	2,900	1,900	1.462	7.728
Straightway	9	4.00	3.01	975	490	3,100	2,040	2.09	9.818
Straightway	10	3.01	2.23	720	470	2,100	1,290	1.795	11.613
Straightway	11	2.23	1.71	669	500	2,100	1,365	2.04	13.653
Straightway	12	1.71	0.90	292	480	3,000	1,970	6.74	20.393

Alloy - Aluminium $1\frac{1}{4}$% Manganese

Table 17 - Showing the elements of energy consumption and the cumulative energy requirements through the rolling schedule

Operation	Pass No.	Entry thickness ins.	Exit thickness ins.	Output tons/hr	Mean V volts.	Mean I amps.	Mean H.P	HP hrs/ton	Cum.
Straightway	1	12.25	11.3	3,650	470	2,100	1,305	0.358	0.358
Straightway	2	11.3	10.65	3,450	490	3,200	2,090	0.650	1.008
Straightway	3	10.65	9.9	3,220	480	3,000	1,910	0.593	1.601
Straightway	4	9.9	9.2	2,975	460	2,300	1,410	0.474	2.075
Straightway	5	9.2	8.5	2,770	490	3,500	2,285	0.824	2.899
Straightway	6	8.5	7.6	2,470	490	4,000	2,630	1.065	3.964
Straightway	7	7.6	6.8	2,200	500	4,000	2,650	1.205	5.169
Straightway	8	6.8	6.0	1,940	480	4,200	2,780	1.435	6.604
Straightway	9	6.0	5.2	1,680	510	4,100	2,800	1.665	8.269
Straightway	10	5.2	4.4	1,425	510	4,000	2,700	1.895	10.164
Straightway	11	4.4.	3.2	1,030	500	3,900	2,580	2.51	12.674
Straightway	12	3.2	2.4	758	460	3,200	1,960	2.597	15.271
Straightway	13	2.4	1.4	452	490	3,000	2,160	4.78	20.081
Straightway	14	1.4	0.7	226	470	3,200	2,000	8.83	28.881

Alloy - Aluminium 2¼% Magnesium

Table 18 - Showing the elements of energy consumption and the cumulative energy requirements through the rolling schedule.

Pass No.	Convective temp. loss °C.	Heat lost to coolant °C.	Heat lost to rolls °C.	Radiation heat loss °C.	Heat gained due to def. °C.	Net temp. change °C.	Slab temp. °C.
1.	0.17	0.17	1.3	0.1	0.42	-1.52	478.48
2.	0.2	0.2	1.5	0.11	0.62	-1.39	477.09
3	0.24	0.24	1.8	0.13	0.77	-1.64	475.45
4	0.29	0.29	2.1	0.16	1.03	-1.81	473.64
5	0.39	0.39	2.7	0.22	1.27	-2.43	471.21
6	0.58	0.58	3.2	0.31	1.76	-2.91	468.30
7	0.87	0.87	3.8	0.47	2.42	-3.59	464.71
8	2.04	2.04	7.7	1.1	6.19	-6.69	458.02
9	6.0	6.0	11.5	3.2	7.91	-18.79	439.23

Measured start temperature 480°C.

Measured finishing temperature 440°C.

Alloy - 99% Aluminium

Table 19 - Showing the calculated temperature losses and gains from all important sources and their net effect on overall slab temperature.

Pass No.	Convective temp. loss °C.	Temp. loss to coolant °C.	Temp. loss to rolls °C.	Radiation temp. loss °C.	Heat gained due to def. °C.	Net temp. change °C.	Slab temp. °C.
1	0.17	0.17	1.1	0.08	0.96	-0.66	469.34
2	0.18	0.18	1.2	0.09	0.76	-0.89	468.45
3	0.20	0.20	1.1	0.10	1.15	-0.45	468.00
4	0.22	0.22	1.4	0.10	1.43	-0.51	467.49
5	0.26	0.26	1.6	0.14	1.23	-1.03	466.46
6	0.31	0.31	1.8	0.16	1.23	-1.35	465.11
7	0.39	0.39	2.2	0.20	1.59	-2.59	462.52
8	0.53	0.53	2.7	0.27	1.95	-2.08	460.44
9	0.85	0.85	3.6	0.40	2.80	-2.90	457.54
10	1.19	1.19	4.4	0.60	2.39	-5.00	452.54
11	1.65	1.65	3.8	0.85	2.74	-5.21	447.33
12	5.30	5.30	10.9	2.75	9.00	-15.25	432.08

Measured starting temperature - 470°C.
Measured finishing temperature - 435°C.

Alloy - Aluminium $1\frac{1}{4}\%$ Manganese

Table 20 - Showing the temperature losses from all important sources and their net effect on overall slab temperature.

Pass No.	Convective temp. loss °C.	Heat loss to coolant °C.	Heat loss to rolls °C.	Radiation temp. loss °C.	Heat gained due to def. °C.	Net temp. change °C.	Slab Temp. °C.
1	0.17	0.17	0.96	0.085	0.48	-0.91	479.09
2	0.17	0.17	0.83	0.90	0.81	-0.45	478.64
3	0.19	0.19	0.96	0.10	0.79	-0.65	477.99
4	0.20	0.20	1.01	0.10	0.64	-0.88	477.11
5	0.21	0.21	1.08	0.11	1.10	-0.51	476.60
6	0.24	0.24	1.37	0.12	1.42	-0.55	476.05
7	0.28	0.28	1.45	0.14	1.61	-0.54	475.51
8	0.32	0.32	1.64	0.16	1.92	-0.50	475.01
9	0.37	0.37	1.90	0.20	2.23	-0.61	474.40
10	0.46	0.46	2.24	0.24	2.53	-0.87	473.53
11	0.71	0.71	3.80	0.37	3.06	-2.59	470.94
12	1.12	1.12	4.20	0.58	3.45	-3.57	467.37
13	2.53	2.53	7.93	1.31	5.25	-9.05	456.32
14	8.43	8.43	13.2	4.33	11.80	-22.53	433.79

Measured starting temperature - 480°C.
Measured finishing temperature - 435°C.

Alloy - Aluminium $2\frac{1}{4}$% Magnesium

Table 21 - Showing the temperature losses from all important sources and their net effect on overall slab temperature.

4.2.3 Mill observations necessary for the calculation of energy curves.

The data measured directly from the mill, and the information which was calculated from this is shown in Tables 10-18, and is plotted in the form of energy curves in Figs. 13 - 15.

4.3 The calculation of the temperature variation during hot rolling of an aluminium slab from theoretical principles

From a series of equations selected from heat theory, and modified to be suitable for predicting temperatures in hot rolling, the effects of various heat sources and heat sinks is shown in Tables 19-21. The calculations made involved three slabs and the information collected to enable the calculations to be made is shown below.

Slab A i) Composition - 99% aluminium
ii) Dimensions 12.75" x 36" x 120"
iii) Measured starting temperature 480°C.
iv) Measured finishing temperature 440°C.

Slab B i) Composition - Aluminium $1\frac{1}{4}$% Manganese
ii) Dimensions 12.25" x 36" x 120"
iii) Measured starting temperature 470°C.
iv) Measured finishing temperature 435°C.

Slab C i) Composition - Aluminium $2\frac{1}{4}\%$ Magnesium

ii) Dimensions 12.25" x 36" x 120"

iii) Measured starting temperature 480°C.

iv) Measured finishing temperature 435°C.

Table 22 Slab data needed to calculate temperature variation during hot rolling.

Other data needed for the calculation of the temperature variation of a slab during hot rolling, concerns the energy expended in rolling (derived from the current and voltage in the mill motor at each pass) the pass schedule, and the rolling speed (which for these slabs is assumed to be constant at 280 f.p.m.) This information for slabs A and B is found in Tables 15 and 16 and for slab C in Table 17. The method of calculating the temperature variation will be dealt with later.

4.4 Hot Compression Testing

Hot compression trials were carried out under the following conditions of lubrication on specimens 1" tall and 0.7" in diameter at 450°C.

i) No lubrication

ii) Lubrication with a high temperature grease-colloidal graphite preparation.

iii) Lubrication with a resin bonded molybdenum disulphide preparation.

iv) Lubrication with a suspension of colloidal graphite and cadmium oxide in distilled water. The composition of this lubricant was given previously.

Since all combinations of lubricants and methods of application did not completely remove the effects of friction, a choice of the best lubricant and the best method of application was made. This was lubricant (iv) and the method of application was that of hot dipping. The lubricant was very effective at reductions up to about 50% but above this some inhomogeneous flow occurred. However the effectiveness of the lubricant can be seen from Fig. 16 which shows the effect of friction on flow in an un-lubricated sample hot compressed 63% and Fig. 17 which shows the reduction in inhomogeneous flow during compression of 65% using lubricant (iv).

4.5 Optical metallography of hot rolled structures

The stages of commercial hot rolling at which samples were taken for metallographic examination are listed below for the alloys H.15 and N.4

4.5.1 Sampling points and metallographic examination of H.15

Samples were cut from a commercial rolling slab at various stages of the rolling schedule. The sample consisted of a full width slice of the rolling blank from 4 to 12 inches wide. A sample of this width avoided including any deformation from the shear in the sample which was to be examined. Samples were taken at the following hot reductions.

i) 68%

ii) 78%

iii) 86%

iv) 93%

Samples were allowed to air cool after cutting, and then specimens were cut from the longitudinal and transverse directions relative to the rolling direction. After polishing with diamond paste and etching, the structures were photographed and are shown in Figs. 18-33.

4.5.2 Sampling points and metallographic examination of N.4

Samples were taken from a slab of commercially rolled N.4 in the same manner as described for H.15. The hot reductions at which these samples were taken were as follows -

i) 68.6%

ii) 82.8%

iii) 94.5%

Samples were cut from the transverse direction for examination by optical microscopy. For revealing the grain size and morphology the samples were anodised after polishing. This process produced sufficient attack at grain boundaries to reveal the grain structure, which could not be shown satisfactorily by chemical etching alone. The anodising conditions were as follows.[77]

Solution composition -	49.5% distilled water
	49.5% industrial alcohol
	1.0% hydrofluoric acid

The polished sample is anodised in the above solution for 3 mins. at a potential of 50 volts using a sheet of aluminium for the cathode. Contrast produced by this solution is sufficiently good to make the use of polarised light for examination unnecessary. The microstructures are shown in Figs. 34-39.

4.6 Optical metallography of hot compression structures

Compression structures from simulated hot rolling schedules were examined and compared with hot rolled structures. Details are given below for the three alloys studied.

4.6.1 Sampling points and metallographic examination of hot compressed structures in H.15

Cylinders of H.15 were deformed by axi-symmetric compression according to schedules derived from commercial practice and the structures were examined metallographically by sectioning the deformed cylinder through its thickness. Structures were always examined on this section where deformation was most uniform. Two sets of micrographs were taken of the structures. Figs. 40-43 show the grain morphology produced at the following hot compression reductions.

i) 50%

ii) 73%

iii) 80%

iv) 86%

In the second series of micrographs shown in Figs. 44-49 a more detailed examination of structure is shown produced by the following reductions.

i) 0%

ii) 14%

iii) 30%

iv) 50%

v) 73%

vi) 86%

4.6.2 Sampling points and metallographic examination of hot compressed structures in N.4

Samples were prepared for metallographic examination from cylinders of axi-symmetrically compressed N.4 alloy, by the same techniques used for the commercially rolled alloy. These structures are shown in Figs. 50-61 which were produced by the following hot compressions.

i) 0%

ii) 20%

iii) 35%

iv) 55%

v) 77%

vi) 83%

Again the compression schedules used were derived from commercial practice.

4.6.3 Sampling points and metallographic examination of hot compressed structures in D.T.D.683.

Cylinders of the alloy D.T.D.683 were deformed in compression following a schedule similar to that used for H.15 since the commercial rolling practices for the two alloys are somewhat similar. The structures produced are shown in Figs.62-71 after hot reductions of -

i) 0%

ii) 20%

iii) 35%

iv) 50%

v) 73%

vi) 85%

4.7 The morphology of intermetallics in hot rolled commercial aluminium alloys

The effect of deformation during hot rolling on intermetallics was studied by optical and electron metallography as described below.

4.7.1 Optical metallographic examination of the effect of hot rolling on intermetallic morphology

A metallographic study was made of the behaviour of the intermetallic constituents in the two alloys N.4 and H.15 under commercial hot rolling conditions. The two alloys are dealt with individually below.

4.7.1.1 Metallographic examination of H.15

The phases studied with particular interest in this alloy were -

a) $CuAl_2$

Fig. 72 shows the effect of 68% reduction on $CuAl_2$ (white phase) which causes a progressive break up of the large particles formed in casting, into roughly spherical, smaller particles. This form of break up (i.e. with no sign of fracture) indicates that the phase has some plasticity under the stress system and temperature of hot rolling.

b) Al(Fe, Mn)Si

Figs. 73 and 74 show the effect of the same conditions (i.e. 68% hot reduction) on the cubic-Al(Fe, Mn)Si (hereafter the prefix "cubic" to the Al(Fe, Mn)Si phase will be abbreviated to "c") phase (dark) which in this case produces considerable fracturing indicating a distinctly limited ability to deform plastically. The two phases $CuAl_2$ and c-Al(Fe, Mn)Si were studied as they represent the major volume fraction of intermetallic present at the rolling temperature in H.15 as can be seen in Fig. 75.

The total number of phases that can be present in this alloy are - $CuAl_2$, c-Al(Fe, Mn)Si, Mg_2Si, Al_2CuMg, Al_7Cu_2Fe, and $(Al, Cu)_6(Mn, Fe, Cu)$. However, the amounts of Mg_2Si and $(Al, Cu)_6(Mn, Fe, Cu)$ were very small and the phase

Al_7Cu_2Fe was not observed at all, hence these constituents were neglected from the study. The phase Al_2CuMg was present in rather small amounts at the rolling temperature partly because the alloy only contains a limited amount and partly because at this temperature most of it is in solution.

4.7.1.2 Metallographic examination of N.4

At the rolling temperature for this alloy (480-505°C.) all the magnesium contained in the alloy is in solution and any intermetallics present are mainly a result of impurities. The phases present will depend upon the amount and relative proportions of impurities, chiefly iron and silicon. The phases that could form are $FeAl_3$, AlFeSi, and Mg_2Si. Since Mg_2Si is quite soluble at the rolling temperature the other two phases are the predominant ones to be found at the hot working temperature. A spectrographic analysis of the slab from which samples were taken for this study reveals that iron is present in much larger quantities than silicon and so the major phase expected will be $FeAl_3$ which is precisely what was observed metallographically. The micrograph shown in Fig. 76 illustrates the relatively small amount of intermetallic (mainly $FeAl_3$) in a commercial rolling slab of N.4 and its distribution after 68.6% hot reduction. Figs. 77 and 78 show the needle-like morphology of the phase and shows that it is badly fractured after this amount of deformation, indicating that the phase has limited plasticity at the hot rolling temperature.

4.7.2 Electron metallographic examination of the effect of hot rolling on intermetallic morphology

Samples were prepared for electron metallographic examination to supplement the observations made in the previous section.

4.7.2.1 Electron metallography of H.15

Samples of the alloy after commercial rolling of 68% were electropolished in a solution of magnesium perchlorate in distilled water and ethanol, at sub-zero temperatures and a potential of 25 volts using an aluminium cathode.[78] From these specimens carbon replicas were made by the "two-stage" method which were then shadowed with a gold palladium alloy and examined in a Phillips EM200 electron microscope.

The greater power and resolution of the electron microscope provides better evidence of the plastic nature of $CuAl_2$ and the brittle nature of c-Al(Fe, Mn)Si at the hot working temperature. Fig. 79 shows the so called "chinese script" like particle of c-Al(Fe, Mn)Si which has been severely fractured while Fig. 80 shows $CuAl_2$ and Al_2CuMg which are free from fracture and roughly spherical in shape. Fig. 81 also shows the unfractured particles of $CuAl_2$.

The phases $CuAl_2$ and Al_2CuMg are expected to be intimately associated as they separate out together during solidification by a eutectic reaction which takes place in the region of the Al-Mg-Mn-Si system occupied by the composition of H.15. However, there is some evidence that the two phases become separated during deformation as seen in Figs. 80 and 82.

4.7.2.2 Electron metallography of N.4

The needle like nature and brittleness of the phase $FeAl_3$ can be clearly seen in Figs. 83 and 84. The straightness of the needles in Fig. 83 which are contained in a matrix that has undergone 68.6% hot reduction, further illustrates its lack of plasticity. Deformation has simply caused fracture of the needles followed by flow of the matrix into the fractures.

4.8 Micro-hardness testing of intermetallic phases

The results of micro-hardness tests carried out on a number of intermetallics are shown in Table 23. In all cases a load of 25gms. was used.

Phase	Measured micro-hardness values	Average VPN
$FeAl_3$	870, 894, 803, 803, 863, 946, 870, 824, 847, 803.	846
$MgZn_2$	345, 357, 339, 357, 345, 306, 383, 383, 370, 351	353
Al_2CuMg	317, 322, 306, 357, 322, 317, 333, 345, 311, 333, 327, 327	326
$CuAl_2$	483, 572, 548, 536, 483, 525, 503, 525, 524, 493	519
c-Al(Fe, Mn)Si	894, 894, 824, 870, 1097, 946, 870, 824, 1003, 1003, 974	927

Table 23 Micro-hardness numbers for some intermetallic phases.

The results tabulated above are compared with the few available results given in the literature and are shown below in Table 24.

Phase	Hardness (this study)	Hardness from the literature
$CuAl_2$	519	390. 560. 780. 400*
c-Al(Fe, Mn)Si	927	....
$FeAl_3$	846	526. 755. 800*
Al_2CuMg	326	....
$MgZn_2$	353	....

Table 24 - A comparison of measured micro-hardness numbers with those given in the literature

(* probably the most reliable values[79])

4.9 Electron micro beam probe analysis

Samples were prepared in the normal way and individual particles of intermetallic contained in the matrix of both N.4 and H.15 were analysed.

4.9.1 Electron micro beam probe analysis of N.4

The particles of intermetallic in this alloy were too small to make a satisfactory analysis, as problems were encountered not only with X-ray excitation from the matrix but also from the edges and sides of the particles because of their smallness and because they projected from the surface of the alloy as a result of preferential polishing. This was unavoidable, as the particles were extremely hard and the matrix soft.

4.9.2 Electron micro beam probe analysis of H.15

The two major phases in this alloy are $CuAl_2$ and c-Al(Fe, Mn)Si, both of which were analysed in the electron beam probe analyser. After correction of the count rates from a $CuAl_2$ particle, for absorption (using Philberts method[80]), and the atomic number effect, the composition was found to be 55.5% copper, 44.5% aluminium compared with the published values of 53.5% copper, 46.5% aluminium[81]. However, it may be pointed out that this phase is not strictly stoichiometric and exists over a composition range although this is fairly narrow. Further corrections may have given a more accurate analysis but the values obtained were considered satisfactory for identification purposes.

The composition given in the literature for the phase c-Al(Fe, Mn)Si is 61.4% aluminium, 16.1% iron, 15.7% manganese, and 6.8% silicon[76], this composition being determined by the chemical analysis of particles extracted from an alloy containing 4% manganese, 2% iron, 3% silicon and 91% aluminium. The same source gives an anlysis of the same phase extracted from an alloy containing 3% manganese, 3% iron, 3% silicon and 91% aluminium as, 18.8% manganese, 11.7% iron, 7.1% silicon and 62.4% aluminium. It is thought that the phase stretches across the Al-Fe-Mn-Si equilibrium diagram from c-AlMnSi to c-AlFeSi linked by a homogeneuity range and that the manganese and iron are interchangeable in the lattice of the phase. Attempts to produce the phase in bulk failed when the first of the two compositions given above was used. From the difficulties encountered, the most likely reason seemed to be the difficulty in completing the peritectic reaction by which c-Al(Fe, Mn)Si forms, as it is well known that the rate of diffusion of the transition metals in aluminium is extremely slow.

The results of probe analysis of the c-Al(Fe, Mn)Si phase are shown below. Although there is some scatter between these results and those given by Phragmen,[76] due to the smallness of the particles analysed, the similarity between the two sets of results is significant.

a) 62.86%Al, 16.09%Mn, 15.45%Fe, 5.60%Si.

b) 55.96%Al, 19.54%Mn, 17.97%Fe, 6.50%Si.

Particles of $(Al, Cu)_6(Mn, Fe, Cu)$ were too small to analyse but the sequence of pictures shown in Figs. 85-88 (produced by photographing the image formed on the cathode ray display tube from the characteristic X-rays excited by the electron beam) show that not only does the phase contain all the elements required but also indicates approximately the amounts present relative to the matrix and $CuAl_2$. Fig. 85 shows the phase contains very much less copper than $CuAl_2$ but slightly more than the matrix. It can be seen from Fig. 86 that the particle of $(Al, Cu)_6(Mn, Fe, Cu)$ contains more manganese than either the matrix or the phase $CuAl_2$, while Fig. 87 illustrates the same relationship for iron. The final picture in this series is shown in Fig. 88 which illustrates that the particle contains less aluminium than the matrix, but slightly more than $CuAl_2$. By considering the phases that can theoretically be present, and the compositions relative to the matrix and $CuAl_2$ the particle can only be $(Al, Cu)_6(Mn, Fe, Cu)$. An analysis of this phase given in the literature obtained by the chemical analysis of particles extracted from an alloy containing 7.75% copper, 0.75% manganese, and 1.5% iron in aluminium was 1.9% copper, 8.5% manganese, 18.7% iron and 70.9% aluminium.

4.10 The identification of intermetallic phases by optical metallography

The identification of intermetallics can be accomplished by the use of etching routines in which colour changes and the degree of etching using various etches under strictly controlled conditions is used to identify the phases.[76, 82, 83, 84] The phases identified in H.15 by this technique were as follows.

i) $CuAl_2$

ii) Mg_2Si

iii) Al_2CuMg

iv) Al (Mn, Fe)Si

v) $(Al, Cu)_6(Mn, Fe, Cu)$

4.11 The simulation of hot rolling schedules using the hot compression test

The three alloys whose rolling schedules were simulated are dealt with individually below.

4.11.1 The simulated rolling schedule for H.15

Since H.15 is known to exhibit an unexplained characteristic during hot rolling (the presence of a "hump" in the energy curve) which was to be investigated, the starting point of this project was the design of a die set to be used for compression testing, to simulate the hot rolling of this alloy.

The data in Table 25 shows the relationship between a commercial rolling schedule (columns A, B, C and D) and the simulated schedule using hot compression, (columns D, E and F). Column B gives the slab thickness after the pass number indicated in column A, and column C gives the slab temperature after this pass derived from a cooling curve plotted from measured values of slab temperature during commercial rolling. Column D gives the time in seconds to complete the schedule up to and including the corresponding pass number in column A. For hot compression, column E gives the temperature of a compression slug (derived from a cooling curve shown in Fig. 89 which was plotted from measured temperature values taken at three points on the specimen) at the times indicated in column D. Column F shows the points in the schedule where samples were taken for metallographic examination. Hence, using this schedule it is possible to say that a compression sample can be deformed to any pass number in the schedule in the

A Pass No.	B Thickness of slab ins.	C Temp. °C.	D Time secs.	E Temp. °C.	F Thickness of cylinder ins.
0	10.0	450	0	450	-
1	9.8	450	0	450	-
2	9.6	449	12	449	-
3	9.5	449	18	448	-
4	9.25	448	24	447	-
5	8.8	447	40	447	-
6	8.3	447	48	446	0.84
7	7.8	446	80	445	-
8	7.4	445	90	443	-
9	7.0	443	108	443	-
10	6.5	440	132	442	0.67
11	5.25	437	194	442	0.504
12	4.0	437	245	436	-
13	3.25	434	302	427	-
14	2.5	426	460	405	0.257
15	1.75	421	500	395	0.195
16	1.1	408	550	389	0.140
17	0.58	389	630	376	-

Table 25 - Showing the commercial rolling schedule and simulated rolling schedule for alloy H.15.

same overall time, and time intervals, and be at approximately the same temperature as a commercially rolled slab following the same nominal schedule.

For each part of the schedule it was intended to complete (say as far as pass number 6) a lead slug was deformed in the die set at room temperature and its thickness measured with a micrometer after each pass (i.e. after the insertion of every shim). Adjustments were made until the percentage deformation at each pass in that part of the schedule was the same as for rolling. However, when the samples of H.15 were deformed, the amount of deformation achieved did not always correspond exactly with the amount of deformation in rolling (for example, pass 16 in hot rolling gives 89% reduction, and in hot compression 86%) but the errors were always within a few percent. The specimens were almost always thicker than they should have been, and this was probably due to elastic distortion of the die set and press.

4.11.2 The simulated rolling schedule for N.4

This alloy is rolled at a higher temperature than H.15 and because the cooling curve of the die set did not coincide exactly (from 480°C.) with that of the rolling slab, the simulation between the rolling and compression schedules was made by noting the

A Pass No.	B Thickness of slab ins.	C Temp. °C.	D Time secs.	E Temp. °C.	F Thickness of cylinder ins.
0	10.0	480	0	-	-
1	9.9	478	0	478	-
2	9.2	477	24	477	-
3	8.5	476	30	476	0.80
4	7.6	475	70	475	-
5	6.8	474	120	474	0.65
6	6.0	473	132	473	-
7	5.2	472	140	472	-
8	4.4	471	168	471	0.45
9	3.2	470	180	470	-
10	2.4	466	216	466	0.230
11	1.4	454	300	454	0.168
12	0.7	438	400	438	-

Table 26 - Showing the commercial rolling schedule and simulated rolling schedule for alloy No. 4

temperatures of the slab after each pass in the rolling schedule and from these temperatures and the cooling curve of the die set from 480°C. it was possible to derive a series of time intervals which could be used in the compression schedule so that the temperature after each pass in rolling and compression was the same. This resulted in only a small foreshortening of the time to complete the reductions by hot compression. The rolling and compression schedules are shown in Table 26.

4.11.3 The simulated rolling schedule for D.T.D.683

Since rolling schedules for D.T.D.683 and H.15 are similar although the rolling temperatures are different, it was decided that the compression schedule used for H.15 would be used for D.T.D.683 as far as reduction and time intervals were concerned, but starting with the die at 410°C. instead of 450°C. Samples were taken for metallographic examination at the following stages of the schedule.

Pass No.	Thickness of compressed sample - ins.	% Reduction
6	0.804	19.6
9	0.677	32.2
11	0.505	49.5
14	0.275	72.5
16	0.147	85.3

Table 27 - showing the stages in the simulated rolling schedule of DTD. 683 at which samples were taken for examination.

4.12 Hot compression testing with load measurement

The materials on which load measurements were made during deformation fall into two groups; pure intermetallics and alloys containing a large volume fraction of intermetallic; and relatively dilute alloys.

4.12.1 Compression testing of pure intermetallics and alloys containing a large volume fraction of intermetallic

Each of the materials in this group are dealt with individually below.

4.12.1.1 Hot compression of pure $CuAl_2$

Hot compression tests were carried out on ½" x ½" dia. samples of pure $CuAl_2$. The effects of deformation on these samples are shown in Figs. 90 and 91. The tests were carried out at a deformation rate of 0.2 ins/min. as were all other tests reported in this section. The load contraction diagrams are shown in Fig. 92.

4.12.1.2 The hot compression of an aluminium alloy containing 40% copper

Similar tests were carried out on an alloy containing approximately 80% by weight of $CuAl_2$ to those conducted on the pure $CuAl_2$ but over a wider temperature range. The effects of temperature are shown in Fig. 93 and the load contraction diagrams are shown in Fig. 94. The microstructures of this alloy at 250°C. and 500°C. are shown in Figs. 95 and 96.

4.12.1.3 The hot compression of an aluminium alloy containing 32% iron

The effect of deformation on an alloy containing approximately 80% by weight $FeAl_3$ over a range of temperatures is shown in Fig. 97, and the load contraction diagrams are shown in Fig. 98.

4.12.1.4 The hot compression of pure $MgZn_2$

The effect of deformation on samples of pure $MgZn_2$ are shown in Figs. 99 and 100 at various temperatures and the load contraction diagrams are shown in Fig. 101.

4.12.2 The compression testing of more dilute alloys

Hot compression tests were carried out on an alloy containing 8% copper. By modifications to the casting practice, the grain size, the distribution of intermetallic, and the size of the intermetallic network were changed. The various conditions of the alloy prior to hot compression were as follows -

i) Chill cast without grain refinement - the microstructures are shown in Figs. 102 & 103 and the load contraction diagram in Fig. 104.

ii) Chill cast without grain refinement and hot rolled 60% - the microstructures are shown in Figs. 105 and 106 and the load contraction curve in Fig. 104.

iii) Sand cast without grain refinement - the microstructures are shown in Figs. 107 and 108 and the load contraction diagram in Fig. 104.

iv) Sand cast without grain refinement and hot rolled 60% - the microstructures are shown in Figs. 109 and 110 and the load contraction diagram in Fig. 104.

v) Sand cast and grain refined with 0.1% titanium - the microstructures are shown in Figs. 111 and 112 and the load contraction diagrams in Fig. 113.

vi) Sand cast without grain refinement - the microstructures are shown in Figs. 114 and 115 and the load contraction diagram in Fig. 113. This alloy condition was repeated for comparison purposes with (v).

All the above conditions of the 8% copper alloy were homogenized for 16 hours at 460°C. and water quenched before compression testing to ensure that the matrix was saturated with copper. Grain refinement where it was used was achieved by the addition of sufficient grain refining hardener (composition 5.7% titanium, 1.1% boron in aluminium) to give a concentration of 0.1% titanium in the alloy.

4.12.3 Flow stress values

From the load contraction diagrams the stress required to produce the onset of deformation were calculated for the following cases -

a) $CuAl_2$ at 460°C. ....11.3 t.s.i.

b) Aluminium saturated with copper ($2\frac{1}{2}$%) at 460°C. ....0.96 t.s.i.

c) $MgZn_2$ at 420°C. ....5.7 t.s.i

4.13 Hot torsion testing

The use of the hot torsion test as a means of assessing hot workability has received a lot of attention in recent years. In this study the test was used to study structural changes in the alloy 2024 but was soon replaced by the hot compression test as insufficient ductility could be obtained from the alloy in the cast state to make the test useful. However, the results obtained did provide some useful information with regard to the relationships between strength and ductility and temperature. Fig. 116 shows the effect of temperature on ductility in both the as cast and homogenized conditions. In these specimens the homogenization was followed by air cooling. The precipitation effects during and after cooling are responsible for the greater strength of the homogenized material. The influence of temperature on strength is shown in Fig. 117 (compared with the results of Field and

Backofen[54]) where the torque at failure is plotted against temperature for both as cast and homogenized conditions. It can be seen in this plot that there is a rapid decrease in strength at temperatures above 250°C. If the data is re-plotted as the logarithm of torque at fracture against temperature, it can be seen in Fig. 118 that the relationship now assumes one in which a straight line undergoes an inflexion at a certain temperature.

The temperature ductility curve shown in Fig. 116 exhibits a maximum in the region of 400°C. for the as cast condition, and about 460°C. in the homogenized condition. This is of interest as the hot working temperature for this alloy is in the region of 460°C. At temperatures above this the ductility decreases rapidly, becoming zero at about 500°C. The liquidus for this alloy is 502°C.

Samples prepared for metallographic examination show that for temperatures below the inflexion point in the plot of the logarithm of fracture torque vs. temperature, extensive fracture and break up intermetallics takes place, as seen in Fig. 119 for a $CuAl_2$ particle. Above this temperature fracturing becomes far less evident.

5. DISCUSSION

5.1 Casting Trials

A satisfactory casting technique was developed, applying the theory of solidification of long freezing range alloys. This technique involved the use of a good degassing practice, the suppression of super heat, and the use of a casting practice which set up thermal gradients in the casting favourable to mass feeding. Only when sound material could be cast was it possible to continue the investigation of the hot working characteristics of aluminium alloys.

5.2 The investigation of slab temperature variation during rolling by experimental temperature measurement

The curves in Fig. 11 show the relationship between temperature and thickness during the hot rolling of a number of slabs. The figure illustrates the point that temperature only begins to drop significantly when the slab thickness is reduced to about two inches or less. The thinner the slab the greater the cooling rate. This implies the expected result that the rate of heat loss is largely dependent on the surface area of the slab. Since all the forms of heat loss in hot rolling are related to surface area - i.e.

i) Radiation losses

ii) Convection losses

iii) Heat losses to the rolls

iv) Heat losses to the roll coolant

and the only source of heat input is from the energy of deformation, it is a logical argument that in the later stages of rolling where the surface area increases rapidly, with each pass, heat losses soon reach a magnitude whereby they cannot be compensated for by the heat input due to deformation despite the fact that this heat input increases steadily through the pass schedule. The rapid growth of surface area can be seen in Fig. 120 which shows the total surface area plotted against thickness for a commercially rolled slab of initial dimensions 12" x 36" x 120". It is of interest that in the work of Kasz and Varley[85] it was reported that temperature drop only became rapid at thicknesses of about ½".

The shape of the cooling curves are very similar to that reported by Von Zeerleder[86] which is also seen in Fig. 11. Von Zeerleder's curve is one of the very few to be found in published literature. The shape of the cooling curves will be dealt with in a later section dealing with calculated cooling curves. (Sec. 5.7)

5.3 The Calculation of Energy Curves in Hot Rolling

The energy curves for a number of commercial alloys were calculated directly from measured values of motor current and voltage and from data relating to rolling speeds and pass reductions etc. For greatest accuracy, an allowance should be made in the calculations for frictional effects in the bearings of the work rolls, and energy losses due to friction in the mill gear box etc. In modern rolling mills with taper roller bearings, frictional losses in the bearings will be small, and to simplify the calculations these losses were assumed to be constant at each pass so that they could be compensated for more easily. The mean horse power consumed in any pass, except for levelling and sealing passes at the start of a schedule and the finishing passes at the end, were fairly constant (this is expected if a pass schedule is designed to give the same rolling load at each pass i.e. a rational rolling schedule) and therefore frictional conditions in the bearings should be similar in all passes. If the rolling load varies widely, then frictional consumption of energy will also vary.

From the mill motor chart (see Fig. 4) the mean values of roll speed, motor current, and voltage are determined. Mean values are necessary, as these parameters vary from the start to the finish of a pass. From the mean current and voltage, the mean horse power developed by the mill motor in each pass is calculated as shown below.

Mean energy consumed per pass = Mean current x mean voltage = watts

$$\text{Therefore mean horse power} = \frac{\text{Mean Watts}}{746}$$

$$\text{Mean time to complete any pass} = \frac{\text{length of slab (ft)}}{\text{mean rolling speed (ft/min)}} = \text{mins.}$$

Output for any pass for continuous rolling

$$= \frac{\text{Slab weight x 60}}{\text{mean rolling time}} = \text{tons/hour}$$

$$\text{Therefore the mean energy consumed per pass} = \frac{\text{Mean H.P.}}{\text{"continuous rolling" output}}$$

$$= \text{H.P. hrs/ton}$$

The value for energy consumption in H.P. hrs/ton is calculated for every pass in the schedule, and the individual values are added together in a cumulative manner. The cumulative units of energy consumption are then plotted linearly against the logarithm of the exit thicknesses for all the passes in the schedule. The resultant energy curves are shown in Figs.13 - 15.

Energy curves have been used to calculate rolling schedules based on the hypothesis that from a curve for a given material the cumulative energy values will be the same whatever the individual pass reductions may be. However, this hypothesis is not strictly true, but nevertheless the curves do provide a convenient visual representation of energy consumption during rolling. Figs. 13 - 15 show energy curves for a range of commercial aluminium alloys in which the shape of the curve can be used to divide the alloys into two general groups. These two groups are often referred to amongst hot rolling operatives as "soft" and "strong" alloys, these terms being derived from the behaviour in hot rolling. The soft alloys exhibit a power curve with an exponential type shape (see Fig. 14) and examples of these alloys are -

i) Commercial purity aluminium

ii) Aluminium $1\frac{1}{4}$% manganese

iii) Aluminium $2\frac{1}{4}$% magnesium

The strong alloys are the highly alloyed materials commonly used for the production of aircraft plate. These alloys have an energy curve with a basically exponential shape but with a distinct "hump" occurring during the early stages of rolling (see Figs. 13 and 15). Examples of the strong alloys are -

i) H.15

ii) D.T.D. 683

Since the factors controlling the development of the "hump" were unknown, the initial objectives of the project were to discover its origin and significance. The significance of the hump is more clearly seen if the slope of the energy curve is plotted against the logarithm of the percentage reduction, instead of cumulative energy consumption against the logarithm of exit thickness. Such plots are shown in Fig. 121. The two groups of alloys are now very clearly divided into one group with an exponential shape to the curve (the soft alloys), and one group with an almost parabolic shape to the curve (the strong alloys).

Since the plot of the slope of the energy curves results in a series of curves showing the change in energy requirements during rolling, it can be said that the soft alloys have an almost constant resistance to deformation during rolling with a very large increase in energy requirements when the slab is reduced to below two inches in thickness. This is to be expected since it has been shown that below two inches in thickness, the temperature of the slab drops rapidly, and therefore the resistance to deformation will rise. Also there will be an increase in the resistance to flow in the roll gap at thinner gauges, due to frictional effects (as the so called "dead zones" approach each other.) For the strong alloys, there is the unexpected result that in the initial stages of deformation, the material has a high resistance to deformation which drops rapidly in the first few passes, assumes a fairly steady value, and then increases rapidly below about two inches in thickness in the same way as the soft alloys, due to the drop in temperature.

Since samples cannot be cut from the rolling slabs during the early stages of rolling because of power limitations in the shear, metallographic examination is not possible as a means of investigating this first stage. However, the hot compression test can be used for simulating these early stages, and the micrographs shown in Figs. 44-49 are most revealing. The micrographs show that at the beginning of the rolling schedule, the structure consists of a cellular network of intermetallics, and that during the first 15-20% hot reduction in H.15 and 20-25% reduction in D.T.D.683, the network is broken down. At the end of this stage, the network is destroyed and further reduction only results in some refinement of the intermetallic particle size. These two observations, i.e. the fact that power requirements fall in the first 20% reduction, and the intermetallic network is broken down in the first 20% reduction (from hot compression), indicate that the intermetallics have an important influence on hot working behaviour.

Since the soft alloys also contain some intermetallic, the size, proportion, distribution and properties of the intermetallics must be the key to the difference in hot working behaviour of the two groups of alloys, or all alloys would show the hump to a lesser or greater extent.

5.4. The influence of intermetallic morphology on hot working behaviour

Since both soft and strong aluminium alloys contain intermetallic compounds, and since the distinguishing feature of cast strong alloys is a well developed cellular structure of intermetallics, a series of casts were produced in the laboratory which had this form of structure, and their hot strengths were compared with alloys with a different intermetallic structure but with the same composition. The alloy H.15 shows the hump very clearly, and at the rolling temperature, the predominant phase in the network is $CuAl_2$ and so samples were prepared of aluminium 8% copper alloy which had a very similar structure to the cast H.15 alloy.

Samples prepared from sand cast material had a cellular structure, whilst samples that were chill cast had a more uniform distribution as can be seen in Figs. 108 and 103. Also samples of both casts were hot rolled to break up the intermetallic structure as seen in Figs. 110 and 106. The load contraction diagrams for these alloy structure variations are shown in Fig.104, and it can be clearly seen that the coarse cellular structure of the sand cast alloy is stronger than the more uniform structure of the chill cast alloy. The figure also shows that hot rolling which breaks up the cast intermetallic networks lowers the strength in both cases. An interesting observation is that the hot rolled sand cast alloy is weaker than the chill cast alloy initially, but becomes stronger as deformation proceeds, until their strengths are similar. This may be connected with the fact that the sand cast - hot rolled alloy still contains some large particles of eutectic which cause the increase in strength later in deformation during compression as they are broken down. All the compression tests were repeated in triplicate on these structures, and in all cases the order of strength was the same, and in all four structures the level of strength exhibited converged at the higher ranges of deformation. This suggests that the structure is important in the early stages of deformation in governing strength, but when the structure becomes broken down, all the structure variations approach the same level of strength and so structure loses its influence on strength.

Because there was a variation in grain size in the above samples (some structures were produced by sand casting, and some by chill casting) the influence of grain size was investigated by comparing the hot strength of two alloys of the same composition, produced under the same conditions of melting and casting, but with largely differing grain sizes produced by the addition of a grain refiner to one sample but not the other. The structures of these samples are shown in Figs. 111, 112, 114 and 115, and the load contraction diagrams are shown in Fig. 113.

It can be seen that the grain refined sample has a grain size many times smaller than the sand casting, without grain refining. Both samples exhibit a cellular intermetallic structure consistent with the slow cooling rate of sand casting, and it is expected from theoretical considerations that the size of the particles will be the same. This is because the particle size is regulated by the dendrite arm spacing, which in turn is a function of cooling rate; the faster the cooling rate, the smaller the dendrite arm spacing. Since both samples were cast under similar conditions, into a mould of the same dimensions and material, from an alloy of the same composition, the particle size should be the same. However, the casting temperature of the grain refined melt was slightly lower than that of the melt without grain refiner and so the cooling rate of the grain refined cast was probably slightly faster. The micrographs exaggerate the difference in particle size because the grain refinement also produces some refinement of the network size (aided by the slightly faster cooling rate) which gives the impression of a finer particle size.

The difference in the network size is fortuitous when the load contraction diagrams are referred to in Fig. 113. These show that there is a significantly higher level of strength in the coarse grained material over that of the grain refined material. Hence it has been shown that a relatively small increase in the size of the cellular $CuAl_2$ network has more effect on hot strength than a very large reduction in grain size (the smaller grain size would be expected to have the higher strength).

To investigate the contribution to hot strength caused by the presence of $CuAl_2$ particles irrespective of their size and distribution, the hot strength of an alloy containing $2\frac{1}{2}\%$ copper was measured. At the temperature used for hot compression, ($460^{o}C.$) the solubility of copper in aluminium is $2\frac{1}{2}\%$ so that these samples consisted of an aluminium solid solution saturated with copper. Therefore, the difference between the hot strength of this alloy and the casts containing 8% copper is due to the presence of the $CuAl_2$ particles, as in all these cases the matrix is saturated with copper. The load contraction diagrams in Fig. 122 shows the quite considerable contribution to hot strength due to the particles.

5.5 Hot Strength Measurements on Intermetallic Compounds

Having shown the important contribution to hot strength provided by intermetallic particles, it became important to measure the strength and deformation characteristics of some intermetallics in order to further develop the argument that these phases have an important influence on hot working.

5.5.1 Hot Strength Measurements on pure $CuAl_2$

The effects of deformation at elevated temperature on this phase are shown in Figs. 90 and 91 and the load contraction diagrams are shown in Fig. 92. These figures show that the phase has considerable strength at temperature, and also a remarkable ability to deform plastically. The sample deformed at 460°C. shows some cracking at one edge, but this was due mainly to splinters breaking away from the edge as a result of cracks already present in the area resulting from contraction stresses which developed during the solidification of the phase, and not from deformation. This was borne out by the observation that some of the splinters were longer than the upset length of the compression slug, indicating that they originated at an early stage of deformation. Also the load contraction diagram shows a dip at the very onset of plastic deformation indicating that splintering took place here.

5.5.2 Hot Strength Measurements on Aluminium 40% copper alloy

Because of the extreme brittleness of pure $CuAl_2$ and its tendency to crack during solidification, even with the slowest of cooling rates, an alloy containing 80% by weight of $CuAl_2$ was cast. In this alloy, the $CuAl_2$ is surrounded by a eutectic containing $CuAl_2$ and an alpha solid solution. This soft component in the eutectic provides a means for the large needles of primary $CuAl_2$ to relieve their contraction stresses and so samples can be made crack free. The deformation characteristics of an alloy with a large volume fraction of intermetallic are virtually the same as the pure intermetallic, and so the composite can be used to further investigate the influence of temperature on the plasticity of $CuAl_2$.

The photograph in Fig. 93 shows the remarkable plasticity of the composite at elevated temperatures, and its brittleness at low temperatures. This is further illustrated in Figs. 95 and 96. The important features then of these results are that the phase is plastic at elevated temperatures (including the range used for hot rolling alloys containing $CuAl_2$) and brittle at low temperatures. The difference in strength between the phase $CuAl_2$ and the matrix of aluminium saturated with copper at the hot rolling temperature of 460°C. helps to illustrate the strengthening effect of the intermetallics since the solid solution has a flow stress of only 0.96 t.s.i., and the $CuAl_2$ has a flow stress of 11.3 t.s.i. The explanation of the origin of the hump in strong aluminium alloy energy curves can now be made as follows.

In the alloy H.15 the predominant phase at the hot rolling temperature is $CuAl_2$. This phase is present in a coarse cellular network, and at the rolling temperature the phase is able to sustain plastic deformation. Also at the working temperature, The $CuAl_2$ is much stronger than the matrix, so that when deformation begins in rolling, the matrix begins to flow but meets considerable resistance due to the stiff intermetallic network. Since the $CuAl_2$ is plastic at the working temperature, the network is broken down by plastic deformation (i.e. necking and not fracture) during the first 15/20% reduction producing no signs of fracture in the $CuAl_2$. Once the network has been destroyed, the alloy offers less resistance to flow, and further deformation only leads to some refinement and re-distribution of the $CuAl_2$ particles.

From hot strength measurements on the 8% copper alloy, it appears that only the coarse networks of intermetallic cause a serious disturbance of flow resulting in increased strength. Therefore the hump in the energy curve for H.15, which represents a region where resistance to deformation is higher than expected, can be said to be due to this mechanism. This is supported by the series of micrographs in Figs. 44-49 which show the break up of the network in cast H.15 during the first 15-20% hot compression.

5.5.3 Hot Strength Measurements on pure $MgZn_2$

The plastic nature of this phase can be seen in Figs. 99 and 100 and its load contraction diagram in Fig. 101. From these figures, it can be seen that the phase behaves in a very similar manner to $CuAl_2$, being brittle at low temperatures and plastic at elevated temperatures.

A commercial high strength aluminium alloy which contains this phase is D.T.D. 683. This alloy also shows the humped effect in its energy curve like H.15, but to a lesser degree. The explanation for this effect is as follows. The alloy D.T.D. 683 is rolled at a lower temperature than H.15, (400-420°C. instead of 450-470°C.) and contains elements that are more soluble in the matrix, so that there will be less intermetallic in the network at the rolling temperature, and the matrix will be stronger. Also, the phase $MgZn_2$ is weaker at the rolling temperature of the alloy than $CuAl_2$; $MgZn_2$ having a flow stress of 5.7 t.s.i. compared with 11.3 t.s.i. for $CuAl_2$ at the respective rolling temperatures for the two alloys. Therefore, because the network occupies a smaller volume fraction, it will disturb flow to a lesser degree, and because the relative difference in strength between the matrix and the intermetallic is much less for $MgZn_2$ than $CuAl_2$, the energy requirements to destroy the network will be proportionately less. Therefore, although the hump appears in the energy curve, it will be less well developed as shown in Fig. 14. The destruction of the network observed metallographically in H.15 is also observed in D.T.D. 683 (see Figs. 67-71)but is by no means as obvious.

5.5.4 Hot Strength Measurements on Aluminium 32% iron alloy

The ability of this phase to deform plasticallyis shown in Fig. 97 and its load contraction diagrams for a range of temperatures are shown in Fig. 98. From these results, it can be seen that the phase does not undergo a transition in plasticity with temperature rise like $CuAl_2$ and $MgZn_2$. The results indicate that strength diminishes with temperature, and if the percentage reduction in height is calculated for the compression slugs shown in Fig. 97, then they are found to drop from 12% at room temperature to 3% at 500°C. This reduction in height is the amount of deformation which takes place before severe cracking occurs (indicated by a rapid drop in load on the load contraction diagram).

The reason for this apparent drop in plasticity with temperature is that the $FeAl_3$ forms in irregular needles, and since the phase is very brittle and susceptible to brittle fracture by stress concentration, it follows that as the temperature is raised the matrix softens and its load bearing capacity falls. The load is then transferred to the needles of $FeAl_3$ which due to stress concentration (resulting from the irregular shape of the needles) fail by brittle fracture leading to failure of the whole sample. Hence the load bearing ability of this phase appears to be very low.

In the commercial alloy N. 4 a major proportion of the intermetallics present is the phase $FeAl_3$ due to iron impurities, particularly if the silicon content is low. Hence because of the small volume fraction present, the needle like morphology of the particles, and the poor load bearing capacity and therefore low strength, the distribution of this phase (not a well formed cellular network) does not offer much resistance to flow and is easily broken down with low energy requirements, so that no hump appears in the energy curve.

Hence the absence of a hump in the energy curve can be accounted for by any one or more of the following factors.

i) The volume fraction of intermetallics is low.

ii) If intermetallics are present they have poor load bearing properties.

iii) Associated with the load bearing properties is probably a high inflexion temperature, i.e. the temperature where the phase begins to show some plasticity. The inflexion temperature of $FeAl_3$ is reported to be 460°C. and for $MnAl_6$ 400°C.[79]

Therefore, due to the factors listed above the soft alloys do not exhibit the hump in their energy curves. For example, commercially pure aluminium contains a relatively small volume fraction of intermetallics based on iron and silicon (similarly with N.4) while for the $1\frac{1}{4}$% manganese alloy most of the phase $MnAl_6$ will be in solution at the working temperature, but the phase has a high inflexion temperature anyway. Hence none of these alloys will be expected to show a hump in their energy curves.

The brittleness of $FeAl_3$ during the hot rolling of N.4 is shown in Fig. 78. The brittleness of another phase c-Al(Mn, Fe)Si which forms in H.15 can be seen in Fig. 74 (which also shows the plasticity of $CuAl_2$ which appears fracture free) and in Fig. 79. A good indication of whether a phase will be brittle at high temperature is its room temperature micro hardness. If this is high then the inflexion temperature will probably be high, although there are some exceptions to this (e.g. $NiAl_3$, room temperature hardness = 950 vpn, inflexion temperature = 290°C.). If the inflexion temperature is high, there is a strong possibility that it will be outside the commercial hot working temperature for the alloy containing it, or very close to it, in either case the phase will probably behave in a brittle manner.

5.6 A Comparison of Hot Rolled Structures and Structures produced by Hot Compression in Simulated Rolling Schedules

Commercial rolling schedules were simulated using hot compression, and the structures produced were compared with rolled structures for points of similarity. The simulation appeared good for two alloys where a direct comparison was possible.

5.6.1 A Comparison of Rolled and Compressed Structures in H.15

The series of micrographs shown in Figs. 18-33 illustrate the hot rolled structures of a commercially rolled slab over a range of reductions from 68% to 93%. In the micrographs in Figs. 40-49 are shown the structures produced by hot compression, using simulated rolling schedules. Both series of micrographs show that the initial cast grains are progressively elongated without any clear indication of recrystallisation taking place. The contrast between grains in the commercial alloy is better than the compression samples probably because the samples were cooled from the rolling temperature more slowly, and because the commercial alloy had a lower magnesium content. The shape of the grains in the compression samples appears to lie half way between the shape produced in the longitudinal and transverse directions by commercial rolling. This effect is due to the absence of any lateral restraint in compression, and the situation in rolling where there is almost complete restraint in the transverse direction, with all the deformation taking place in the longitudinal and short transverse directions.

The two series of micrographs also show the break down of the intermetallics, from a network structure to a highly directional structure of particles and stringers. To get the degree of similarity of structure shown in the two series of micrographs, it is necessary to pay careful attention to homogenization treatments and preheats so that the simulation embraces these variables as well as the temperatures and reductions etc. of the schedule itself.

5.6.2 A Comparison of Rolled and Compressed Structures in N.4

The series of micrographs shown in Figs. 34-39 show the structures produced over a series of reductions of 68.6% to

94.5% in commercially hot rolled material. The structures illustrated in Figs. 50-61 are produced by hot compression simulating a commercial schedule. Both series of micrographs show a very strong similarity in structure. The specimens used for examination of the rolling structures were cut from the transverse direction. Again it appears as though little or no recrystallisation has taken place. The simulation of structure appeared in this case to be even better than for H.15, but again care is needed in simulating the thermal treatments.

5.6.3 Hot Compression Structures of D.T.D. 683

The structures produced by hot compression of this alloy are shown in Figs. 62-71. In this case no commercially hot rolled samples are available for comparison purposes, but the structures appear to be very similar to those shown by the commercially rolled H.15 alloy, which has a similar rolling schedule.

5.7 The Calculation of the Temperature Variation of a Rolling Slab during Hot Rolling

The derivation of the equations used for calculating the temperature of a rolling slab at any stage of its rolling schedule will be shown below, and any assumptions required will be stated and justified. The sources of heat loss or heat generation in the rolling slab will be dealt with individually.

5.7.1 Convective Heat Losses

From the basic theory of heat flow, two dimensionless parameters used in the analysis of problems concerning convective heat flow and fluid mechanics are -

Grashof number $= \dfrac{\alpha g \theta D^3}{\nu^2} = Gr$ .... (1)

Prandtl number $= \dfrac{C_p \rho \nu}{K} = Pr$ .... (2)

For all diatomic gases, and carbon dioxide the Prandtl number

$Pr = 0.74.$

For conditions of convective streamlined flow, a third dimensionless number, the Nusselt number, is expressed as follows -

$$Nu = \gamma_s (Gr \, . \, Pr)^{0.25}$$

and for turbulent convective flow this parameter is expressed as follows -

$$Nu = \gamma_t (Gr \, . \, Pr)^{0.33}$$

The terms γ_s, γ_t are constants whose values vary for different geometric shapes, and positions of these shapes relative to the direction of flow of the convective fluid.

5.7.1.1 Rate of Heat Loss in Streamlined Flow

The rate of heat loss in streamlined convection is as follows.

$$Nu = \gamma_s (Gr \,.\, Pr)^{0.25} \qquad Pr = 0.74$$

$$\therefore Nu = \frac{HD}{\theta K} = \gamma_s (Gr \,.\, Pr)^{0.25}$$

$$H_s = \frac{\gamma_s (0.74\, Gr)^{0.25}\, K\theta}{D}$$

$$= \frac{\gamma_s K (0.74)^{0.25} \left(\frac{ag\theta D^3}{\upsilon^2}\right)^{0.25} \theta}{D}$$

$$\therefore H_s = \underline{\underline{\gamma_s K (0.74)^{0.25} \left(\frac{ag}{\upsilon^2}\right)^{0.25} \theta^{1.25} D^{-0.25}}} \; . \; . \; . \; . \; (3)$$

5.7.1.2 Rate of Heat Loss in Turbulent Flow

The rate of heat loss in turbulent convection is as follows.

$$Nu = \frac{HD}{K\theta} = \gamma_t (Gr \,.\, Pr)^{0.33}$$

$$HD = \gamma_t (Gr \,.\, Pr)^{0.33}\, K\theta$$

$$H_t = \frac{\gamma_t (0.74)^{0.33} \left(\frac{ag\theta D^3}{\upsilon^2}\right)^{0.33} K\theta}{D}$$

$$\therefore H_t = \underline{\underline{K\gamma_t (0.74)^{0.33} \left(\frac{ag}{\upsilon^2}\right)^{0.33} \theta^{1.33}}} \; . \; . \; . \; . \; (4)$$

Substituting into equations (3) and (4) for the constants, using values for large vertical surfaces of irregular shape, the following expressions are arrived at.

$$Hs = 1{\cdot}03 \times 10^{-4} \times D^{-0{\cdot}25} \times \theta^{1{\cdot}25} \quad \text{Cals./sq.cm/sec.}\ldots\ldots\ldots(5)$$

$$Ht = 2{\cdot}7 \times 10^{-5} \times \theta^{1{\cdot}33} \quad \text{Cals./sq.cm/sec.}\ldots\ldots\ldots(6)$$

At the point where the term log. (Gr.Pr) reaches a value of approximately 9, the conditions of flow in a convective air stream flowing over a heated body, changes from streamline to turbulent, i.e. when $Gr.Pr = 10^9$.[88] From this experimental observation, a useful empiric approximation can be used to determine if conditions are streamline or turbulent in a particular problem. The approximation is that the value of GrPr can be estimated knowing the size of the hot body, and the mean temperature difference between the hot body and the convective stream. The mean temperature difference is given as follows.

Mean temperature difference for any given period of cooling (or heating) $= \dfrac{(Ts - Ta) + (Tf - Ta)}{2} = \theta$

Ts = The temperature of the hot body at the start of the cooling period.

Tf = The temperature of the hot body at the end of the cooling period.

Ta = Ambient temperature i.e. the temperature of the air surrounding a hot body as it cools.

The value of Ts will almost certainly be known in any problem, but the value of Tf may not. In such a case, it is sufficient to estimate its value by consideration of the problem, in conjunction with any experience obtained on similar problems. The estimate of the value of GrPr can now be made from the following equation.

$$\mathrm{GrPr} = 10^2 D^3 \theta \qquad \ldots\ldots\ldots(7)$$

For the problem under consideration, i.e. a rolling slab, it can be assumed that for a slab of N.4 the starting temperature is 480°C. (the hot rolling temperature) and that during rolling it falls to 300°C., by the end of the schedule which is probably somewhat lower than the actual finishing temperature, which for the moment we assume cannot be measured. If it is also assumed that the dimensions of the slab are much greater in width and length than in thickness, which is perfectly reasonable particularly towards the later stages of rolling, (thus we are determining the flow conditions over the large flat surfaces of the slab, neglecting the edges) and that the slab measures 60" x 60" (i.e. approx. 150 cm.sq.), the mean temperature difference between the slab and the surrounding air is $\frac{(480-20) + (300-20)}{2} = 370°\mathrm{C}$.

Substituting into equation (7)

$$\mathrm{Gr.Pr} = 10^2 \times 370 \times (150)^3$$

$$= 10^6 \times 370 \times 3{\cdot}37 \times 10^6$$

$$= \underline{1{\cdot}2 \times 10^{11} > 10^9}$$

Therefore conditions are turbulent for the convective flow conditions around the rolling slab. This means that equation (6) must be used to calculate the convective heat losses from the slab. However, equation (6) should strictly speaking, be used for large vertical surfaces, whereas a rolling slab has its largest area in the horizontal plane.

Corrections to equation (6) for the orientation of the surface can be made in the following way. For a horizontal plate, the heat losses from the upward facing surface are about 30% greater than for a vertical surface, and for the downward facing surface, they are about 35% less. Since this only gives an overall difference of 5%, and since there is some side area (which is vertical) for which the equation applies directly, no adjustment will be made to the equation. These correction factors are available from a number of published sources, e.g. ref. 69.

Another correction will also be necessary to equation (6) since this equation is derived for natural convective conditions. The correction is necessary since the slab will be moving during rolling, and so equation (6) is likely to severely underestimate the heat losses. It is possible to obtain a correction factor by reference to published data[70], provided the relative velocity between the air current and the hot body is known. In this case it is the rolling speed, which for simplicity is assumed to remain constant at 200 f.p.m. Under these conditions heat will be lost by forced convection at a rate approximately 1.7 times faster than under natural convective conditions; equation (6) now becomes -

$$Ht = 1{\cdot}7 \times 2{\cdot}7 \times 10^{-5}\,\theta^{1\cdot33} \quad \text{Cals./sq.cm/sec.}$$

$$= 4{\cdot}59 \times 10^{-5}\,\theta^{1\cdot33} \quad \text{Cals./sq.cm/sec.}$$

5.7.2 Radiation Heat Losses

The heat losses due to radiation from a hot body obey the Stefan-Boltzmann law of radiation. From this law the following equation has been developed.

$$H = E\,\sigma\,(T1^4 - T2^4) \qquad \text{Cals./sq.cm/sec.}$$

Assuming the value for emmisivity for aluminium is 0.15 (from published values[68]), the conductivity of aluminium is 0.260 cal/cm/sec/°C. (also from published data,[68]) and equating radiated heat loss to the heat lost by the slab, the temperature drop of a plate of any size, in any time, at any temperature, due to radiation is given by the following expression.

$$\text{Temp. drop} = \frac{0{\cdot}15 \times 1{\cdot}36 \times 10^{-12} \times A \times t_p \times (T_1^{\,4} - T_2^{\,4})}{M \times C_p.}$$

$$= \frac{0{\cdot}205 \times 10^{-12} \times A \times t_p \times (T_1^{\,4} - T_2^{\,4})}{0{\cdot}26 \times M}$$

5.7.3 Heat Losses at the Roll Face

The two major heat losses at the roll face are as follows.

a) Heat conducted into the rolls

b) Heat taken away by spillage of lubricant-coolant onto the hot slab.

Due to the good contact between the rolls and the slab in hot rolling, (a) is probably greater than (b) and since it is almost impossible to determine the interface conditions between the slab and the coolant, and also difficult to determine the proportion of coolant flow which comes into contact with the slab surface, the dwell time of the coolant on the slab surface, and the proportion boiled off as steam, some empiric or assumed allowance must be made for this heat loss. In the case being considered, the amount of heat lost to the coolant is assumed to be of the same order as the heat lost by convection. In both cases the most important factor affecting the degree of heat loss is the surface area of the rolling blank, so that heat losses due to the two heat sinks discussed above will both increase proportionately during rolling. Therefore, the heat loss allocated to the coolant will be said to be equal to the heat loss by convection.

The problem of determining the heat losses to the rolls lies in defining the conditions for heat transfer and the value for the heat transfer coefficient. From the work of Kutateladze and Borishanski[71] an equation for the thermal resistance for heat flowing from a hot plate into a semi-infinite cooler plate is given by the following expression.

$$R = \frac{1}{\pi k^{\circ}} \ln \frac{4a}{b}$$

Therefore, assuming that the conditions in hot rolling, where a hot slab, which is small in comparison with the rolls, (particularly towards the end of rolling) approximates to the above hypothetical conditions, the thermal resistance for one square centimetre of plate is as follows.

$$R = \frac{1}{3{\cdot}142 \times 0{\cdot}14} \ln 4$$

$$= \underline{3{\cdot}142}$$

Also from the work of Kutateladze and Borishanski, the rate of heat transfer can be calculated from this value of thermal resistance.

Rate of heat transfer = $\frac{t_i - t_o}{R} = \frac{420}{3.14}$ = 134 Cals./sq.cm/sec.

This value for the rate of heat transfer, applies for a slab whose mean rolling temperature is 420°C. A different value will have to be calculated if the mean rolling temperature varies. The mean rolling temperature is taken as the mathematical mean of the starting temperature minus the ambient temperature and the finishing temperature minus the ambient temperature.

The temperature drop per pass can now be calculated from the rate of heat transfer given above, the contact area between the rolls and the slab (calculated from the roll dimensions, the slab dimensions, and the size of the pass) and the length of time taken to complete the pass as shown below.

$$\text{TEMP DROP } \Delta T = \frac{q \times A_c \times t}{M \times C_p}$$

5.7.4 Heat gained by the Slab due to Deformation

Since a very large proportion of the energy actually expended in producing deformation is converted into heat, the amount of heat generated within the slab per pass, can be calculated from the current and voltage measured across the mill motor at each pass. However, the electrical energy is also consumed in each pass in overcoming the following losses.

a) Friction in the roll bearings

b) Friction in the mill gear box

c) Inertia of the rolls in each pass (reversing mill)

The measurements needed to allow the calculations to be made for predicting the temperature of a rolling slab were made on a mill of very modern design, but in spite of this such losses will still be significant. For example, the weight of the gears and rolls which have to be stopped and reversed at every pass is in excess of 400 tons.

The energy consumed in the roll bearings can be quite a large proportion of the total. In an example given by Larke[89] the energy consumed by roller bearings and bronze bearings for the same rolling schedule were respectively a maximum of 21% and 84% of the total energy consumed in a particular pass. Because of these losses it was assumed that the energy losses plus the energy of deformation not converted into heat was equal to an average of 40% of the total energy expended on every pass. The calculation of heat input was then as follows.

ENERGY OF ROLLING PER UNIT MASS

$$= \frac{F \times 550 \times E \times I}{746 \times Q} = \text{ft lbs/lb.}$$

778 ft lbs = 1 B.Th.U.

$$= \frac{0\cdot6 \times 550 \times E \times I}{746 \times Q \times 778} = \text{B.Th.U}/\text{lb}$$

$$= \frac{252 \times 0\cdot6 \times E \times I}{746 \times Q \times 778 \times 454} = \text{Cals}/\text{gm.}$$

$$\therefore \text{TEMPERATURE DROP} \quad \Delta T = \frac{252 \times 0\cdot6 \times 550 \times E \times I}{746 \times Q \times 778 \times 454 \times C_p}$$

5.7.5 The Estimation of Slab Surface Area and Pass Time

In calculating the heat losses due to radiation and convection, it is necessary to know the following.

a) The area of the slab loosing heat at each pass.

b) The time over which heat is lost at each pass.

In this study, a pass was considered to be that element of rolling which takes place between the slab entering the roll gap on one side of the mill, the actual reduction, and the period before the slab re-enters the roll gap on the other side of the mill. By this definition, the slab has two areas; the exit area, and the entry area for each pass. Since the slab spends more time on the exit side per pass by this definition, a weighted average was taken for each pass in which the pass area was said to be two thirds the exit area plus one third the entry area. Total areas were calculated using combined face and edge areas.

The time taken for each pass was calculated from the length of the slab and the rolling speed, which gives the time to effect the reduction, and added to this is a period of six seconds which is the mean time taken to stop the slab, and reverse it, ready for the next reduction. This period was arrived at by consulting a report[90] containing data concerning the elemental times for the rolling of slabs of the type and dimensions used in these calculations. The data in the report was collected from the same mill used for this study.

The temperature variations of three slabs of different composition were calculated from the above equations and the results can be seen in Fig. 123 together with the measured starting and finishing temperatures. The calculated finishing temperatures were extremely close to the measured finishing temperatures as shown below in Table 28, indicating that the method is valid, accurate, and the assumptions on which it is based are reasonable.

Alloy	Calculated finishing temp.	Measured finishing temp.
99% Al	444°C.	440°C.
Al - $1\frac{1}{4}$% Mn.	435°C.	440°C.
Al - $2\frac{1}{4}$% Mg.	434°C.	435°C.

Table 28 - Showing the calculated and measured finishing temperatures for three commercial aluminium alloys.

The validity of the method is further shown in Fig. 124, which compares a calculated temperature variation curve with a measured one, for the aluminium $2\frac{1}{4}\%$ magnesium alloy (N. 4). The comparison can be seen to be extremely good indeed.

6. CONCLUSIONS

6.1 The Simulation of Hot Rolling Structures

The use of an axi-symmetric hot compression test has been found to give structures very similar to those produced by commercial hot rolling. To achieve a good simulation, care must be taken in providing efficient lubrication, and in using the same pre-heats as those used in industrial fabrication practices. The hot compression test is experimentally simpler, and also less costly than hot torsion testing as a means of simulation. The simulated rolling schedules are particularly useful in studying structural changes early in rolling, when it is difficult to take representative samples from a rolling slab. This is because the slab is too thick to shear, and because if a partially rolled slab is allowed to cool, structural changes may take place giving unreliable results, apart from the high cost and wastage entailed by such a technique.

The simulated rolling schedules allowed a study to be made on the behaviour of intermetallics and certain distributions of intermetallic during the early stages of rolling. These experiments, in conjunction with another series of experiments in which the resistance to deformation of a number of different distributions of intermetallic were measured, showed that the resistance to flow of certain high strength alloys was unexpectedly high in the early stages of deformation, and dropped rapidly as deformation proceeded. These stages were then followed by an increase in the resistance to flow as a result of a decrease in the temperature of the slab. The initially high resistance to deformation was shown to be due to a function of both the volume fraction of intermetallic, the properties of the intermetallic, and also the size and distribution of the intermetallic network. Because of the high concentration of alloying elements in the strong aluminium alloys, and the mechanisms by which they solidify, they produce in industrial castings, a structure shown to be of a form that produces high initial resistance to deformation, and therefore the possibility of difficulties in hot working. Moreover, the properties of the intermetallics contained in these alloys are also favourable in producing an increase in strength in the hot working range. These properties are as follows -

a) The intermetallic possesses the ability to become plastic at the working temperature, and therefore deforms with the matrix consuming energy.

b) The intermetallic possesses considerably higher strength than the matrix at the rolling temperature, and therefore contributes more to hot strength than its relatively small volume fraction might be expected to.

c) Because in the high strength alloys the intermetallic has a high ~~coherency~~ bond strength with the matrix, (the basis of age hardening in these alloys) the necessity to maintain ~~coherence~~ high bond strength increases the effects due to (a) and (b)

In the group of so called soft aluminium alloys, which do not show any great difficulty in hot working in the early stages, these effects are not manifest. This is because -

a) The intermetallics do not in the main exhibit any plasticity in the hot working temperature range, and therefore fracture. Since brittle fracture consumes less energy than plastic deformation, this process has little effect on overall energy consumption during working.

b) The intermetallics although capable of high strength, do not exhibit this property because they lack the plasticity required to achieve it. These intermetallics frequently occur in the form of needles and plates, and like most brittle materials are very sensitive to the stress concentration produced by notches. Since the needles are often irregular in shape, the notches are inherent, and so little energy is required to fracture them.

c) The brittleness of these phases originates largely from their complex crystal structure. Since complex crystals generally have large lattice parameters, the parameters of the lattices of the brittle phases will probably be much larger than that of aluminium so that ~~coherency~~ bond strength will be weak. Hence ~~coherency~~ bonding strains are small and do not contribute much to the resistance to deformation. In the strong alloys, the phases (eg. $CuAl_2$ and $MgZn_2$) present are the ones which produce age hardening by the lattice strain associated with coherency, and so the lattice parameters will be similar to that of aluminium. Table 29 illustrates these points by listing the lattice parameters of the phases occurring in strong alloys and soft alloys (high ~~coherency~~ bond strength and low ~~coherency~~ bond strength respectively between the phase and the matrix).

A list of the major phases, generally accepted as being present in the alloys studied in this project[78] is shown below. Certain phases occurring in very small quantities and metastable phases are not included.

<u>N3</u> - <u>Al-Mn</u>
$MnAl_6$, $Al_6(Mn_x\ Fe_{1-x})$, α ((Al-Mn-Si)(Fe))

<u>N4</u> - <u>Al-Mg</u>
Al_3Fe, $Al_6\ Mn$, plus small quantities of $Al_3\ Mg_2$

H15 Al-Cu-Mn-Mg

Al_2Cu, Al_2CuMg, Al_6Mn, Al_5Mg_4Cu

DTD5050 Al-Zn-Mg-Cu

$MgZn_2$, $Al_2 Mg_3$, $CrAl_7$

1B 99.5%Al

Al_4Si_2Fe, (Al_7SiFe_2), $(Al_9Si_2Fe_2)$, Al_3Fe, $(Al_{12}Fe_3Si)$

The above list shows that the "soft" alloys contain phases which are brittle at the hot working temperature, i.e. those based on the transition metals and silicon, whilst the strong alloys contain phases that are plastic at the hot working temperature, e.g. Al_2CuMg, Al_2Cu, $MgZn_2$

It was also shown that the morphology of the intermetallics in strong alloys is extremely important in determining the resistance to deformation during the first 15-20% deformation. Cellular networks are effective in increasing resistance to flow. If these networks can be removed, then an improvement in workability might be expected.

Dendrite arm spacing has a large influence on the size of intermetallic particles, and the chief factor affecting the dendrite arm spacing is the rate of cooling during solidification.[91] It has been shown that for cooling rates beyond 500 degrees per minute, the cooling rate has very little effect on dendrite arm spacing. Increasing the cooling rate has a two-fold advantage of making the

Phase	Crystal system	Lattice constants			Type of alloy acting as host to phase
		a_1 kX	a_2 kX	a_3 kX	
$CuAl_2$	Tetragonal	6.052	-	4.878	Strong
Al_2CuMg	Orthorhombic	4.00	9.23	7.14	Strong
Mg_2Si	Cubic	6.391	-	-	Strong
$MgZn_2$	Hexagonal	5.15	-	-	Strong
c-Al(Fe, Mn)Si	Cubic	12.63	-	-	Soft
$FeAl_3$	Orthorhombic	48.04	15.59	8.10	Soft
Aluminium	f.c.c.	4.0946	-	-	

Table 29 - showing the lattice parameters of intermetallic phases found in soft and strong commercial alloys compared with the lattice parameter of aluminium.[93]

intermetallic particles progressively smaller in size and also preventing the formation of certain undesirable intermetallic compounds at borderline compositions such as plates of AlFeSi or plates and rhomboids of (Fe, Mn)Al_6 in H.15. Refinement of the macro grain size has no effect on the dendrite arm spacing or on the particle size of the intermetallics. Any increase in the cooling rate beyond 500 degrees per minute, has further little effect on micro-structure which suggests that once the cooling rate has been raised to this level, there is little to be gained in the direction of reducing the cell size and particle size of the intermetallics by cooling any faster.

Certain important observations have been made[92] in the aluminium - $CuAl_2$ eutectic system for binary alloys containing 2, 3, 4 and 5% copper at cooling rates of 6.0 - 3,000 degrees per minute. The effects of cooling rate on dendrite arm spacing was found to be in agreement with the above statements, indicating that 500 degrees per minute was the optimum. A very important observation was that the structure of cast aluminium copper alloys show a change from a linear arrangement of spherical divorced $CuAl_2$ particles at high rates of solidification to a cellular pattern in which $CuAl_2$ occurs in the normal eutectic at low rates of solidification. At a given rate of solidification, there is a greater tendency to form spheroids of divorced $CuAl_2$ particles the lower the copper concentration of the alloy, while higher copper concentrations favour a cellular structure. Hence it follows that if adjustments can be made to casting practice to attain a minimum cooling rate in a rolling slab of 500 degrees per minute, the undesireable cellular structure can be suppressed and replaced by a more uniform distribution of intermetallics. This should not only make hot working easier, but also produce less directionality in the final fabricated material.

Any section through the branches of a dendrite will have a cellular structure, in which the cells are outlined by the material that solidifies last. For a wide range of aluminium alloys including the following -

i) H.15 Al-Cu-Mg-Si
ii) D.T.D.683 Al-Zn-Mg-Cu
iii) N.6 Al-Mg.
iv) H.20 Al-Zn-Si-Cr

with size ranges of 5.5" - 20" in diameter for extrusion billets, and 6.5" x 20" - 10" x 36" for rolling slabs, cooling rates have been determined[91] by measuring the cell size at various points through the section of castings, and calculating the freezing rate from the freezing rate - cell size relationship. The results show that only in small castings i.e. extrusion billets of 5" diameter and less are freezing rates of 500 degrees per minute achieved or exceeded. For rolling slabs with dimensions of the order of 10" x 36" the maximum cooling rate anywhere in the cross section is not likely to exceed about 250 degrees per minute, and therefore it would appear that with the present methods of D.C. casting it is not possible to produce a slab without the cellular structure.

6.2 The Comparison of Calculated and Measured Slab Temperature Variations during Hot Rolling

The comparison made in Section 5.7.5 between the measured and calculated variation in temperature of a slab during hot rolling, showed that not only was the comparison good, but also that the method appears to be valid. This is important, as the knowledge of such a variation, and particularly a method of calculating it, is of fundamental importance in the study of hot workability of a material, and to the calculation of rolling schedules.

The important conclusions to be made from this section of the study are the need to temper enthusiasm for a purely theoretical solution to the problem, with the difficulties of determining the conditions of heat transfer. Because of the difficulties in this area, it is more practical to overcome the problem by using an approach with an empirical bias by substituting theoretical heat transfer conditions for conditions based largely on assumptions which must be justified by careful thought and analysis of the problem. Having constructed a model it is then necessary to test it by comparing predicted results with measured ones and only if the difference between the two sets of results is small can the model be said to have any validity.

6.3 The Properties of Intermetallic Phases

The series of experiments which investigated the deformation behaviour of intermetallics illustrated the following points -

a) That at least some intermetallics undergo a transformation at some temperature (the inflexion temperature) above which they possess the ability to deform plastically.

b) When an intermetallic has plasticity, it is able to exhibit mechanical strength, and at the hot working temperature range for aluminium alloys, this strength will probably be significantly greater than the aluminium matrix in most cases.

Therefore in a consideration of the hot working properties of aluminium alloys, it is not enough to regard the relatively small volume fraction of intermetallics as an inert collection of particles that may or may not deform during fabrication and which have little effect on workability. It has been shown that the properties of the particles (as well as their distribution) have a significant and measureable effect on workability. This was shown most clearly in the energy curves in Figs. 13, 14 and 15 where the presence of strong plastic second phase particles in relatively small amounts produces a hump in the curve, showing that more energy is used to break up and redistribute them than brittle phases which show no hump in the energy curve of alloys containing them.

6.4 The Increase in Hot Strength caused by the presence of a Second Phase

The presence of second phase particles in a continuous matrix phase results in localised internal stresses which modify the plastic properties of the continuous phase. Many factors must be considered for a complete understanding of strengthening from second phase particles. These factors include the size, number and distribution of the second phase particles, the strength, and ductility, of the matrix and second phase, the crystallographic fit between the phases and the interfacial energy and interfacial bonding between the phases. It is virtually impossible to vary these factors independently in experiments, and it is very difficult to measure many of these quantities with any degree of accuracy. Therefore, our existing knowledge of the effect of second phases on mechanical properties is largely empirical and incomplete.

In a multi-phase alloy, each phase contributes something to the overall properties of the aggregate. If the contributions from each phase are independent, then the properties of the multi-phase alloy will be a weighted average of the properties of the individual phases. For example, the density of a two phase alloy will be equal to the sum of the volume fraction of each phase times it s density. However, for the structure sensitive mechanical properties, the properties of the aggregate are generally influenced by interaction between the two phases. Two simple hypotheses may be used to calculate the properties of the two phase alloy,[95] from the properties of the individual phases. If it is assumed that the strain in each phase is equal, then the average stress in the alloy for a given strain will increase linearly with the volume fraction.

$$\sigma_{avg.} = f_1\sigma_1 + f_2\sigma_2$$

The volume fraction of phase 1 is f_1 and $f_1 + f_2 = 1$

The diagram shown in Fig. 125a shows the calculated flow curve for an alloy with 0.5 volume fraction of phase 2 on the basis of the equal strain hypothesis.

An alternative hypothesis is to assume that the two phases are subjected to equal stresses. The average strain in the alloy at a given stress is then given by

$$\epsilon_{avg.} = f_1 \epsilon_1 + f_2 \epsilon_2$$

Fig. 125b shows the flow curve for a 0.5 volume fraction alloy on the basis of the equal stress hypothesis. Both of these hypotheses are simple approximations, and the strengths of alloys containing two ductile phases usually lie between the predicted values from the two models described above.

The model described above can be used in the following way to predict the effect on hot strength of a small volume fraction of a second phase provided that the stress-strain curves for the second phase and the matrix are available for the temperature of interest.

For an aluminium copper alloy containing 8% copper by weight, the thermal equilibrium diagram shows that at 460°C. $2\frac{1}{2}$% copper is in solution in the matrix, and therefore the amount of second phase present must be formed from the remaining $5\frac{1}{2}$% copper. The composition of the second phase ($CuAl_2$) is as follows - 53.5% copper, 46.5% aluminium.

Therefore, in 100 gms. of the alloy, the amount of aluminium reacting with copper to form the second phase is

$\frac{5.5 \times 46.5}{53.5} = 4.8$ gms.

Therefore the weight of $CuAl_2$ in 100 gms. of alloy is $= 4.9 + 5.5 = 10.3$ gms. and hence the weight of matrix must be 89.7 gms.

The density of $CuAl_2$ is 4.34 gms./cm^3.

The density of the matrix is 2.7 gms./cm^3.

Therefore, in 100 gms. of the alloy, the volume of the two phases are as follows -

$$\text{Volume of } CuAl_2 = \frac{10.3}{4.34} = 2.38 \text{ cms.}^3$$

$$\text{Volume of matrix} = \frac{89.7}{2.7} = 33.2 \text{ cms.}^3$$

Hence the volume fraction of the second phase can now be calculated.

$$\text{v.f. of } CuAl_2 = \frac{2.38}{33.2 + 2.38} = 0.067$$

Having obtained a value for the volume fraction of the second phase it is now possible to calculate the stress strain curve for the aluminium 8% copper alloy, using the equal strain hypothesis. The figures shown below are extracted from the stress strain curve for pure $CuAl_2$ compressed at 460°C.

Reduction ins.	Stress lbs/in^2
0	0
0.05	16,150
0.10	19,850
0.15	18,400
0.20	17,400
0.25	15,800

Similar figures are extracted from the stress strain diagrams for aluminium 8% copper and aluminium 2½% copper; these are shown below.

Reduction ins.	Stress lbs./in^2	Reduction ins.	Stress lbs./in^2
0.05	3,350	0.05	2,320
0.10	3,360	0.10	2,470
0.15	3,350	0.15	2,500
0.20	3,380	0.20	2,540
0.25	3,400	0.25	2,590

Aluminium 8% copper — Aluminium 2½% copper

Since the hypothesis of equal strain states that

$$\sigma_1 f_1 + \sigma_2 f_2 = \sigma_{avg.}$$

it follows that the stress strain curve for the aluminium $CuAl_2$ composite can be calculated from the following equation.

$$0.067\ \sigma\ CuAl_2 + 0.935\ \sigma\ \text{matrix} = \sigma\ \text{alloy}$$

The data given below shows a comparison between the measured and calculated stress at various strains.

Strain ins.	Stress lbs. /in^2	Strain ins.	Stress lbs. /in^2
0	0	0	0
0.05	3,350	0.05	3,240
0.10	3,360	0.10	3,630
0.15	3,350	0.15	3,550
0.20	3,380	0.20	3,525
0.25	3,400	0.25	3,470

Measured values Calculated values

These figures show quite good agreement, when it is remembered that the method is only an approximate one. For comparison purposes, the stress strain curve (measured) for the 8% copper alloy in the sand cast state was chosen. This was because the structure of the alloy in this condition ensured that the second phase underwent deformation. This statement is supported by the fact that the stress strain curve for the alloy in this condition was above the stress strain curves for the other conditions, where the second phase was either partially distributed throughout the matrix by alteration of the casting technique, or by prior hot working.

The importance of the above illustration is that the resistance to deformation of an alloy may be estimated if the deformation characteristics of the matrix, the intermetallic phases, and the volume fractions of these phases are known. The analysis conducted above, although simple, illustrates the important contribution to hot strength provided by a relatively small amount of second phase, i.e. the presence of 6.7% by volume of $CuAl_2$ in a matrix of aluminium accounts for 30% of the stress required to deform the composite. A consideration of the suitability of a wide range of casting alloys for high temperature applications (graded according to the method used by the Light Alloy Founders Association), shown in Table 30, indicates that the best alloys are those containing the transition elements. This is because the transition elements combine with aluminium to form intermetallics with high inflexion temperatures. This means that if these phases possess the ability to deform plastically then they retain a high level of strength to a high temperature and therefore impart a proportion of this property on the alloy. The beneficial effect of transition elements can be seen in Table 30, where the grading of an Al-Si alloy is raised from C to A by the addition of copper and nickel. The grading results in the division of the alloys roughly as follows -

A) Al-Ni-Mg-Cu
Al-Cu-Si-Mg
Al-Cu-Ni-Mg
Al-Cu-Ni-Si-Mg

B) Al-Si-Cu-Mn

c) Al-Si
Al-Si-Cu
Al-Si-Mn

The ideal properties for an intermetallic to give good hot strength are -

1) The ability to retain strength to a high temperature.

2) The phase should be relatively insoluble in the matrix, to prevent dissolution or coagulation.

3) The phase should have good coherence with the matrix.

The intermetallics formed between aluminium and the transition elements possess most of these properties, especially the second one, and it is well known that the rate of diffusion of the transition elements in aluminium is very slow, which is ideal in high temperature materials, but unfortunately these elements have very low solubilities in the matrix. This low solubility means that aging mechanisms cannot be used to produce a strength increase, as not enough zones can be formed to accomplish this. The low solubilities of these elements are discussed below along with some of the more important aspects of the thermal equilibria that exist between the transition elements and aluminium.

Aluminium-Titanium

The addition of titanium to aluminium produces a rising

No.	B.S.1490	Cu	Mg	Si	Fe	Mn	Ni	Zn	Pb	Sn	Ti	Co	Nb	Suitability for high temp. applications
1	LM6M	.1	.1	10-13	.6	.5	.1	.1	.1	.05	.2	-	-	C
2	LM20M	.4	.15	10-13	.7	.5	.1	.2	.1	.05	.2	-	-	C
3	LM9P	.1	.2-.6	10-13	.6	.3-.7	.1	.1	.1	.05	.2	-	-	C
4	LM13WP	.5-1.3	.8-1.5	11-13	.8	.5	.7-2.5	.1	.1	.1	.2	-	-	A
5	LM18M	.1	.1	4.5-6	.6	.5	.1	.1	.1	.05	.2	-	-	C
6	LM8P	.1	.3-.8	3.5-6	.6	.5	.1	.1	.1	.05	.2	-	-	C
7	LM2M	.7-2.5	.3	9-11.5	1	.5	1	1.2	.3	.2	.2	-	-	C
8	LM24M	3-4	.1	7.5-9.5	1.3	.5	.5	3	.3	.2	.2	-	-	C
9	LM4M	2-4	.15	4-6	.8	.3-.7	.3	.5	.1	.05	.2	-	-	B
10	LM21M	3-5	.1-.3	5-7	1	.3-.6	.3	2	.1	.05	.2	-	-	B
11	LM22M	2.8-3.8	.05	4-6	.7	.3-.6	.15	.15	.1	.05	.2	-	-	C
12	LM16W	1-1.5	.4-.6	4.5-5.5	.6	.5	.25	.1	.1	.05	.2	-	-	C
13	LM12WP	9-11	.2-.4	2.5	1	.6	.5	.8	.1	11	.2	-	-	A
14	LM1M	6-8	.15	2-4	1	.6	.5	2-4	.3	.2	.2	-	-	A
15	LM11W	4-5	.1	.25	.25	.1	.1		.05	.05	.3	-	-	B
16	LM14WP	3.5-4.5	1.2-1.7	.6	.6	.6	1.8-2.3	.1	.05	.05	.2	-	-	A
17	D.T.D. 741A	3.5-4.5	1.2-2.5	.5	.5	.1	.1	.05	.05	-	-	.5-1	.05-.3	A
18	LM10W	.1	9.5-11	.25	.35	.1	.1	.1	.05	.05	.2	-	-	B
19	LM5M	.1	3-6	.3	.6	.3-.7	.1	.1	.05	.05	.2	-	-	B
20	LM3M	2.5-4.5	.1	1.3	1	.5	.5	9-13	.3	.05	.2	-	-	C
21	2L5Z	1.3-2	.5-1.7	.6-2	.8-1.4	.1	.5-2	.1	.05	.05	.05-.3	-	-	A
22	LM23P	.8-2	.05-.2	1.5-2.8	.8-1.4	.1	.8-1.7	.1	.1	.1	.05-.3	-	-	B

Table 30 - Suitability of cast aluminium alloys for elevated temperature applications. Alloys ranked according to the Light Alloy Founders Association Grading Convention[95].

A = Particularly recommended
B = Suitable but not especially recommended
C = Not recommended in cases where heat resistance is likely to be an important consideration

liquidus and solidus, but at about 655°C. on the liquidus (at 0.15%Ti) there is a peritectic reaction with the phase $TiAl_3$ to form a solid solution of titanium in aluminium with 1.15% Ti. Above 655°C. the melt is in equilibrium with solid $TiAl_3$ which melts peritectically at 1340°C. $TiAl_3$ is tetragonal in crystal structure with a = 5.435 Å, c = 8.591 Å.

Aluminium Manganeses

Aluminium and manganese give a complex equilibrium diagram, but the only two compounds of interest in aluminium technology are $MnAl_6$ and $MnAl_4$. $MnAl_6$ contains 25.34% manganese and has an orthorhombic structure with 28 atoms to the unit cell (a=6.498 Å, b=7.552 Å, c=8.87 Å). $MnAl_6$ is formed primarily from 2% to 4.1% between 658.5°C. and 710°C. A peritectic reaction of the melt with a complex solid solution occurs at 710°C. Supercooling produces strong supersaturation here. Supercooling or liquid quenching may produce a strong supersaturation of the solid solution of manganeses in aluminium to produce zones not yet detected. The addition of manganese to aluminium produces a eutectic at 658.5°C. and about 2% manganese and at this temperature the solidus is at 1.82% manganese. As the temperature falls the manganese concentration falls and is ejected from the lattice as secondary $MnAl_6$. The solid solubility is 0.95% manganese at 600°C. and 0.35% manganese at 500°C.

Manganese is the major alloying element in a series of alloys called the Al-Tran alloys which are a fairly new series of alloys (patented in 1950) for high temperature applications. It is claimed that the alloys have been developed with substantial complex zone formations, which are produced by high cooling speeds or constitutional effects.

Aluminium-Vanadium

The Al-V system is also a complicated one, and the only feature of technical interest is the existence of a phase of approximate composition $Al_{11}V$, with a f.c.c. type crystal structure, with a=14.586 Å, and 192 atoms per unit cell.

Aluminium-Nickel

The addition of nickel to aluminium forms a eutectic at 640°C. and 5.7% nickel, between a solid solution of 0.05% nickel in aluminium and the compound $NiAl_3$. This forms at 854°C. by peritectic reaction between melt containing 28.4% nickel and $NiAl_3$, and has an orthorhombic structure with a=6.611 Å, b=7.366 Å, c=4.812 Å. The solid solubility of nickel in aluminium at 500°C. is 0.006%.

Aluminium-Cobalt

The addition of cobalt to aluminium forms a eutectic at 657°C. and 1% cobalt between a solid solution of less than 0.02% cobalt in aluminium and the compound Co_2Al_9. This phase forms at 943°C. by peritectic reaction between melt containing 20% cobalt and Co_4Al_{13} and is monoclinic with 4 cobalt and 18 aluminium atoms per unit cell (a=8.5564 Å, b=6.290 Å, c=6.213 Å, beta = 94.76°).

Aluminium-Chromium

This system undergoes a peritectic reaction at 661°C., between melt with 0.4% chromium and solid $CrAl_7$. The solid solubility is 0.77% at 661°C. and 0.15% at 300°C. Zones can be expected to form as chromium diffuses into vacancies along certain matrix planes when an alloy with 0.5% chromium is quenched from the alpha range. The final evolution product of the zones is $CrAl_7$ with a=20.47 Å, b=7.64 Å, c=25.36 Å, beta = 155.13° Other transition elements can partially replace chromium without modifying the crystal type.

Aluminium-Iron

This system forms a eutectic at 655°C. The important phase in the system is $FeAl_3$ which is monoclinic. Zone formation has not yet been investigated but it is improbable because aluminium can take so little iron into solution (0.052% iron at 655°C.)

Hence, although the use of the transition elements is attractive, it is obvious that conventional aging mechanisms are not possible. Reference has already been made to the Al-Tran alloys which are used for elevated temperature applications. These alloys are based on a binary aluminium 4% manganese alloy with additions of iron, iron plus titanium, and iron plus titanium plus cobalt. As mentioned earlier, it is possible, using special heat treatment techniques to form zones in aluminium manganese alloys, and it is claimed that the Al-Tran alloys contain complex zones.

However, there is still a method by which the properties of the transition element intermetallics could be used. Since the phases of interest have high inflexion temperatures and are insoluble in the matrix, it may be possible to work an alloy containing such phases at a fairly low temperature (say 250°C.) at which the intermetallics are brittle and fracture, becoming dispersed in the matrix, which is soft enough (due to negligible solid solution hardening)to fill the fractures in the hard phases. The fine dispersion of the intermetallics produced may result in conferring high temperature strength to the alloy.

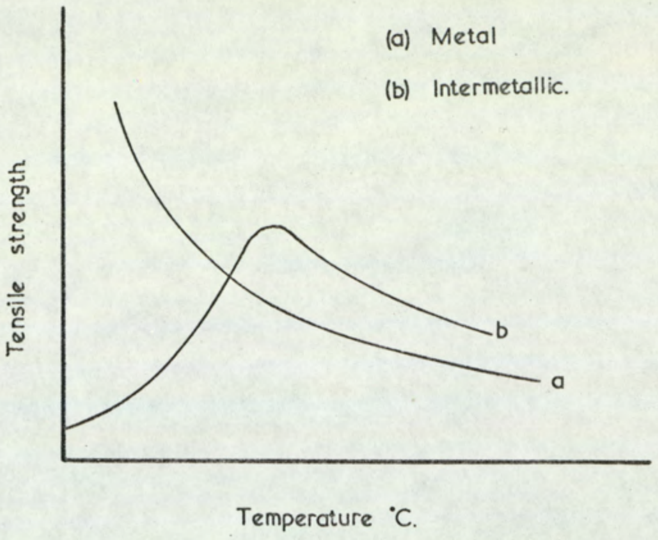

Fig. 1. The variation of strength with temperature for a pure metal and an intermetallic.[59]

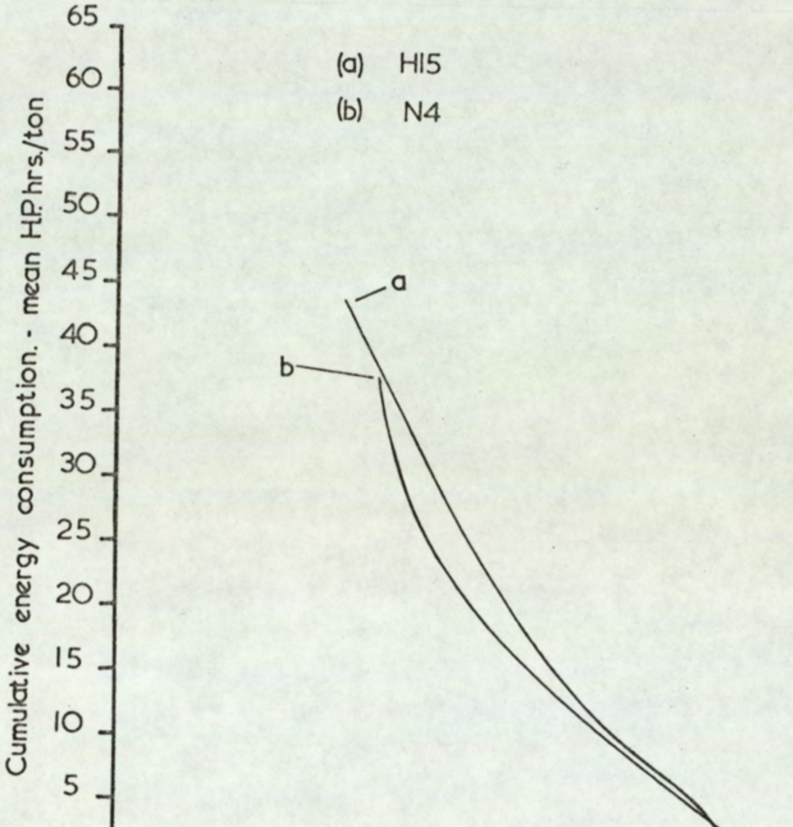

Fig. 2. Energy curves for "soft" and "strong" commercial aluminium alloys.

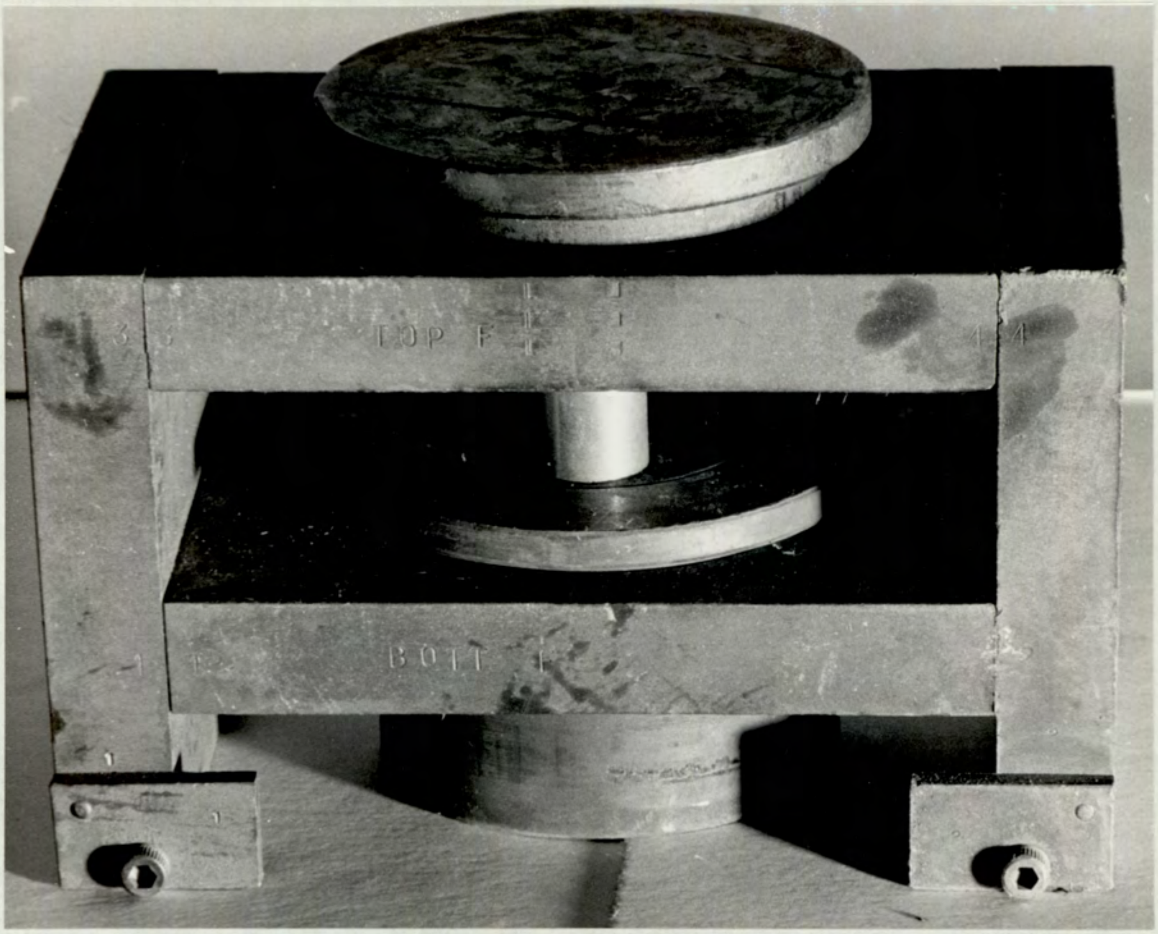

Fig. 3a. The die-set used for the simulation of hot rolling schedules. The die holders can be seen (fully mobile in the vertical direction) with a compression slug between them. The stops attached to the base of the side-pieces of the die-set are for easy location in the press as seen in Fig. 3b.

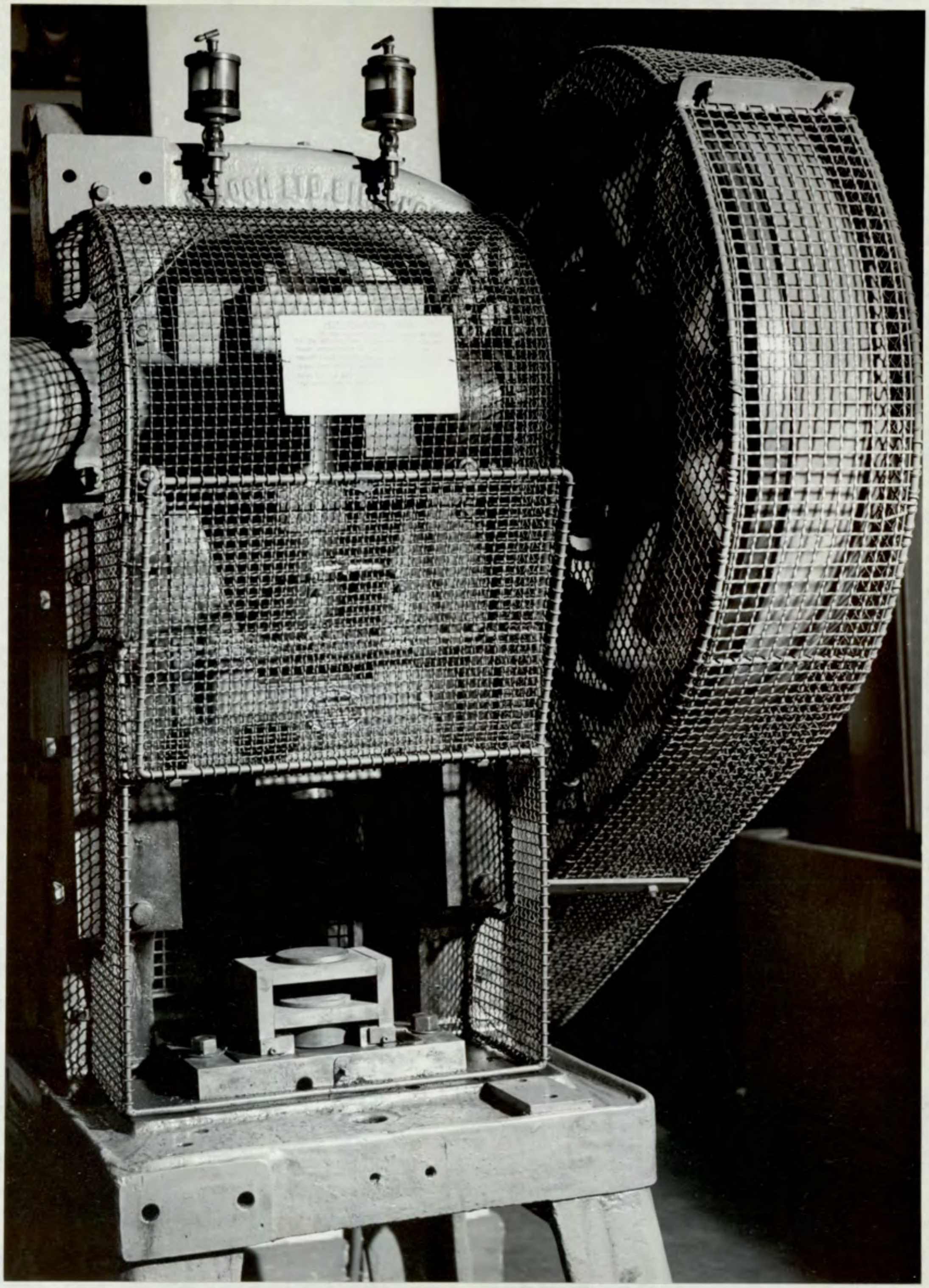

Fig. 3b. Upsetting press with die-set assembly in place, used for the simulation of hot rolling schedules.

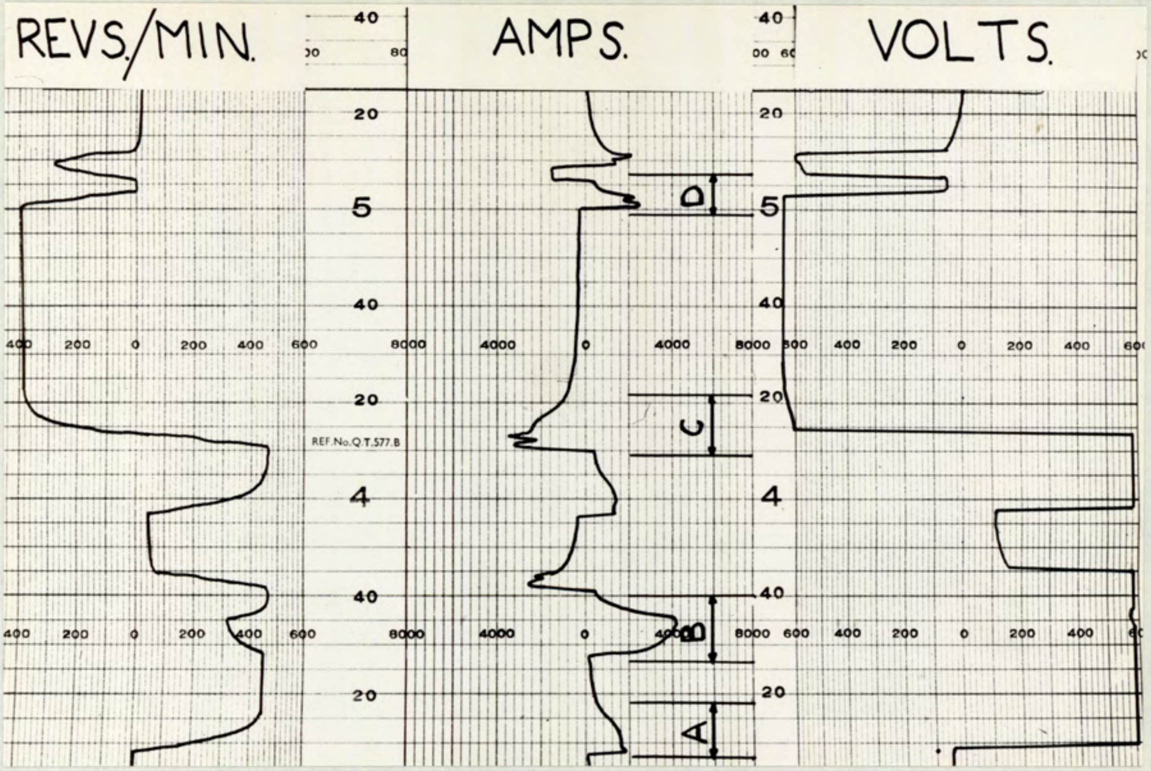

Fig. 4. Mill motor recorder chart showing speed, voltage, and current characteristics.

a) the current characteristic when the mill motor is started from rest.

b) the current characteristic due to the execution of a single pass.

c) the current characteristic when the mill motor is stopped and reversed simultaneously.

d) the current characteristic when the mill motor is stopped.

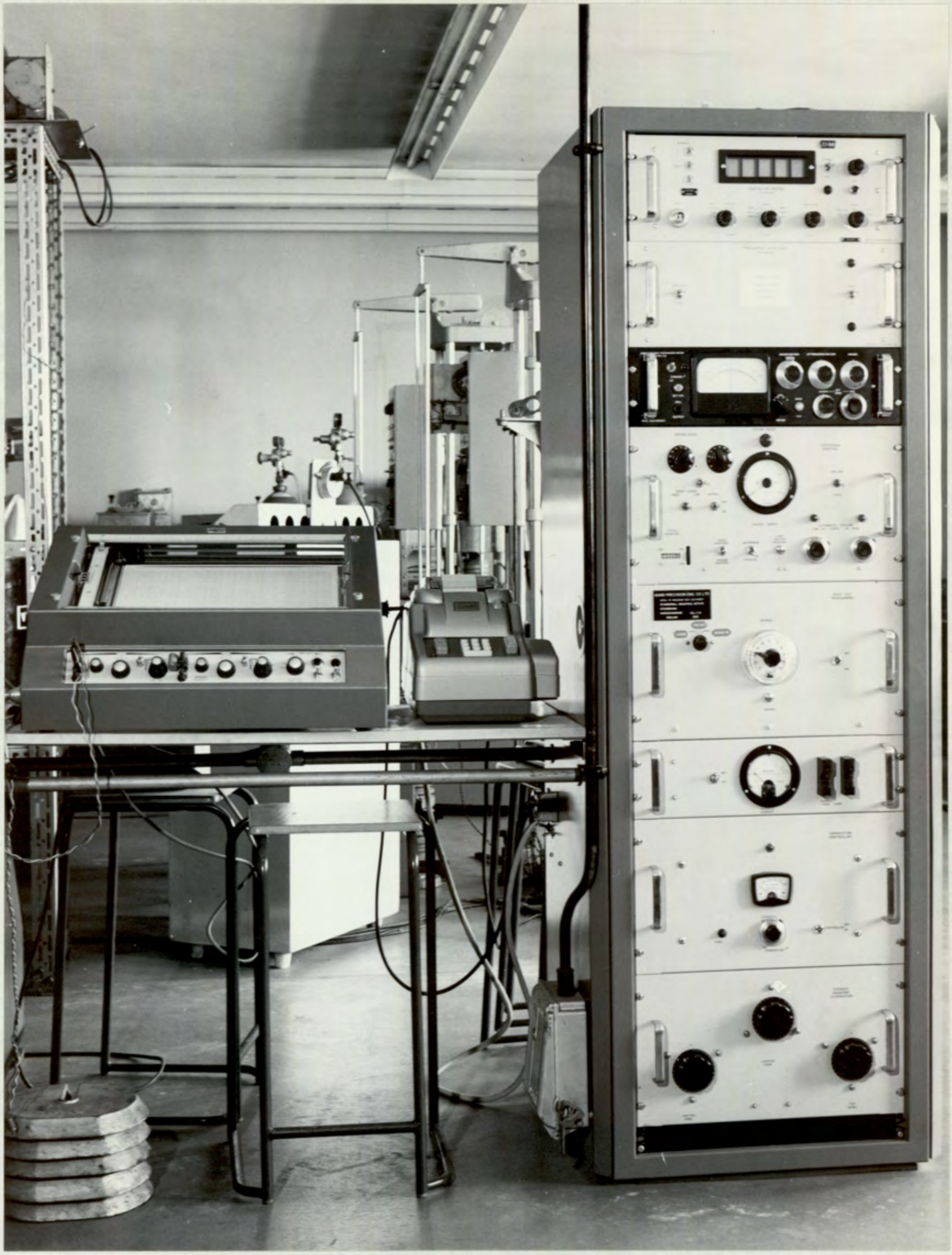

Fig. 5. Equipment used for compression testing with load measurement.

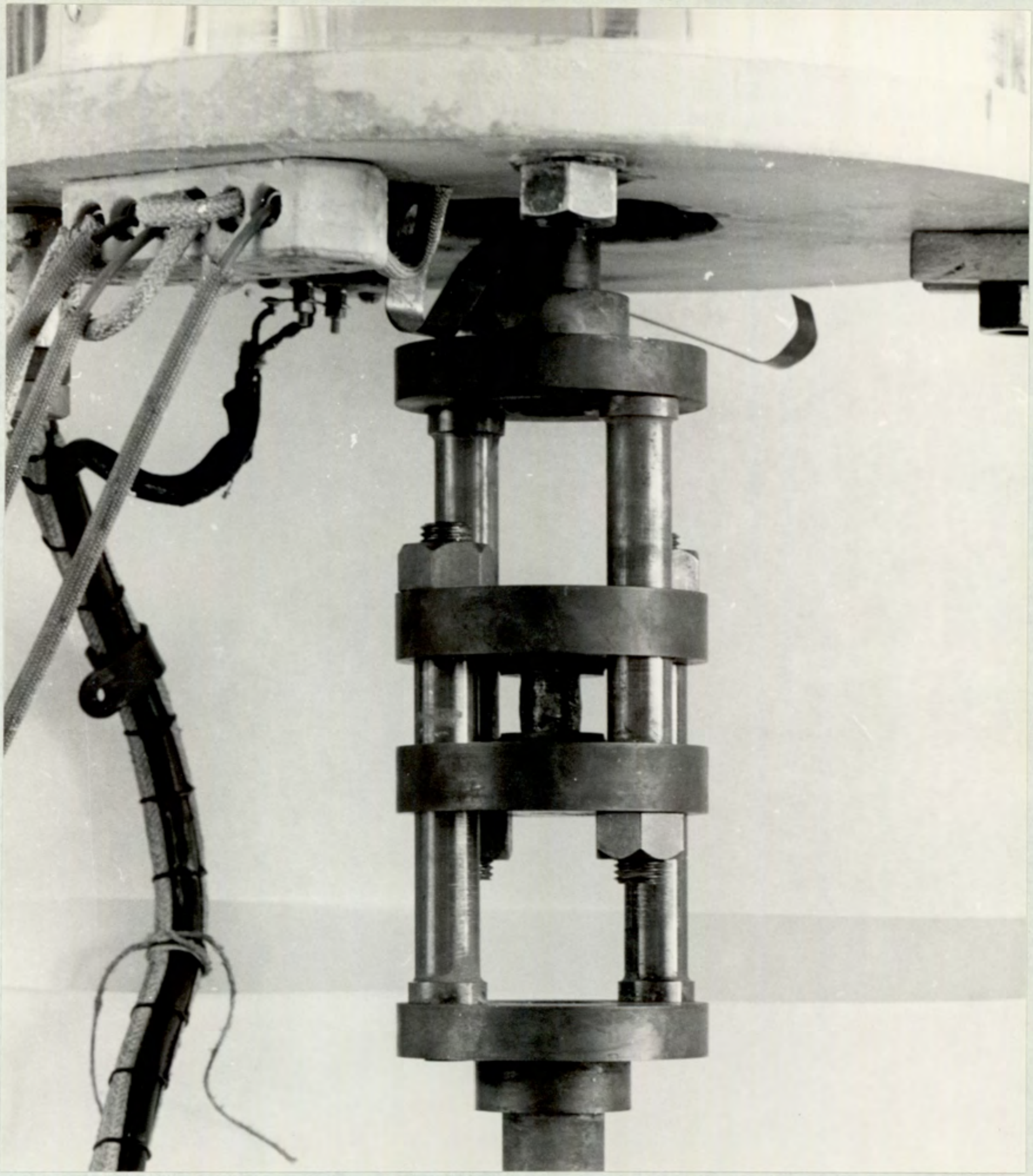

Fig. 6. Compression jig used for compression testing with load measurement. The three zone tube furnace can be seen in the raised position.

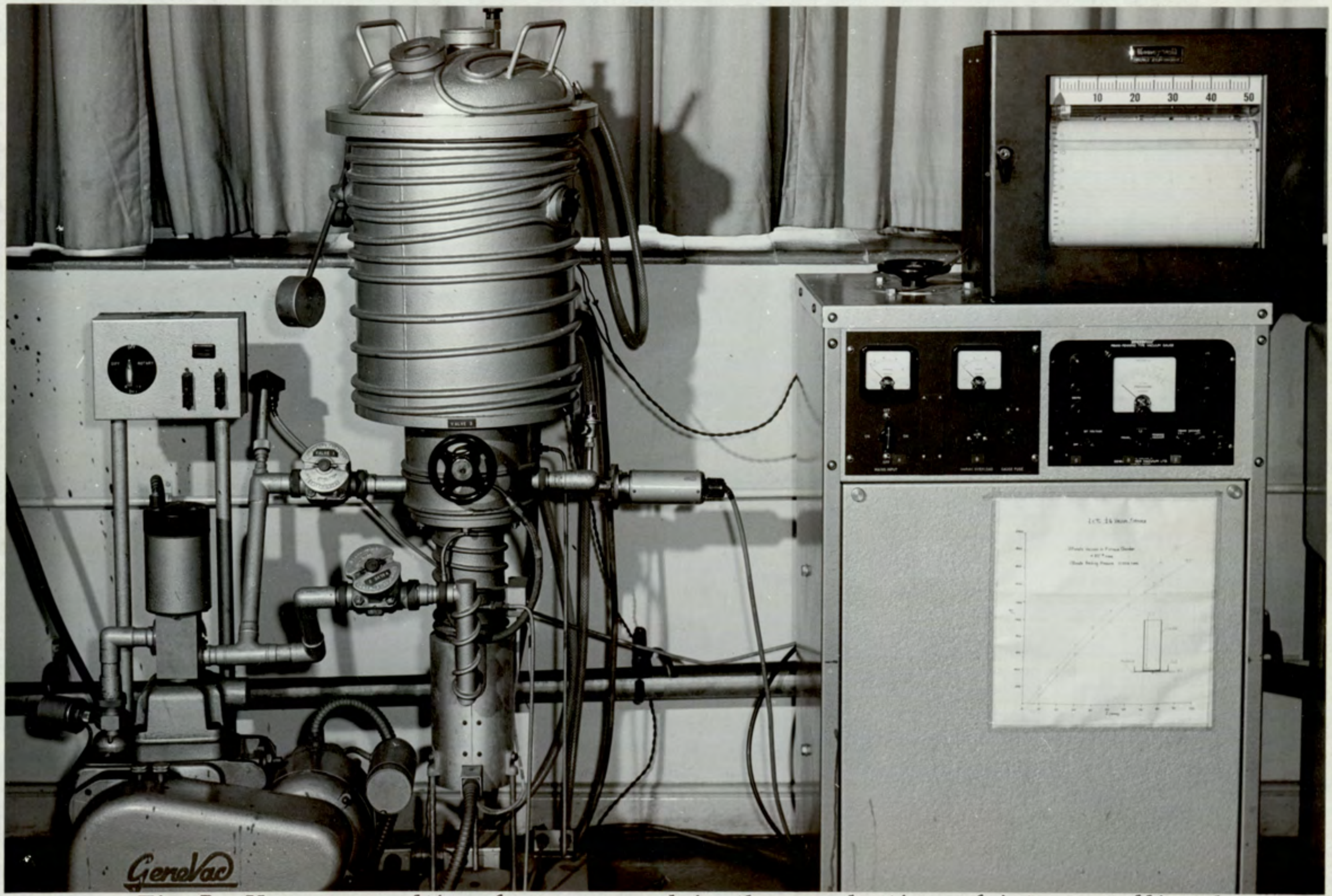

Fig. 7 Vacuum melting furnace used in the production of intermetallic phases.

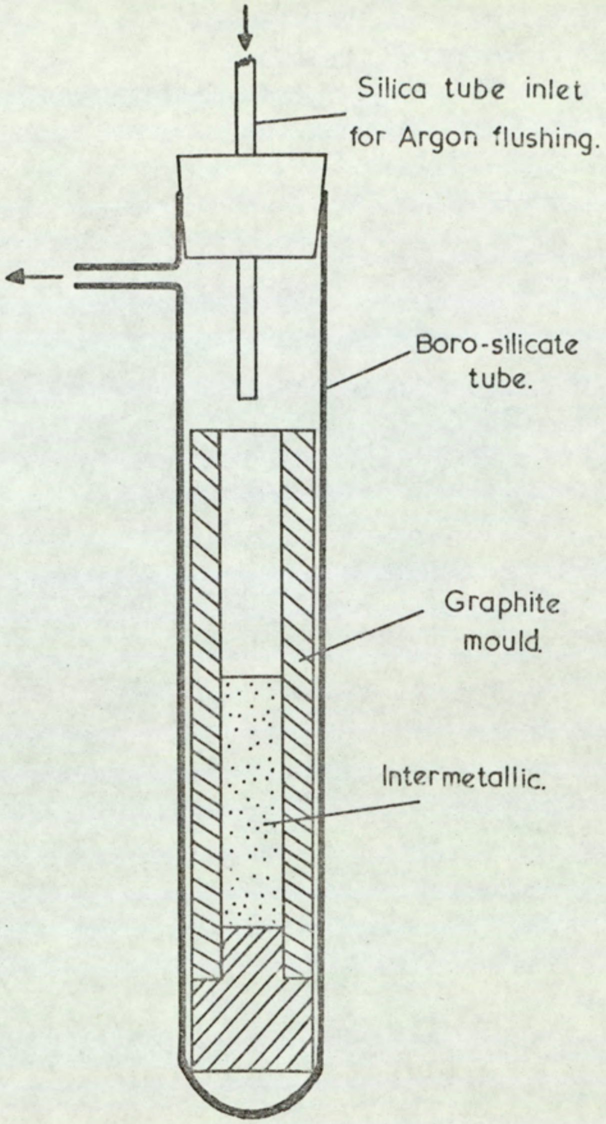

Fig. 8 Apparatus used for the remelting and solidification of intermetallic phases.

Fig. 9 Cracking induced in a sample of pure $CuAl_2$ by the pattern of internal contraction stresses. Approx x2 actual size.

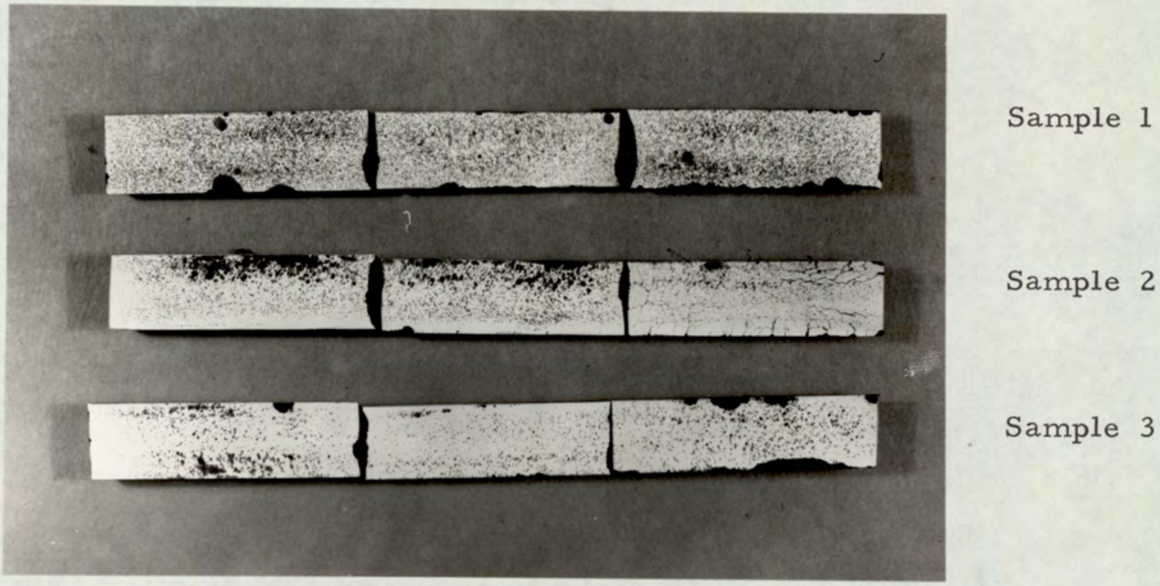

Fig. 10. Dye penetrant tests showing micro-porosity in chill cast H15 alloy
Sample 1 - Normal casting technique
Sample 2 - Cast into tilted mould
Sample 3 - Melt allowed to stand in furnace for 20 mins. before being poured into a tilted mould.
Approx. 1/3rd actual size.

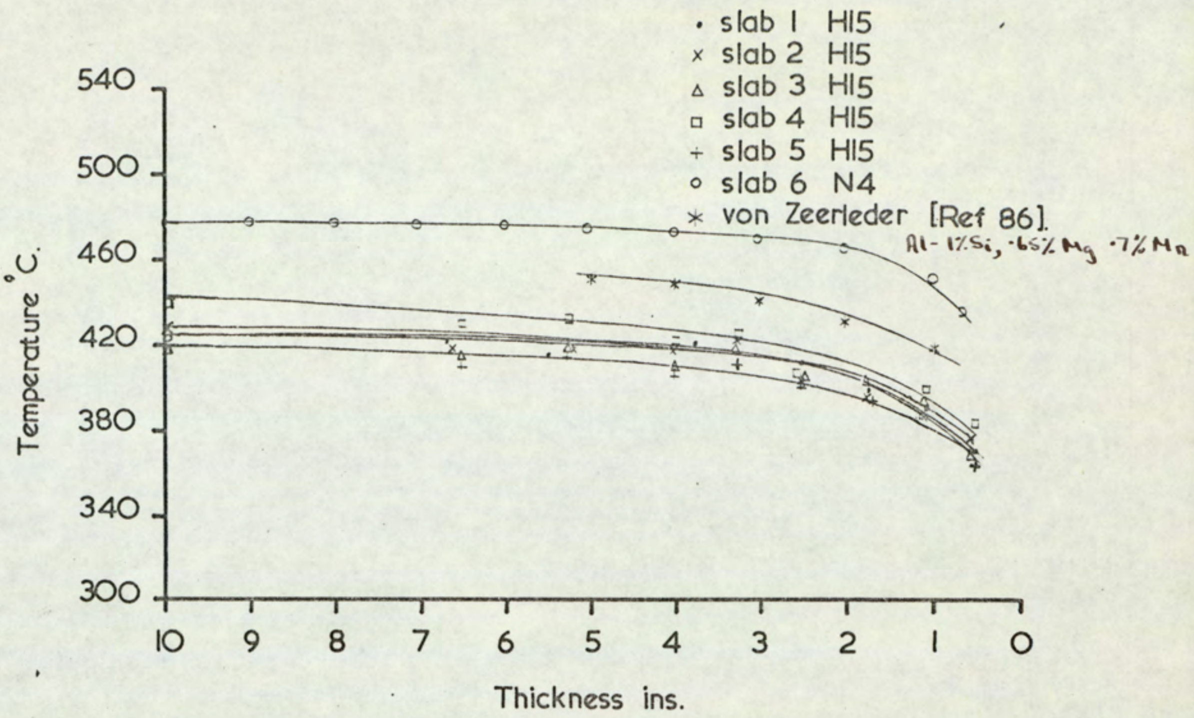

Fig. 11 Plot of temperature vs. thickness for the hot rolling of H.15 and N.4 from measured values.

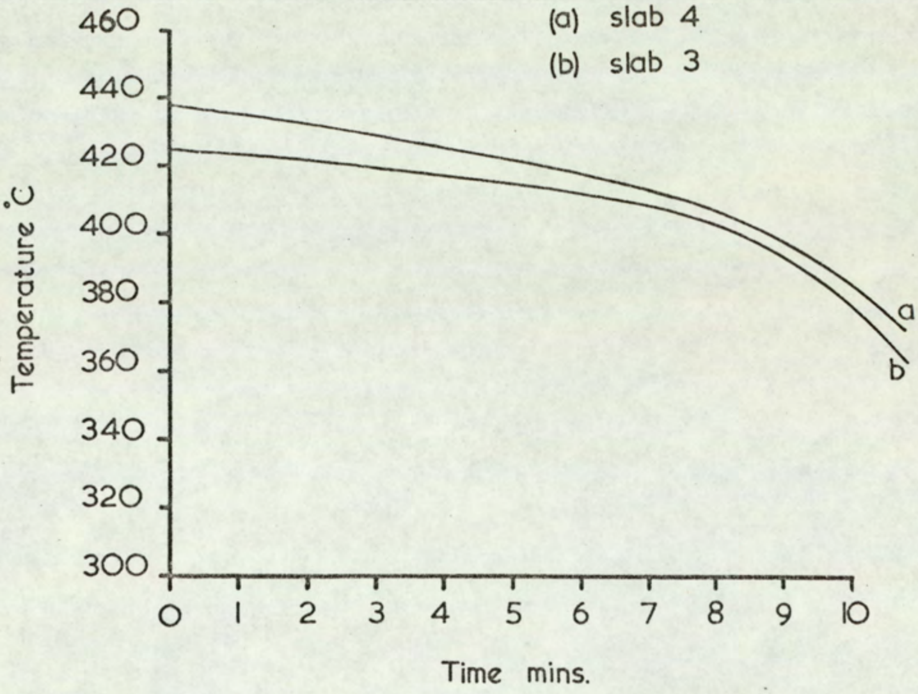

Fig. 12 Plot of time vs. temperature for the hot rolling of H15. and N.4 from measured values.

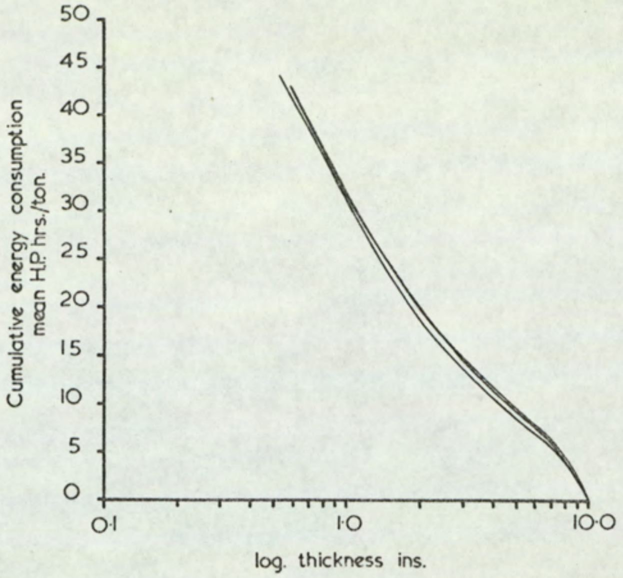

Fig. 13 Energy curves for the hot rolling of H15.

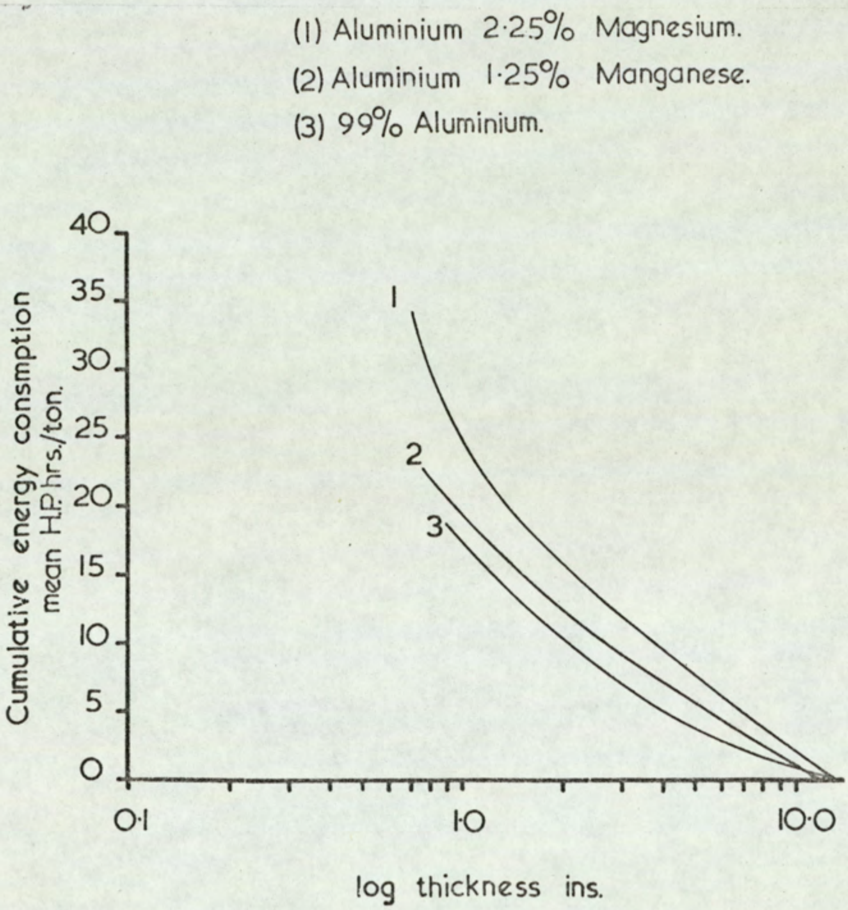

Fig.14 Energy curves for the hot rolling of (1) Al-2$\frac{1}{4}$% Mg, (2) Al-1$\frac{1}{4}$%Mn, (3) 99% Al.

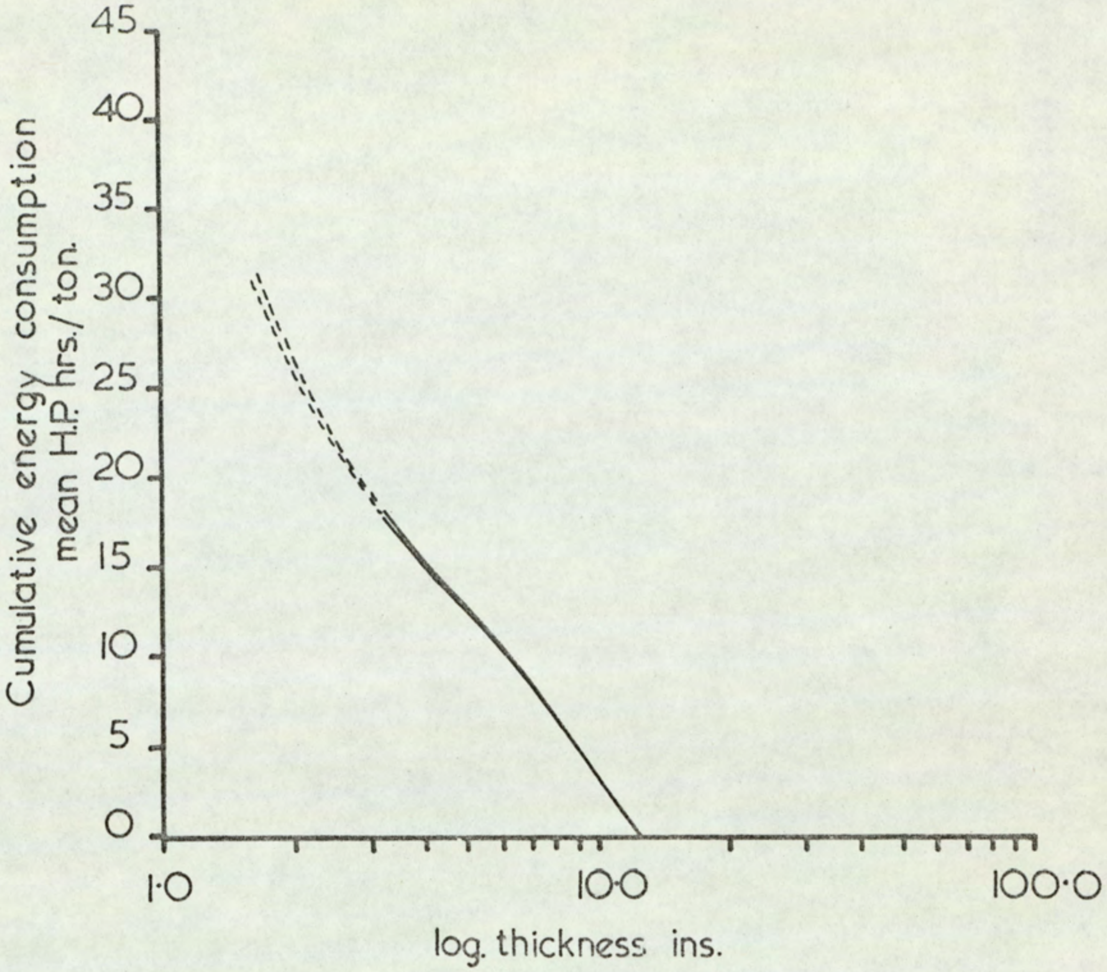

Fig. 15 Energy curves for hot rolling of DTD 683.

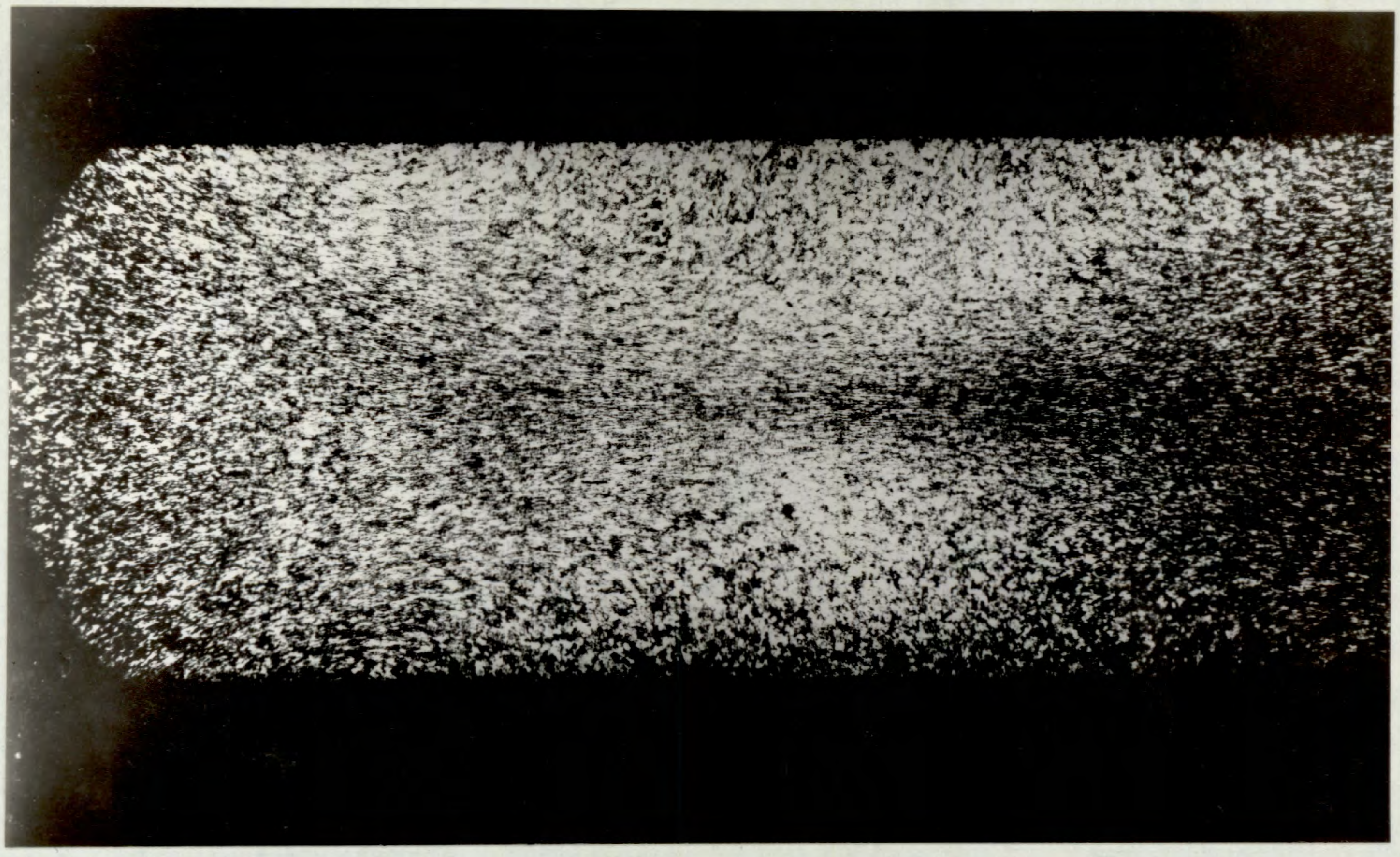

Fig.16 Inhomogeneous flow in H.15 during unlubricated hot compression (63%).

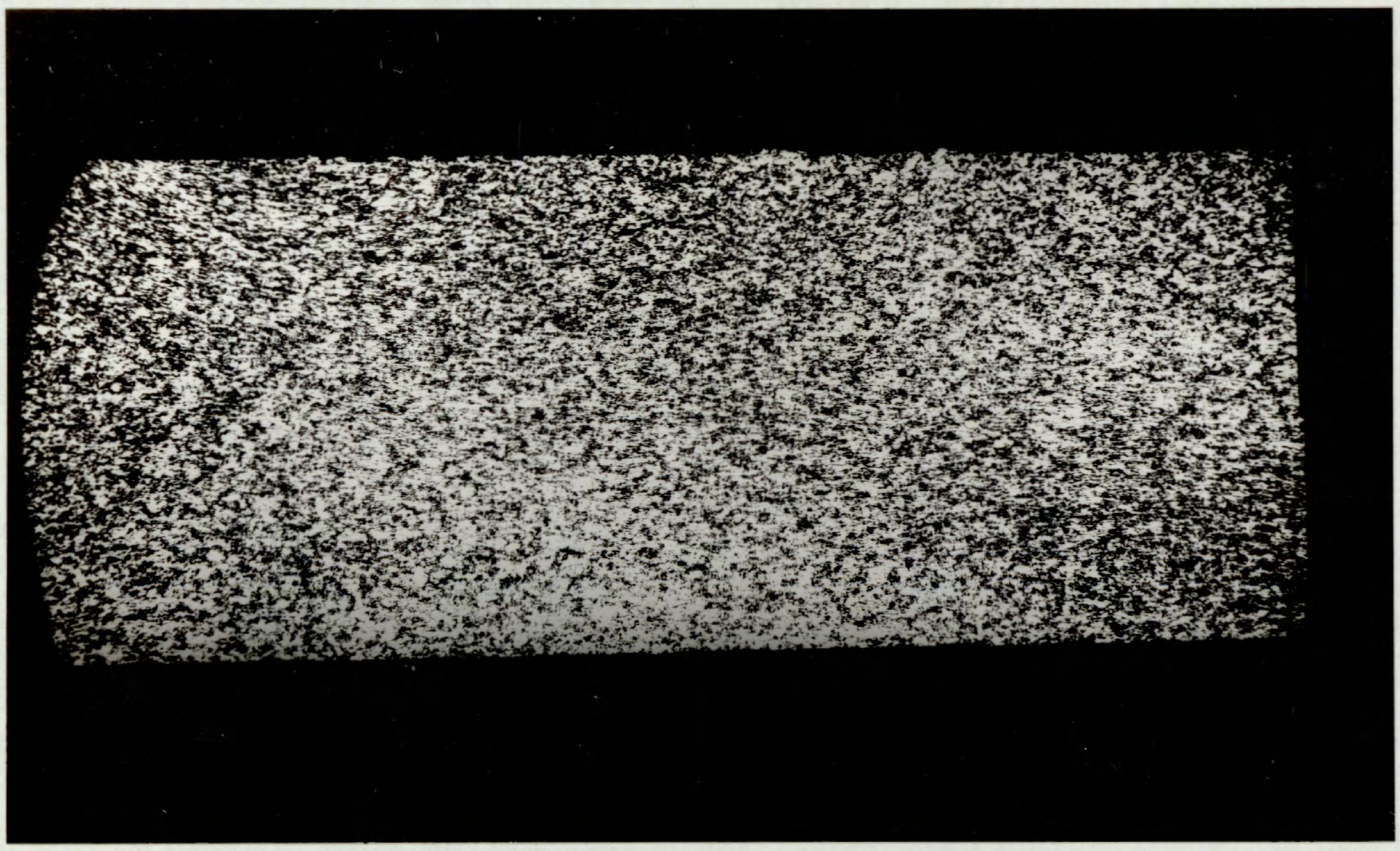

Fig. 17. The reduction in inhomogeneous flow in H.15 during hot compression using lubricant (iv) (65%).

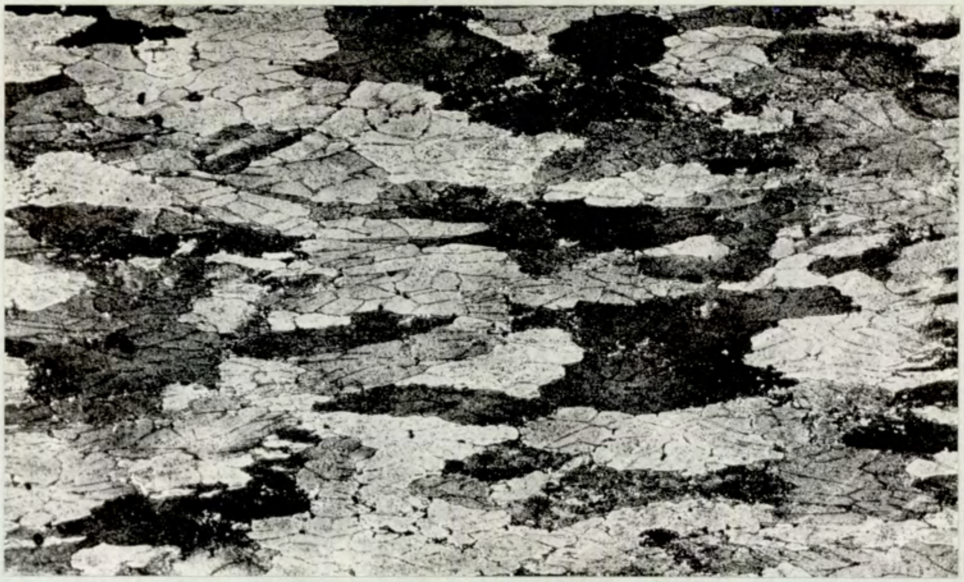

Fig. 18. Microstructure of H.15 commercially hot rolled 68%. Transverse section, Mag. x75, Etch-mixed acids.

Fig. 19. Microstructure of H.15 commercially hot rolled 68%. Transverse section, Mag. x500, Etch-$\frac{1}{2}$% HF.

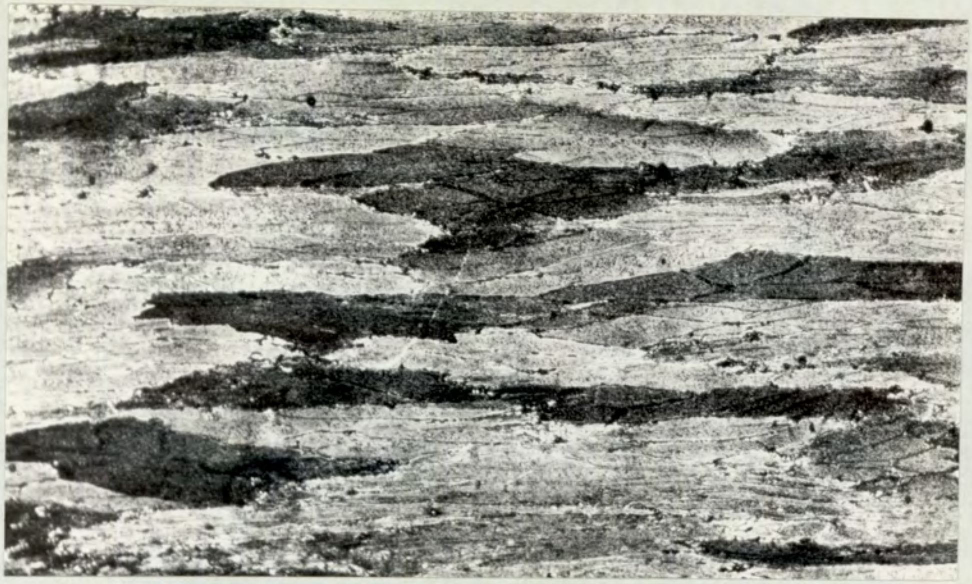

Fig. 20. Microstructure of H.15 commercially hot rolled 68%. Longitudinal section, Mag. x75, Etch-mixed acids.

Fig. 21. Microstructure of H.15 commercially hot rolled 68%. Longitudinal section, Mag. x500, Etch-$\frac{1}{2}$% HF.

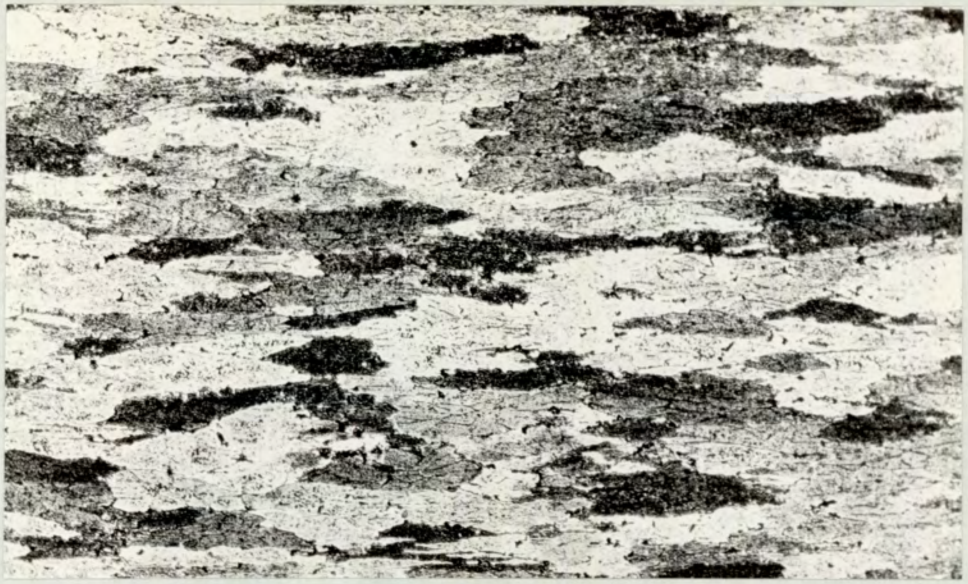

Fig. 22. Microstructure of H.15 commercially hot rolled 78%. Transverse section, Mag. x75, Etch-mixed acids.

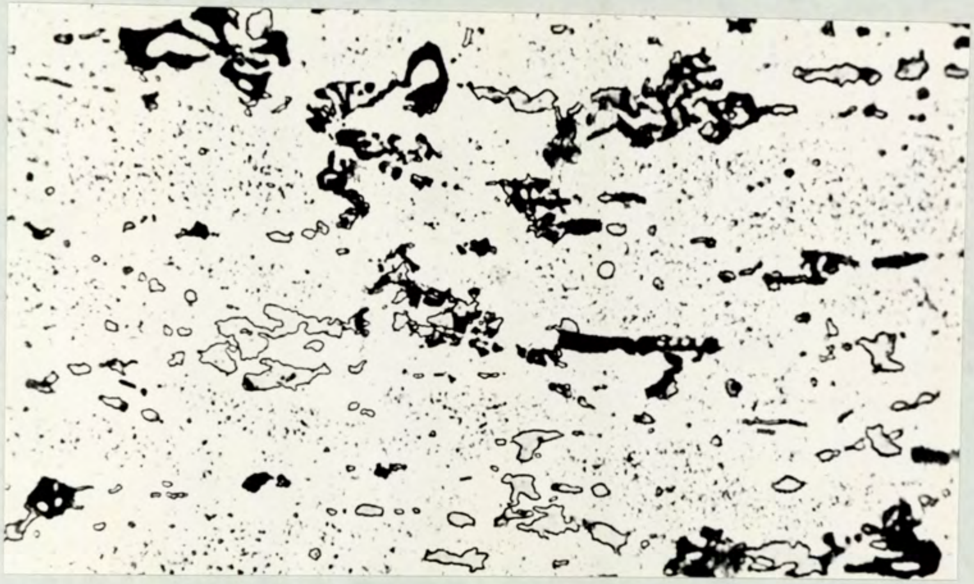

Fig. 23. Microstructure of H.15 commercially hot rolled 78%. Transverse section, Mag. x500, Etch-$\frac{1}{2}$% HF.

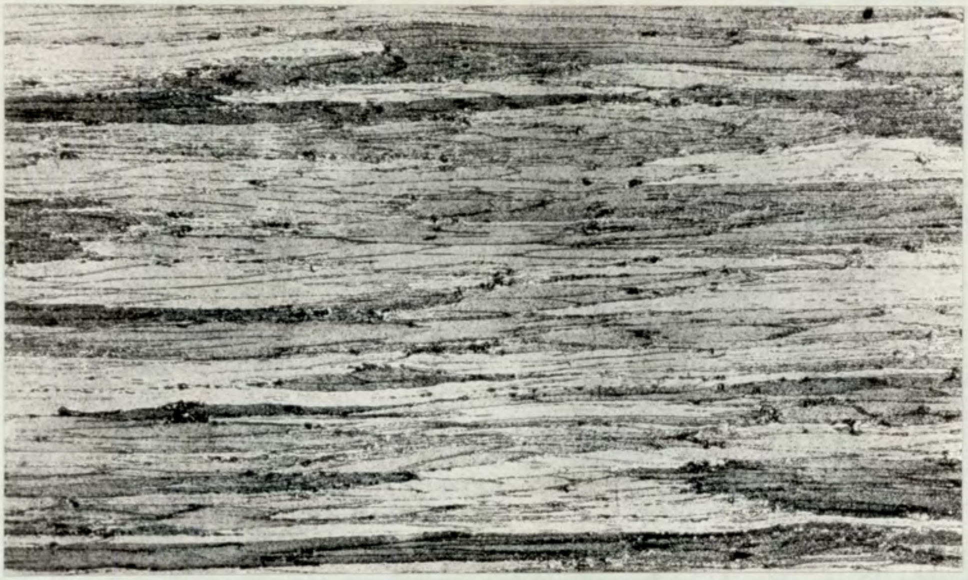

Fig. 24. Microstructure of H.15 commercially hot rolled 78%. Longitudinal section, Mag.x75, Etch-mixed acids.

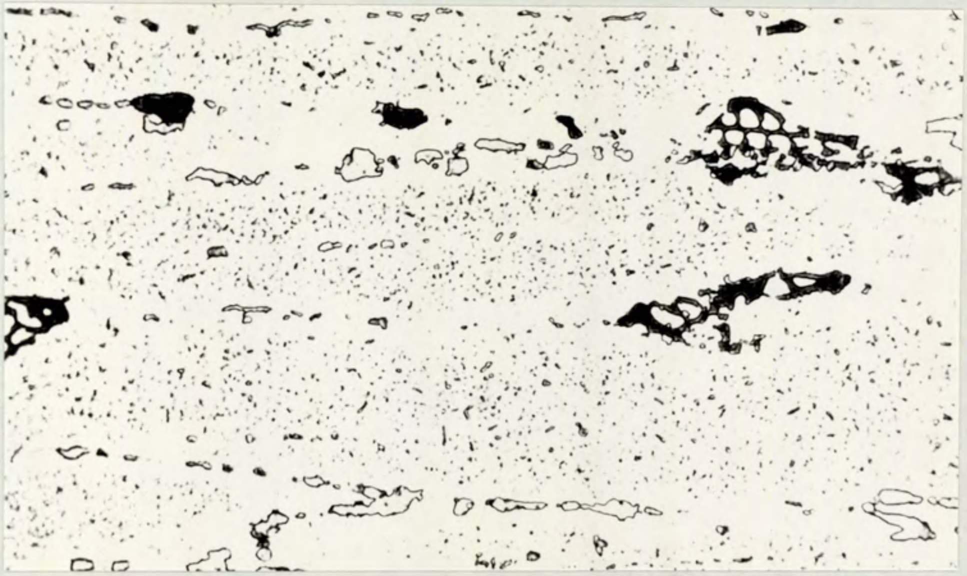

Fig. 25. Microstructure of H.15 commercially hot rolled 78%. Longitudinal section, Mag.x500, Etch-$\frac{1}{2}$% HF.

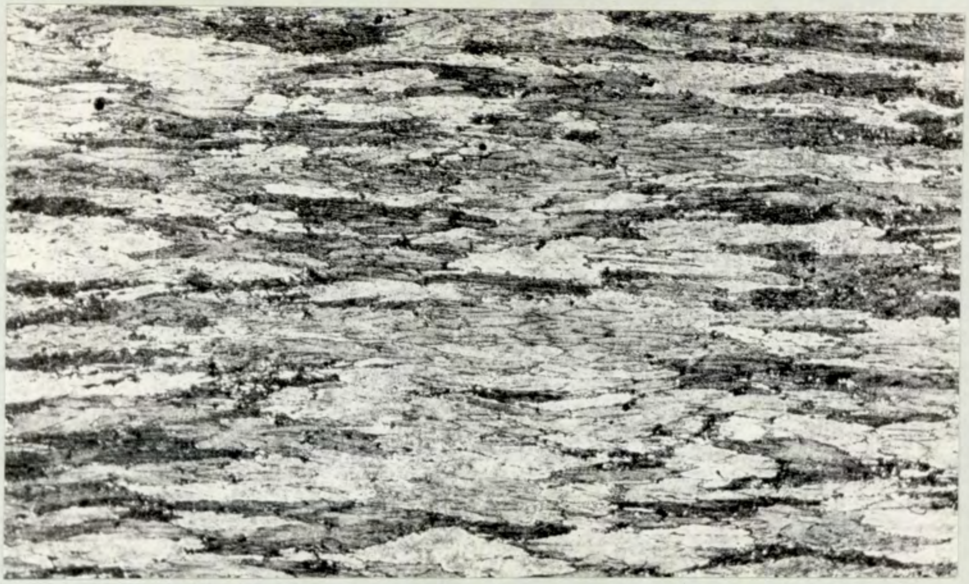

Fig. 26. Microstructure of H.15 commercially hot rolled 86%. Transverse section, Mag.x75, Etch-mixed acids.

Fig. 27. Microstructure of H.15 commercially hot rolled 86%. Transverse section, Mag.x 500, Etch-$\frac{1}{2}$% HF.

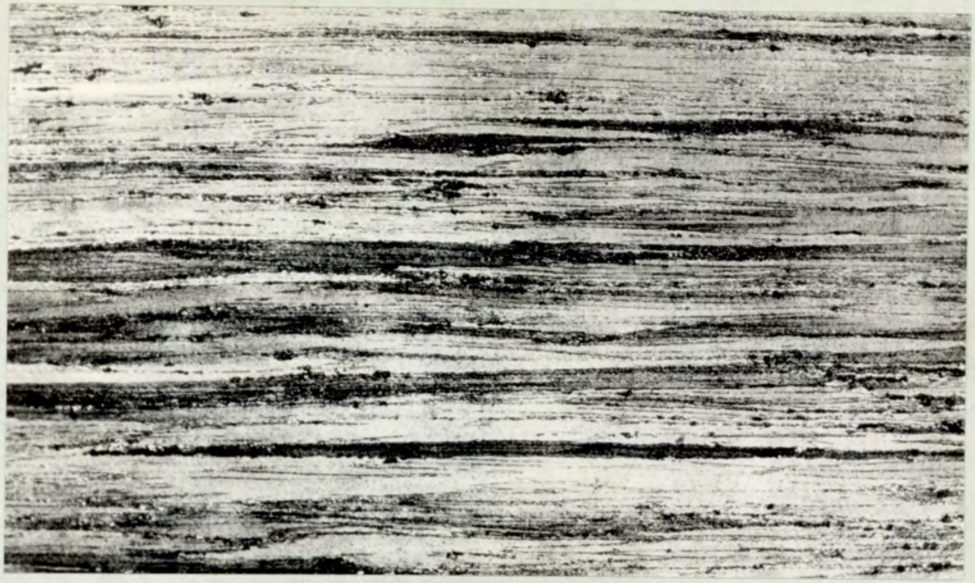

Fig. 28. Microstructure of H.15 commercially hot rolled 86%. Longitudinal section, Mag. x75, Etch-mixed acids.

Fig. 29. Microstructure of H.15 commercially hot rolled 86%. Longitudinal section, Mag. x500, Etch-$\frac{1}{2}$% HF.

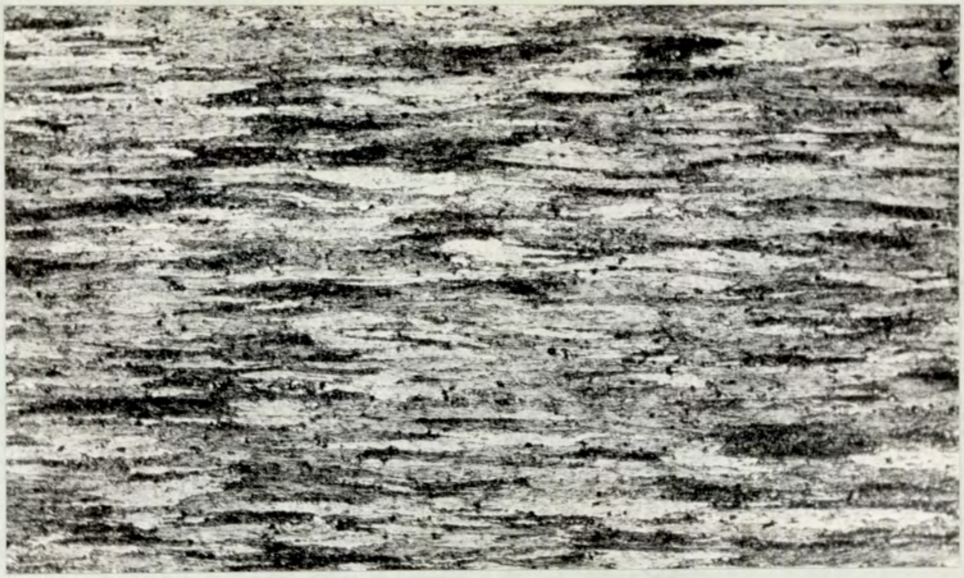

Fig. 30. Microstructure of H.15 commercially hot rolled 93%. Transverse section, Mag.x 75, Etch-mixed acids.

Fig. 31. Microstructure of H.15 commercially hot rolled 93%. Transverse section, Mag. x 500, Etch-$\frac{1}{2}$% HF.

Fig. 32. Microstructure of H.15 commercially hot rolled 93%. Longitudinal section, Mag. x 75, Etch-mixed acids.

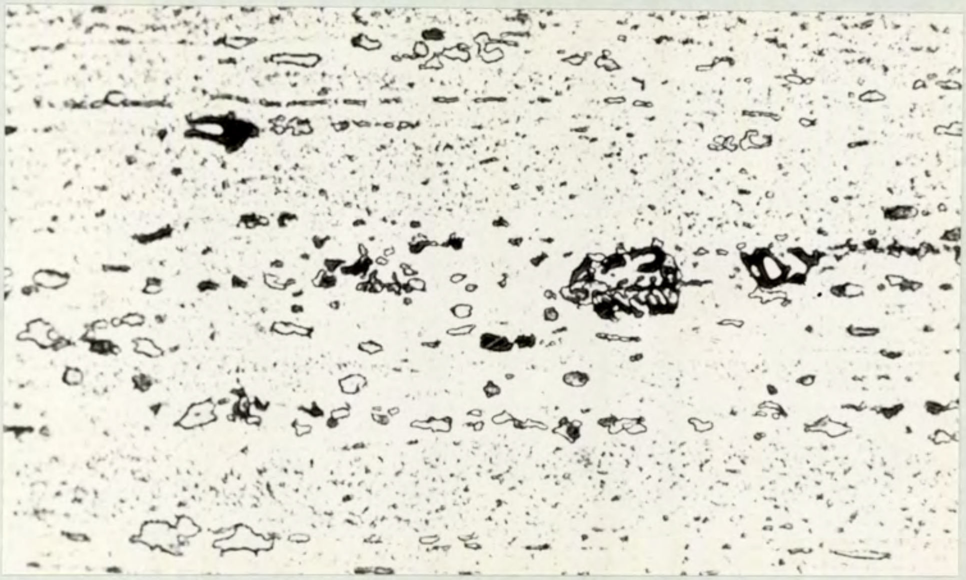

Fig. 33. Microstructure of H.15 commercially hot rolled 93%. Longitudinal section, Mag. x 500, Etch-$\frac{1}{2}$% HF.

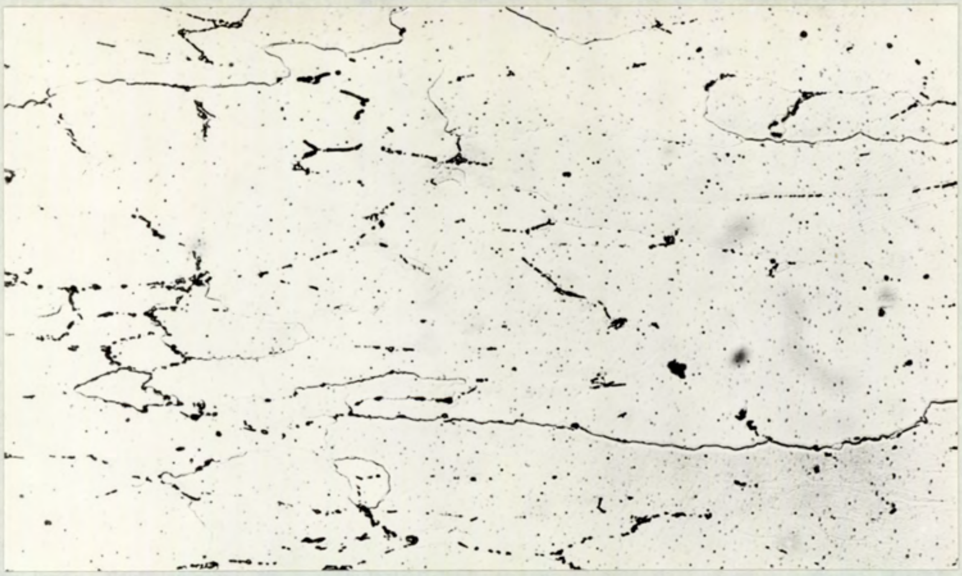

Fig. 34. Microstructure of N4 commercially hot rolled 68.6%
Transverse section, Mag. x 200, Sample anodised.

Fig. 35. Microstructure of N4 commercially hot rolled 68.6%.
Transverse section, Mag. x 750, Etch-$\frac{1}{2}$% HF.

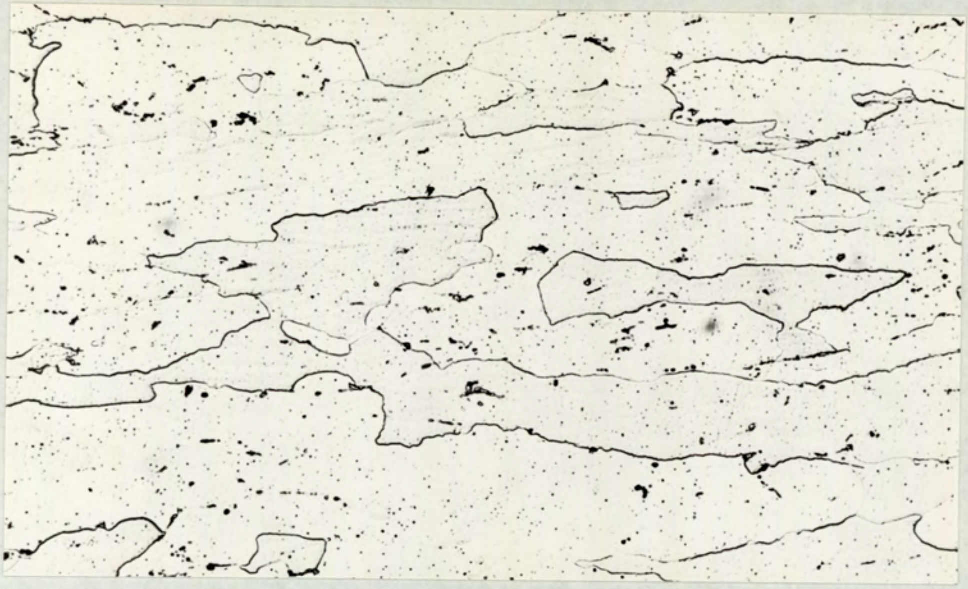

Fig. 36. Microstructure of N4 commercially hot rolled 82.8%. Transverse section, Mag. x200, Sample anodised.

Fig. 37 Microstructure of N4. commercially hot rolled 82.8% Transverse section, Mag. x750, Etch-$\frac{1}{2}$% HF.

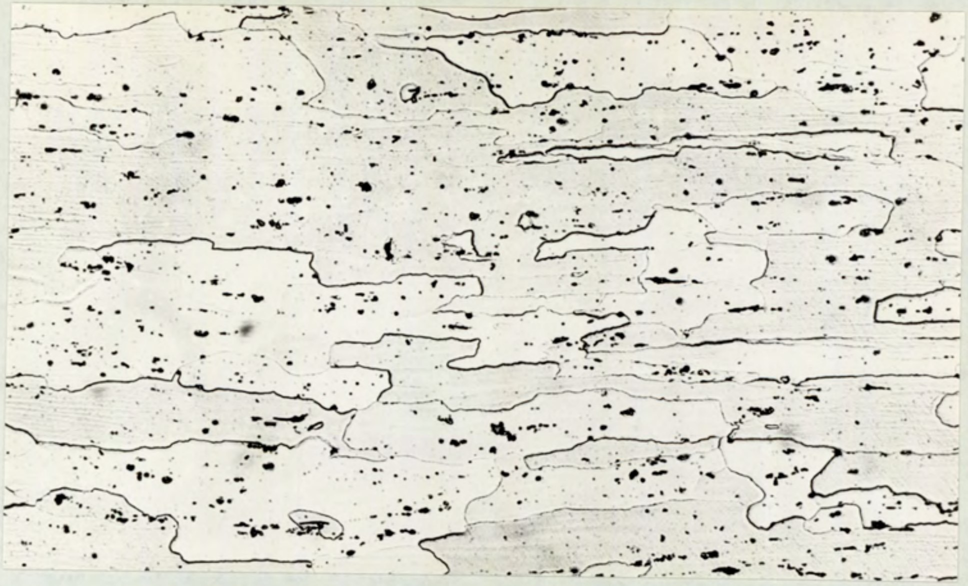

Fig. 38. Microstructure of N4. commercially hot rolled 94.5%. Transverse section, Mag. x200, Sample anodised.

Fig. 39. Microstructure of N4 commercially hot rolled 94.5%. Transverse section, Mag. x 750, Etch-$\frac{1}{2}$% HF.

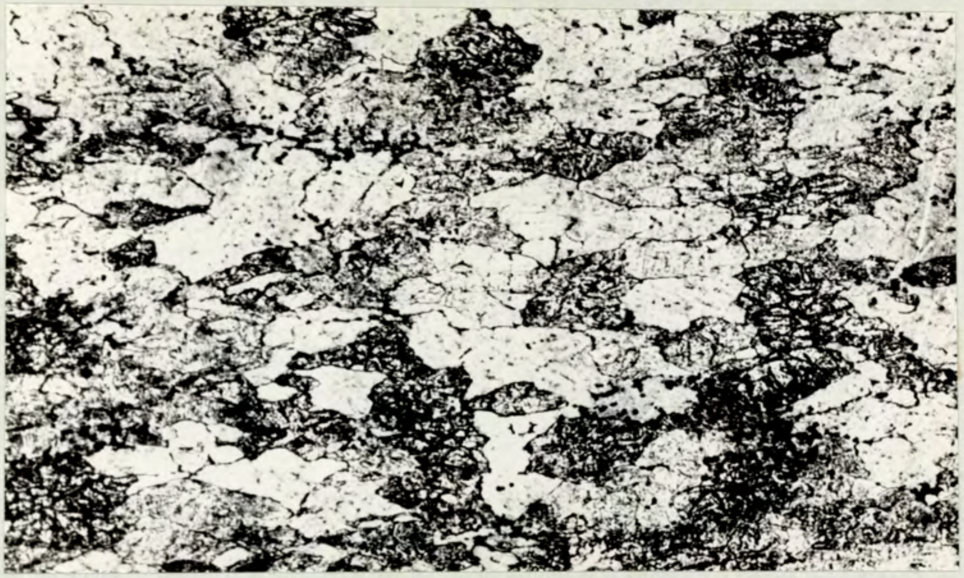

Fig. 40. Microstructure of H.15 hot compressed 50%. Transverse section, Mag. x75, Etch-mixed acids.

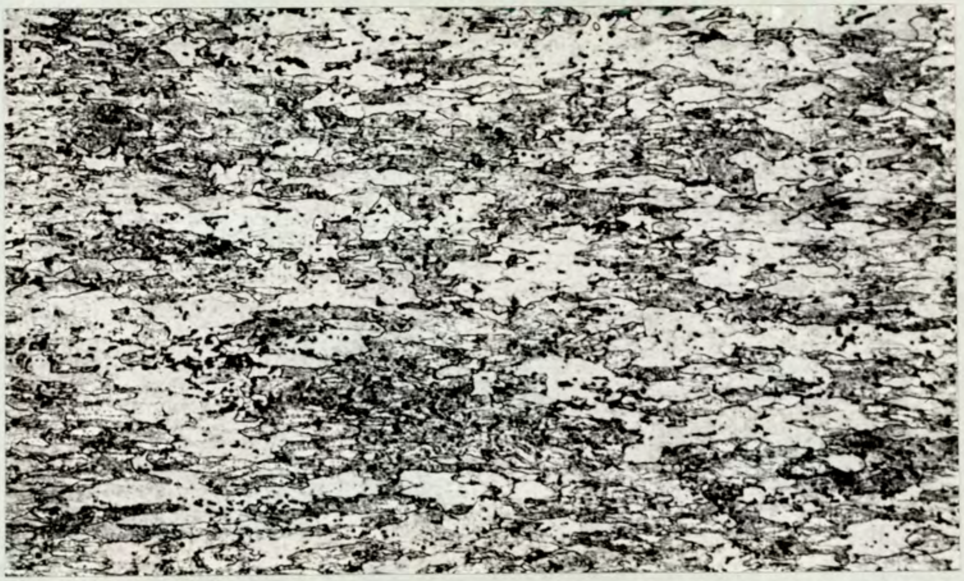

Fig. 41. Microstructure of H.15 hot compressed 73%. Transverse section, Mag. x75, Etch-mixed acids.

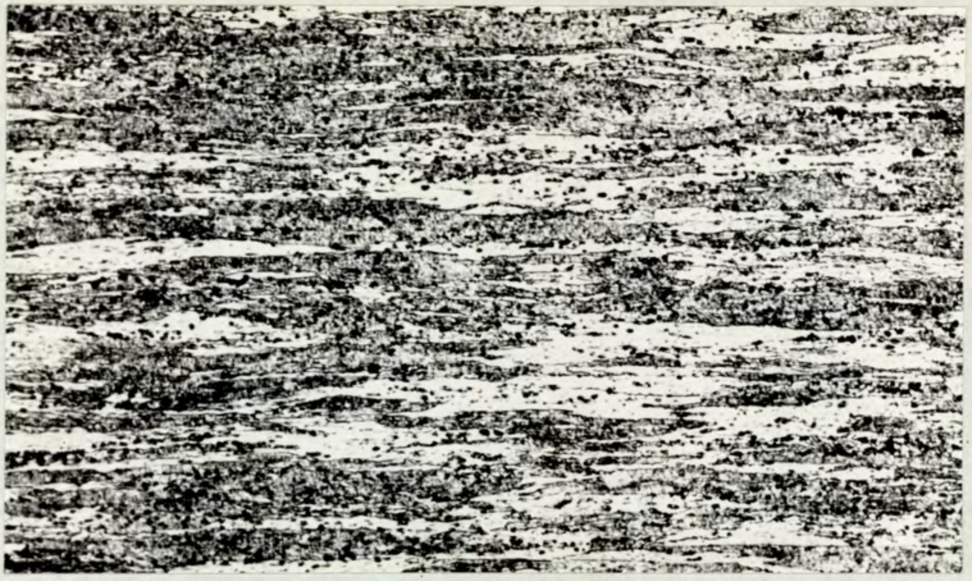

Fig. 42. Microstructure of Hl5. hot compressed 80%. Transverse section, Mag. x 75, Etch-mixed acids.

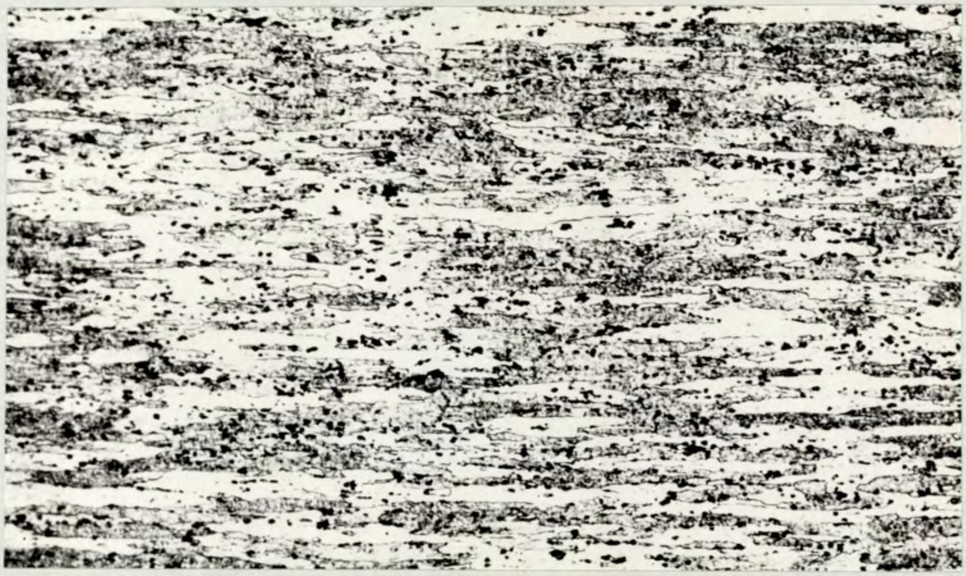

Fig. 43. Microstructure of Hl5. hot compressed 86%. Transverse section, Mag. x75, Etch-mixed acids.

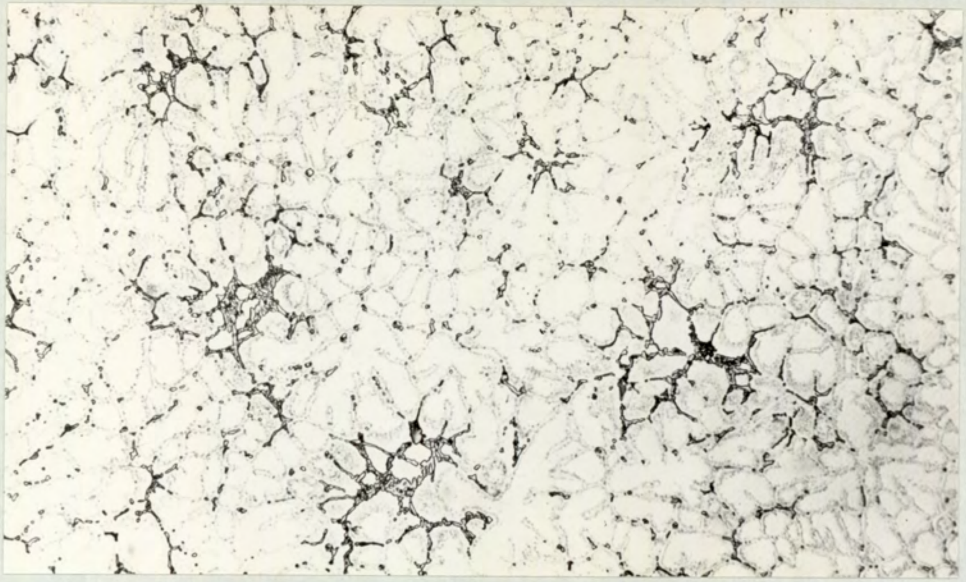

Fig. 44. Microstructure of H15 hot compressed 0%. Transverse section, Mag. x 150, Etch-$\frac{1}{2}$% HF.

Fig. 45. Microstructure of H.15 hot compressed 14%. Transverse section, Mag. x150, Etch-$\frac{1}{2}$% HF.

Fig. 46. Microstructure of H15 hot compressed 30%. Transverse section, Mag. x150, Etch-$\frac{1}{2}$% HF.

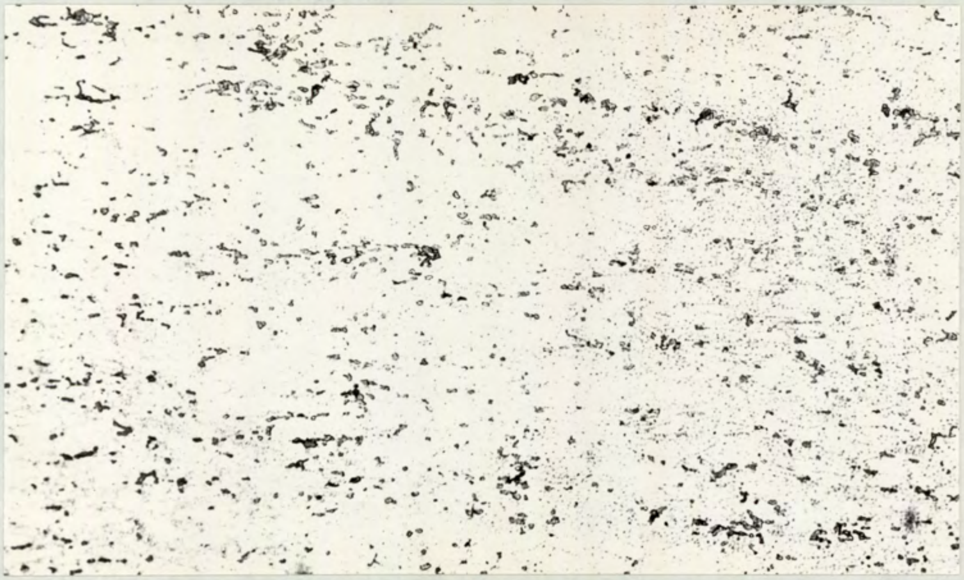

Fig. 47. Microstructure of H15 hot compressed 50%. Transverse section, Mag. x150, Etch-$\frac{1}{2}$% HF.

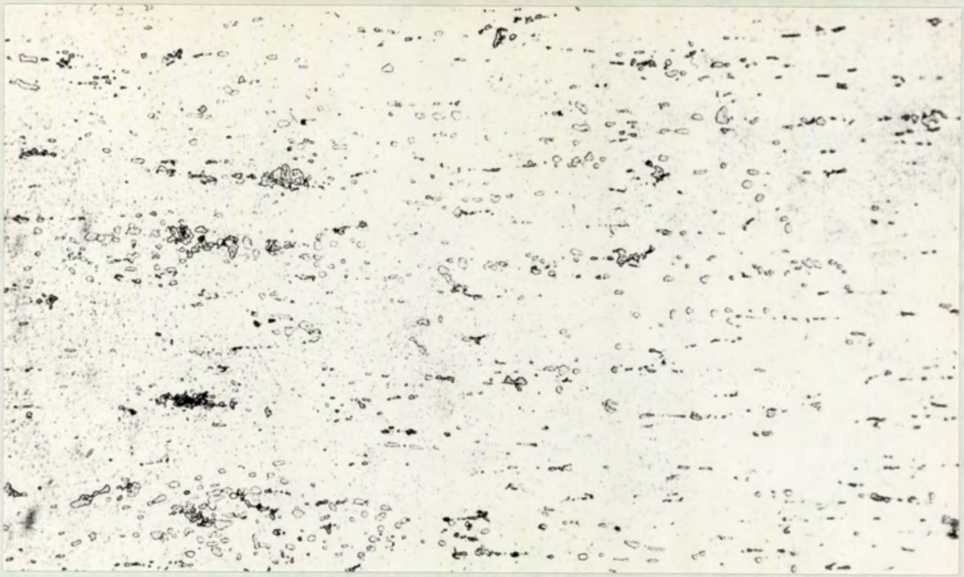

Fig. 48. Microstructure of H15 hot compressed 73%. Transverse section, Mag. x150, Etch-$\frac{1}{2}$% HF.

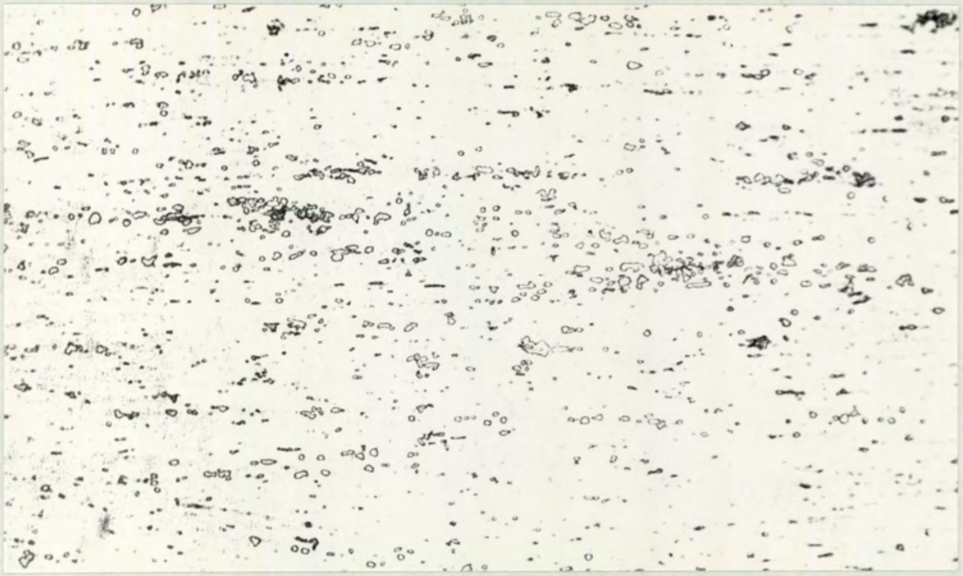

Fig. 49. Microstructure of H15 hot compressed 86%. Transverse section, Mag. x150, Etch-$\frac{1}{2}$% HF.

Fig. 50. Microstructure of N4 hot compressed 0%. Transverse section, Mag. x120, Sample anodised.

Fig. 51. Microstructure of N4 hot compressed 20%. Transverse section, Mag. x120, Sample anodised.

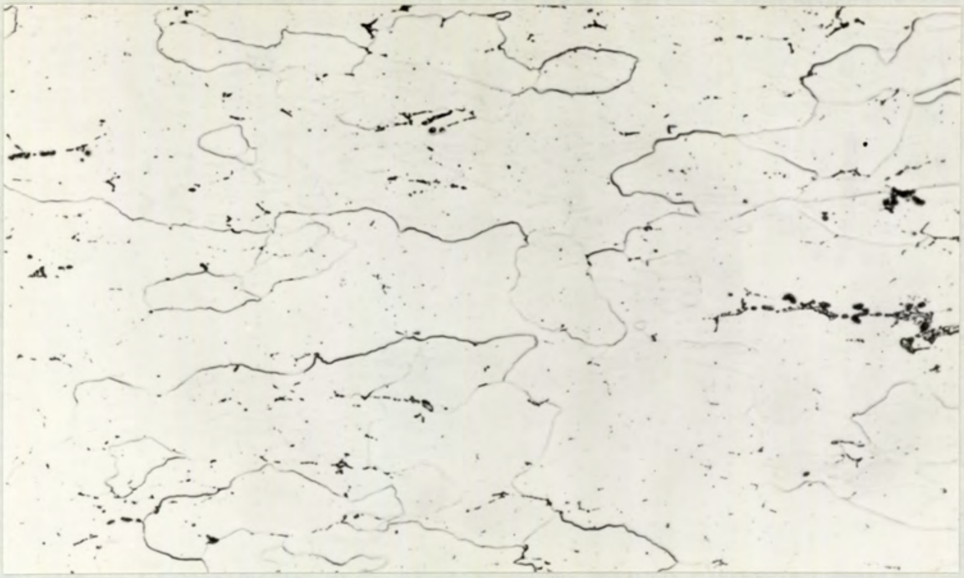

Fig. 52. Microstructure of N4 hot compressed 35%. Transverse section, Mag. x120, Sample anodised.

Fig. 53. Microstructure of N4 hot compressed 55%. Transverse section, Mag. x120, Sample anodised.

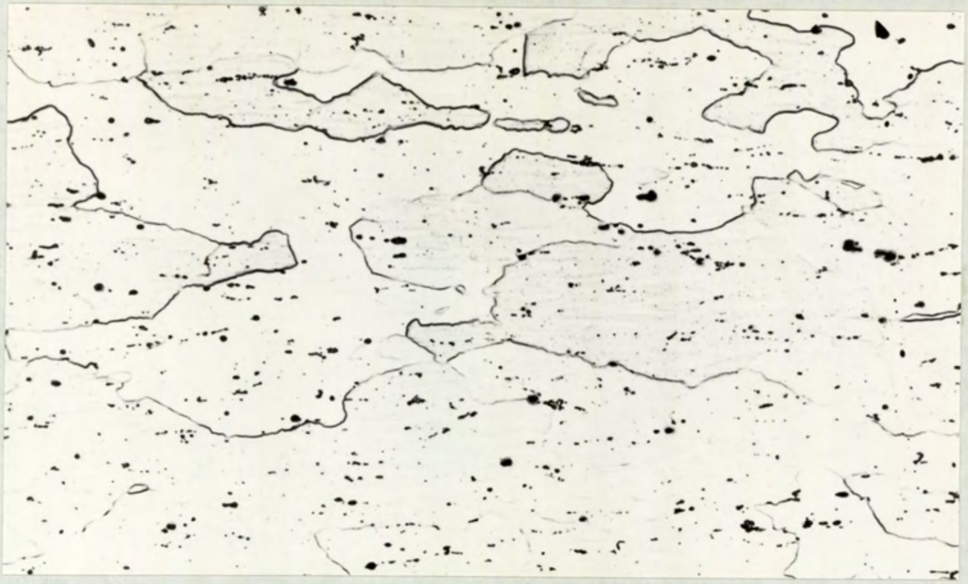

Fig. 54. Microstructure of N4 hot compressed 77%. Transverse section, Mag. x120, Sample anodised.

Fig. 55. Microstructure of N4 hot compressed 83%. Transverse section, Mag. x120, Sample anodised.

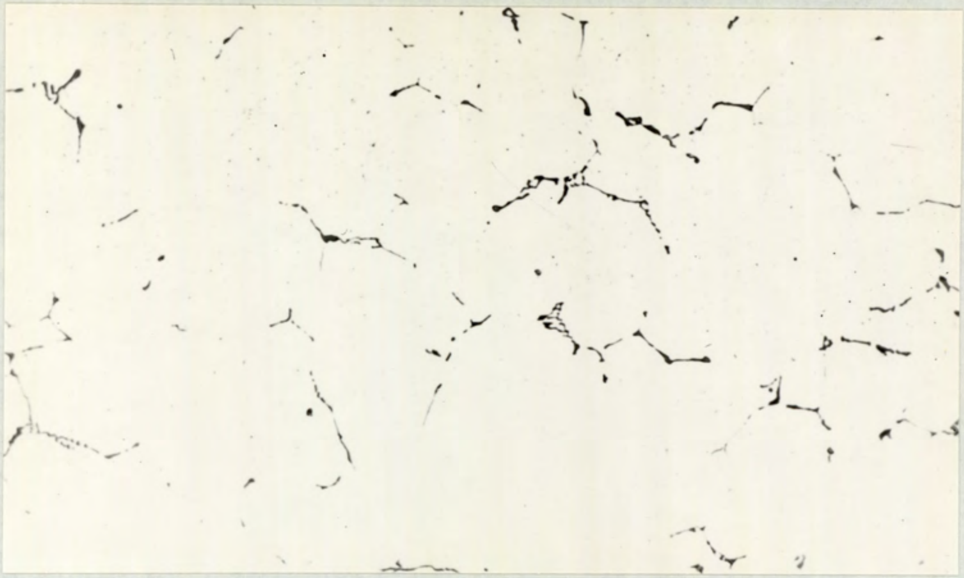

Fig. 56. Microstructure of N4 hot compressed 0%. Transverse section, Mag. x300, Etch-$\frac{1}{2}$% HF.

Fig. 57. Microstructure of N4 hot compressed 20%. Transverse section, Mag x300, Etch-$\frac{1}{2}$% HF.

Fig. 58. Microstructure of N4 hot compressed 35%.
Transverse section, Mag. x300, Etch-$\frac{1}{2}$% HF.

Fig. 59. Microstructure of N4 hot compressed 55%.
Transverse section, Mag. x300, Etch-$\frac{1}{2}$% HF.

Fig. 60. Microstructure of N4 hot compressed 77%. Transverse section, Mag. x300, Etch-$\frac{1}{2}$% HF.

Fig. 61. Microstructure of N4 hot compressed 83%. Transverse section, Mag. x300, Etch-$\frac{1}{2}$% HF.

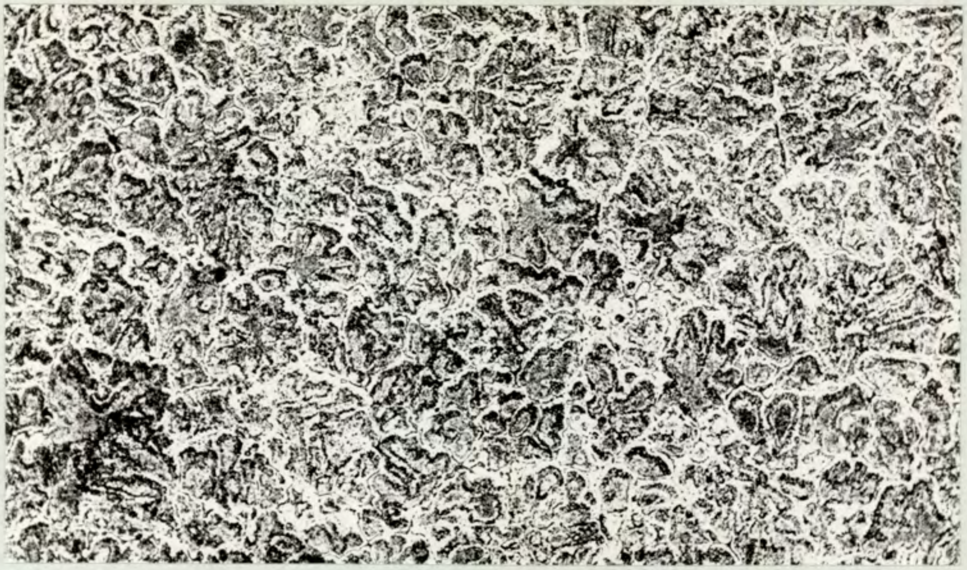

Fig. 62. Microstructure of DTD 683 hot compressed 0%. Transverse section, Mag. x120, Etch-10% NaOH.

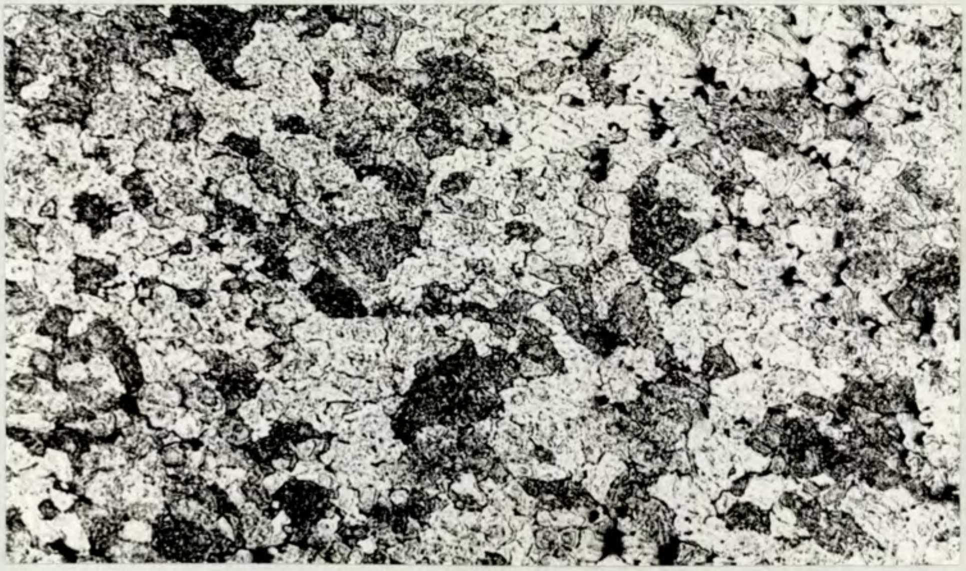

Fig. 63. Microstructure of DTD 683 hot compressed 20%. Transverse section, Mag. x120, Etch-10% NaOH.

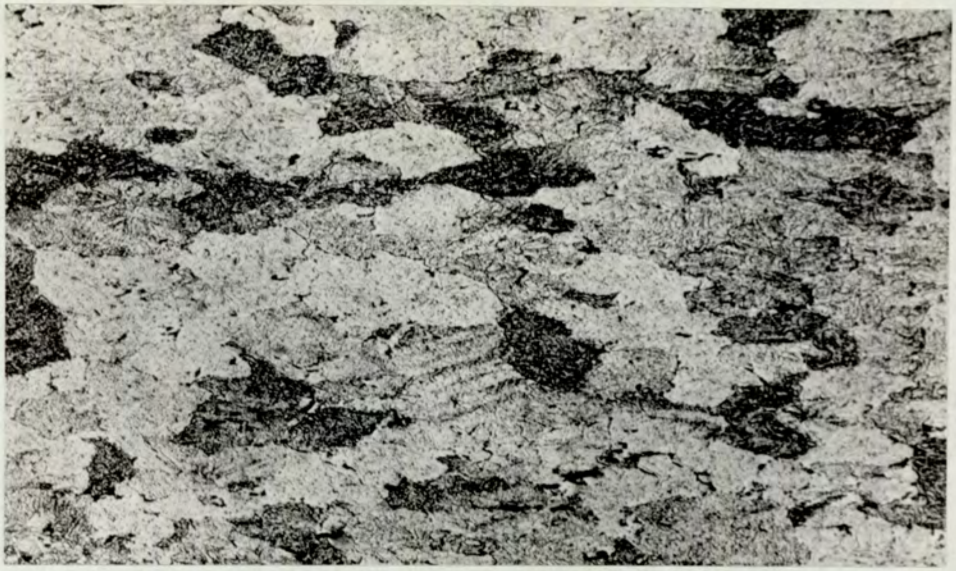

Fig. 64. Microstructure of DTD 683 hot compressed 35%. Transverse section, Mag. x120, Etch-10% NaOH

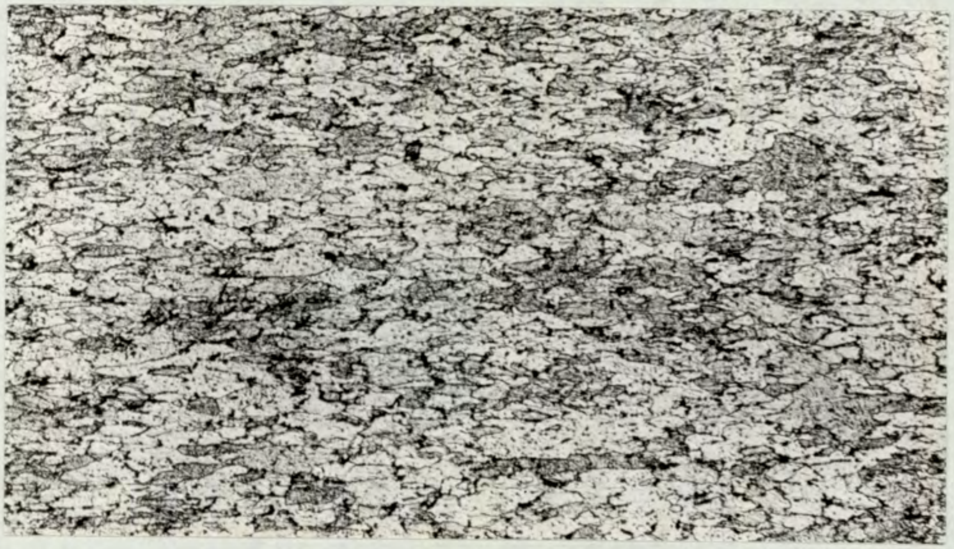

Fig. 65. Microstructure of DTD 683 hot compressed 73%. Transverse section, Mag. x120, Etch-10% NaOH

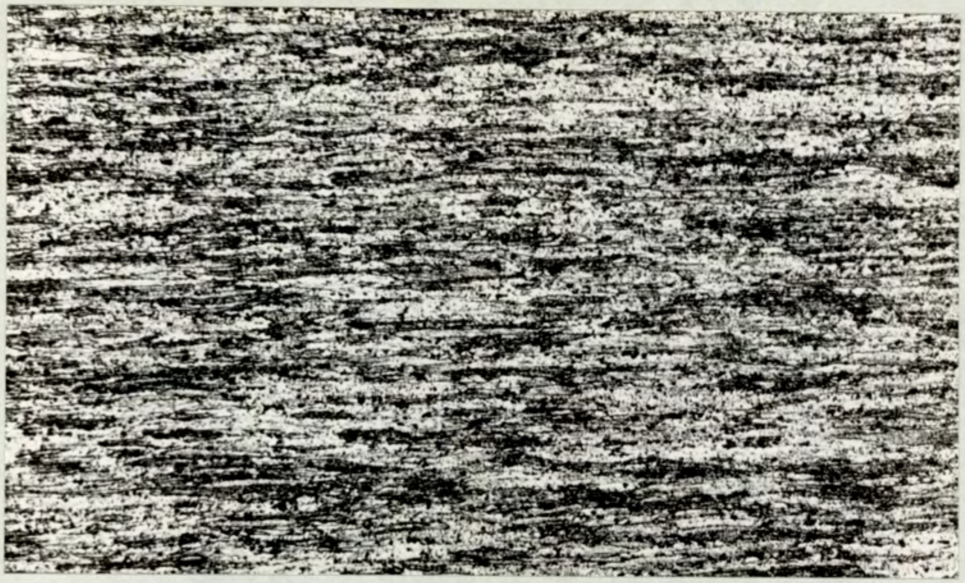

Fig. 66. Microstructure of DTD 683 hot compressed 85%. Transverse section, Mag. x120, Etch-10% NaOH

Fig. 67. Microstructure of DTD 683 hot compressed 0%. Transverse section, Mag. x450, Etch-$\frac{1}{2}$% HF.

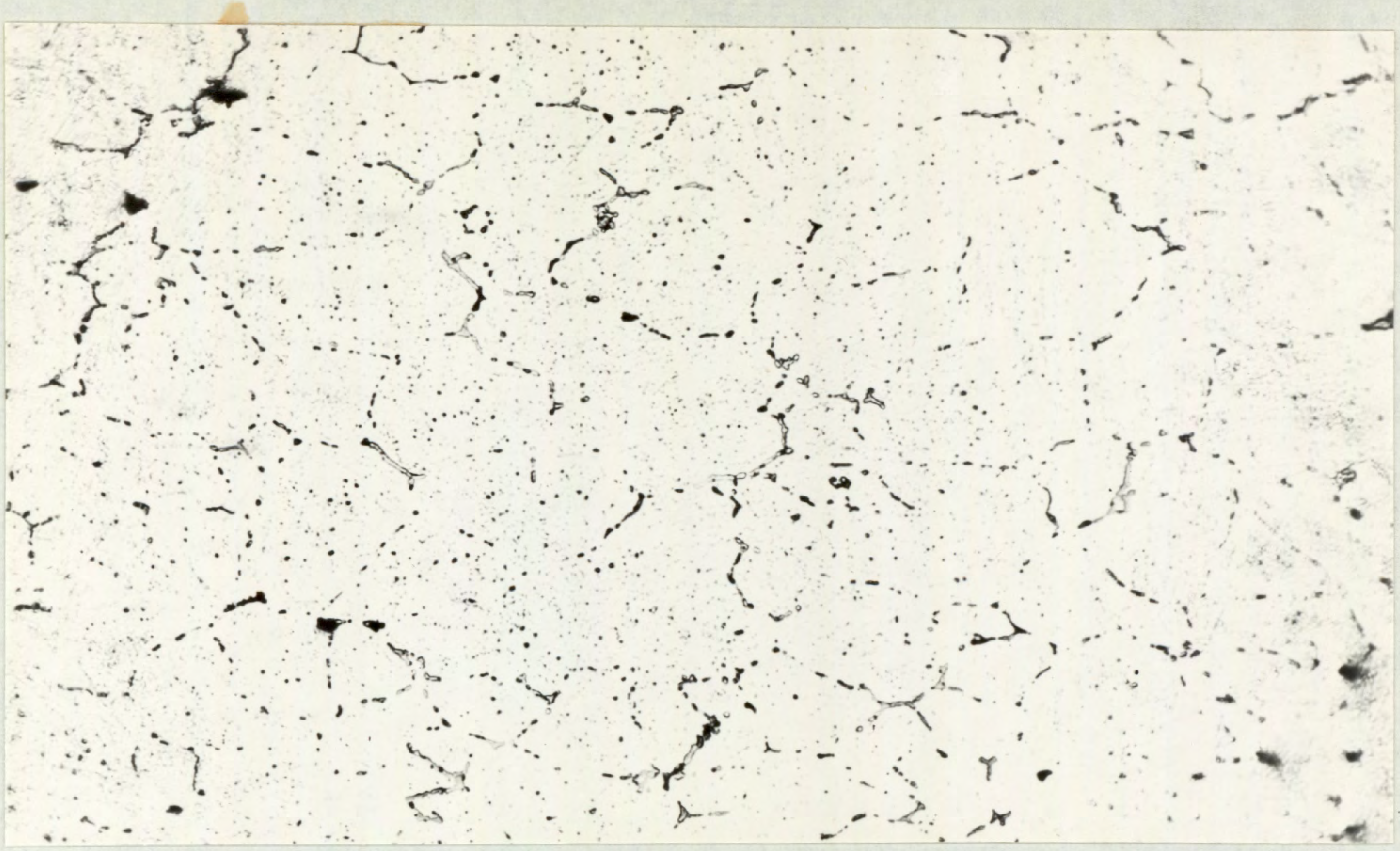

Fig. 68. Microstructure of DTD 683 hot compressed 20%. Transverse section, Mag. x450, Etch-$\frac{1}{2}$% HF.

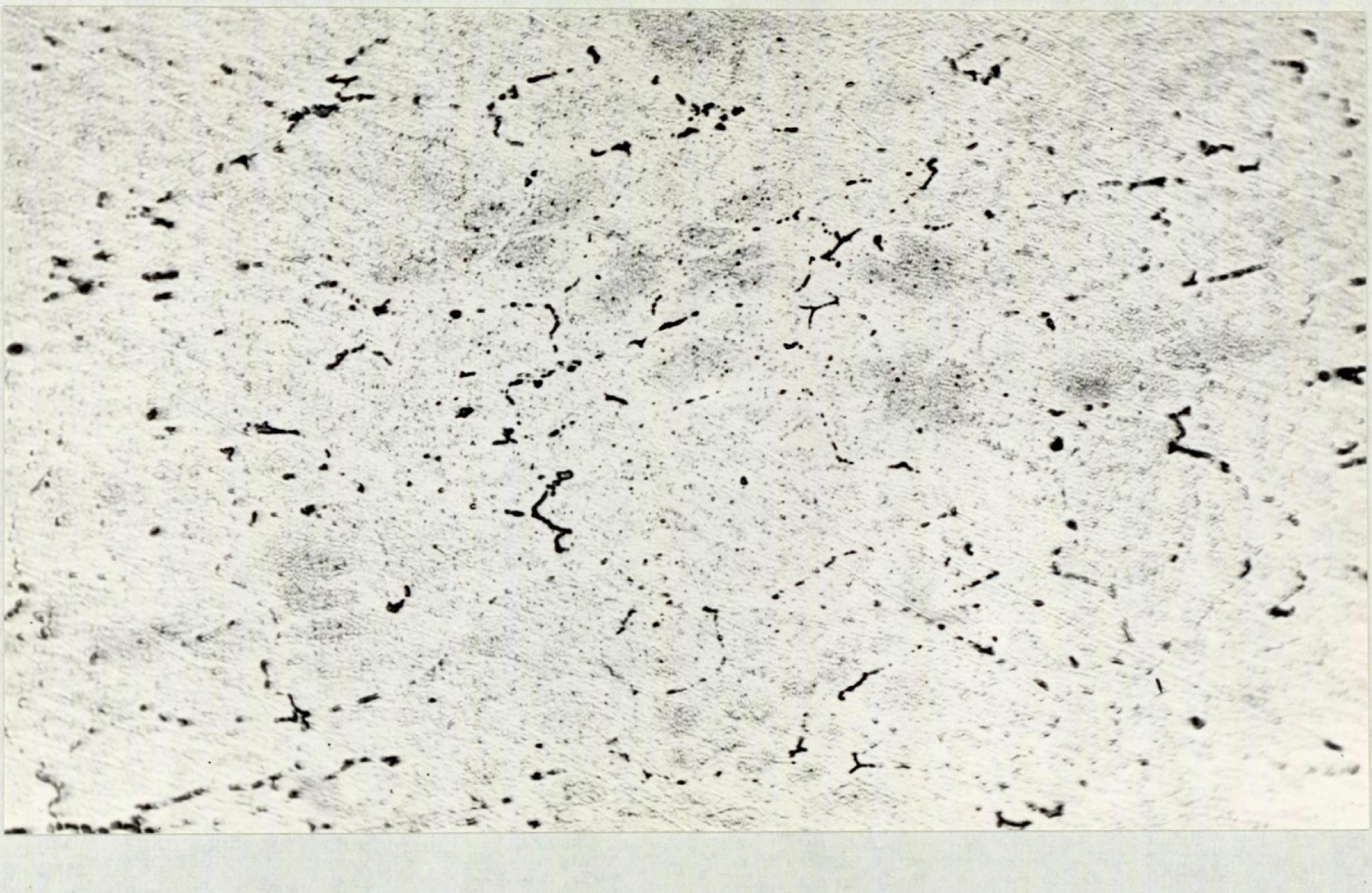

Fig. 69. Microstructure of DTD 683, hot compressed 35%. Transverse section, Mag. x450, Etch-$\frac{1}{2}$% HF.

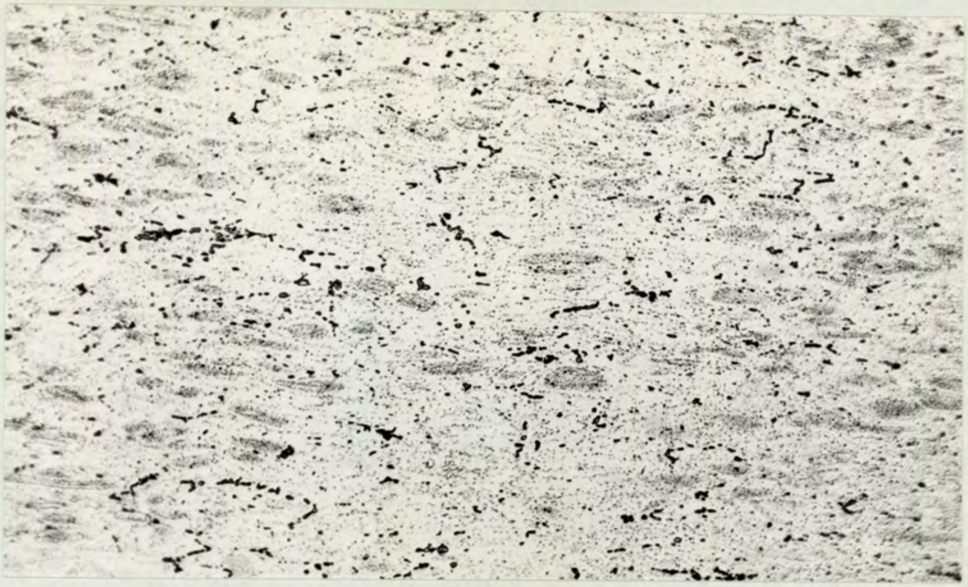

Fig. 70. Microstructure of DTD 683 hot compressed 73%. Transverse section, Mag. x450, Etch-½% H.F.

Fig. 71. Microstructure of DTD 683 hot compressed 85%. Transverse section, Mag. x450, Etch-½% HF.

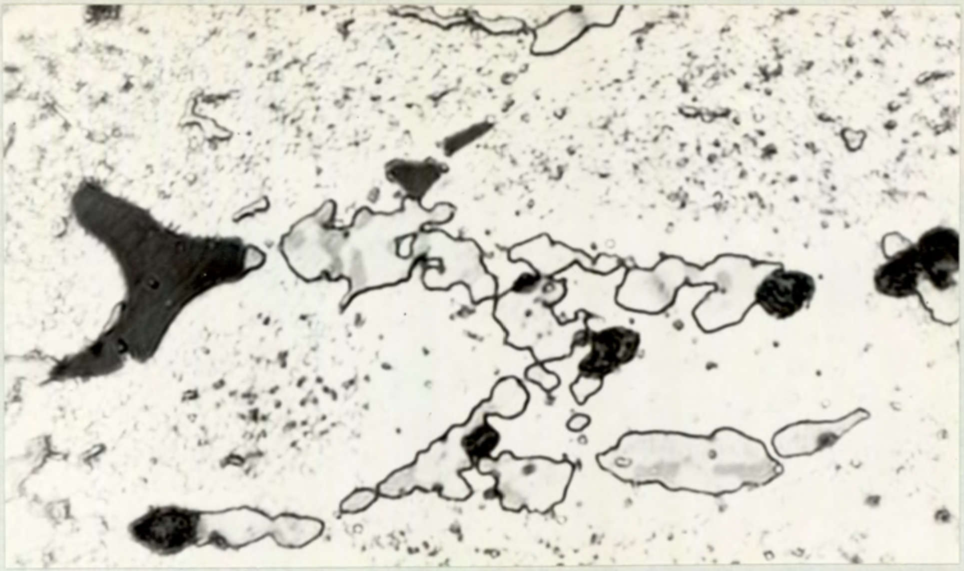

Fig. 72. Microstructure of Hl5 showing mechanical breakdown of the phase $CuAl_2$. Mag. x2500, Etch-$\frac{1}{2}$% HF.

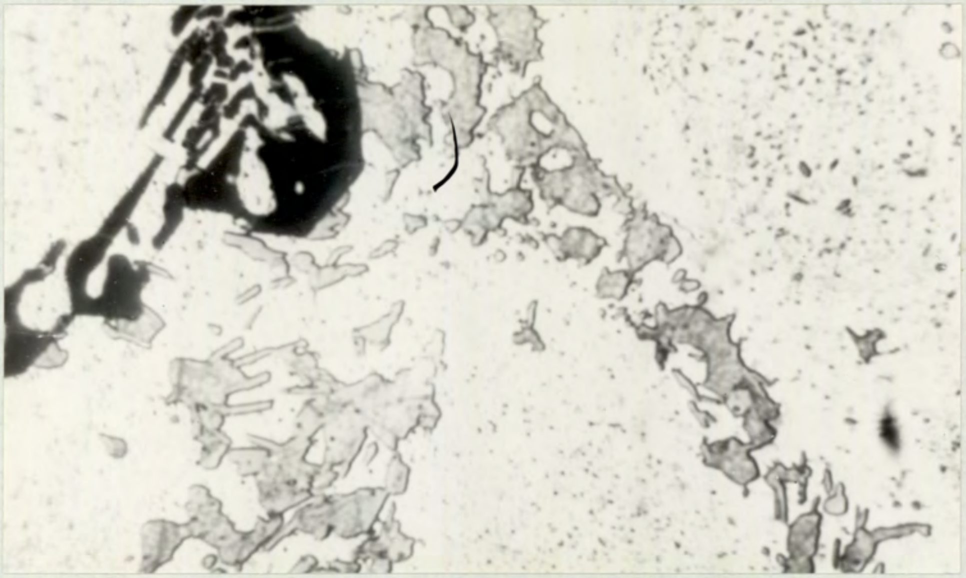

Fig. 73. Microstructure of Hl5 commercially hot rolled 68% showing fracture of c-Al(Mn, Fe)Si phase. mag. x2000, Etch-$\frac{1}{2}$%HF.

Fig. 74. Microstructure of H15 commercially hot rolled 68% showing the effects of working on $CuAl_2$ and c-Al(Mn, Fe)Si. Mag. x1000, Etch -$\frac{1}{2}$% HF.

Fig. 75. Microstructure of H15 commercially hot rolled showing the amount and distribution of the two major phases; $CuAl_2$ and c-Al(Mn, Fe)Si. Mag. x75, Etch - $\frac{1}{2}$% HF.

Fig. 76. Microstructure of N4 commercially hot rolled showing the amount and distribution of the major phase $FeAl_3$ Mag. x 75 Etch -$\frac{1}{2}$% HF.

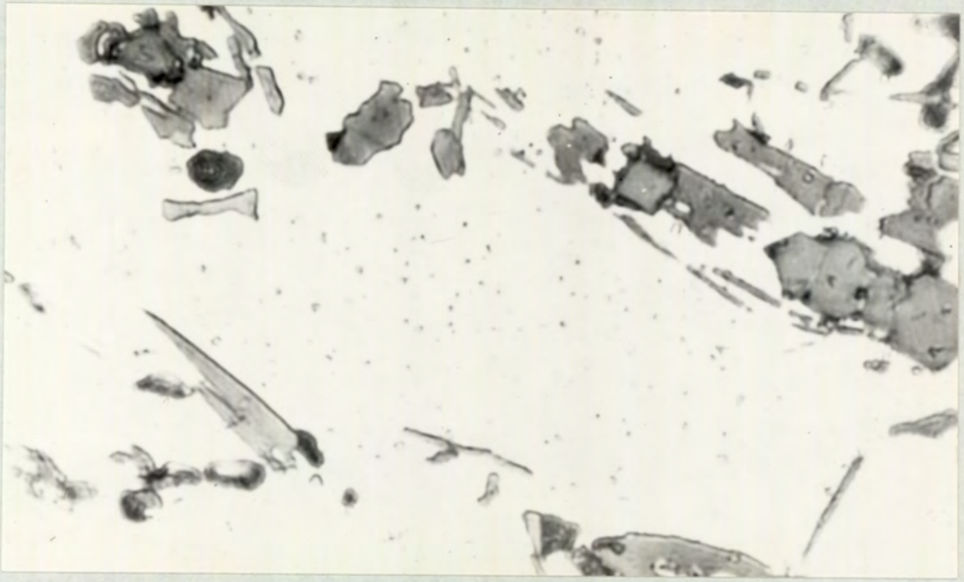

Fig. 77. Microstructure of N4, commercially hot rolled showing fracture of $FeAl_3$ needles. Mag. x3000, Etch - $\frac{1}{2}$% HF.

Fig. 78. Microstructure of N4 commercially hot rolled showing fracture of $FeAl_3$ needles. Mag. x1000, Etch - ½% HF.

Fig. 79. Electron micrograph of fractured c-Al(Mn, Fe) Si phase in commercially hot rolled H15. alloy. Mag. x5000, Carbon replica of sample in the electropolished condition.

Fig, 80. Electron micrograph of unfractured particles of $CuAl_2$ and Al_2CuMg in commercially hot rolled H15 alloy. Mag. x8000, Shadowed carbon replica of the sample in the electropolished condition.

Fig, 81. Electron micrograph of unfractured particles of $CuAl_2$ and Al_2CuMg in commercially hot rolled H15 alloy. Mag. x6000, Shadowed carbon replica of sample in the electropolished condition.

Fig. 82. Electron micrograph showing tendency for the two phases $CuAl_2$ and Al_2CuMg to separate during hot rolling. Mag. x5000, shadowed carbon replica of sample in the electropolished condition.

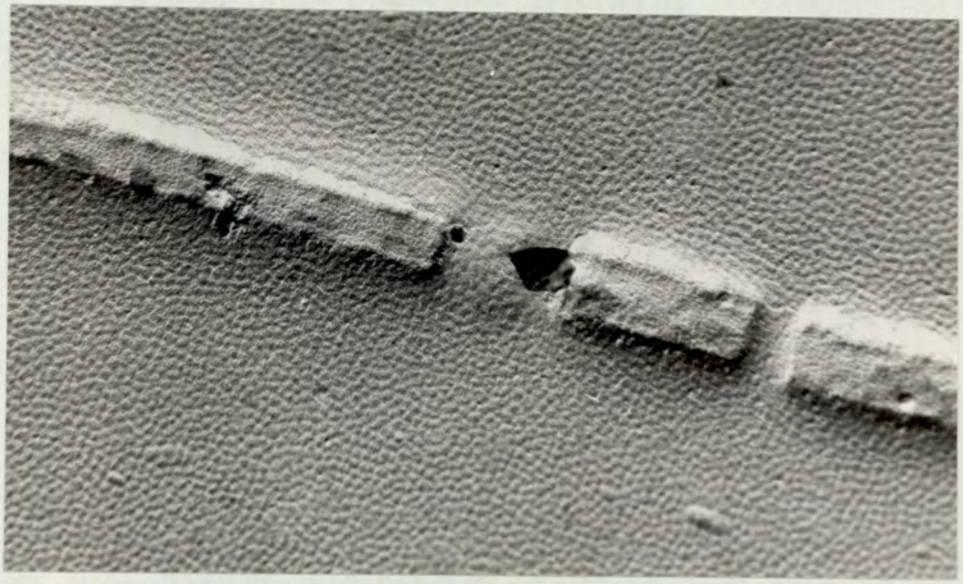

Fig. 83. Electron micrograph showing the fracture of $FeAl_3$ needles during the commercial hot rolling of N4. Mag. x6000, shadowed carbon replica of sample in the electropolished condition.

Fig. 84. Electron micrograph showing the fracture of $FeAl_3$ needle during the commercial hot rolling of N4. Mag. x10000 shadowed carbon replica of sample in the electropolished condition.

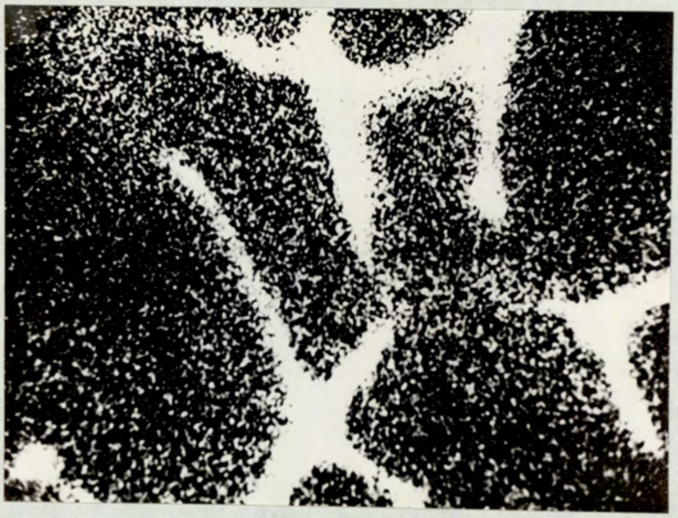

Fig. 85. Copper distribution in the intermetallics and matrix of hot rolled H15. Mag. x800.

Fig. 86. Manganese distribution in the intermetallics and matrix of hot rolled H15. Mag. x800.

Fig. 87. Iron distribution in the intermetallics and matrix of hot rolled H15. Mag. x800.

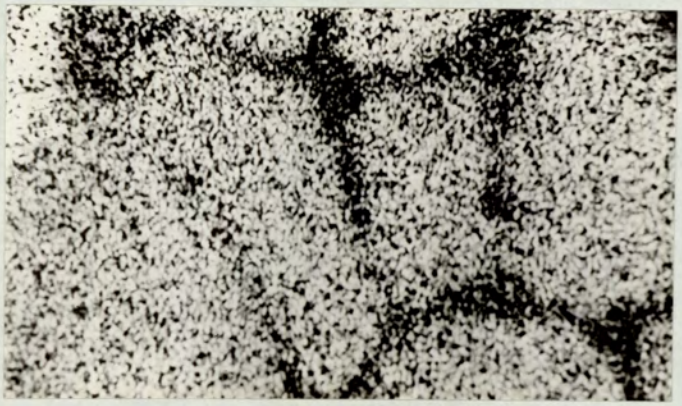

Fig. 88. Aluminium distribution in the intermetallics and matrix of hot rolled H15. Mag. x800.

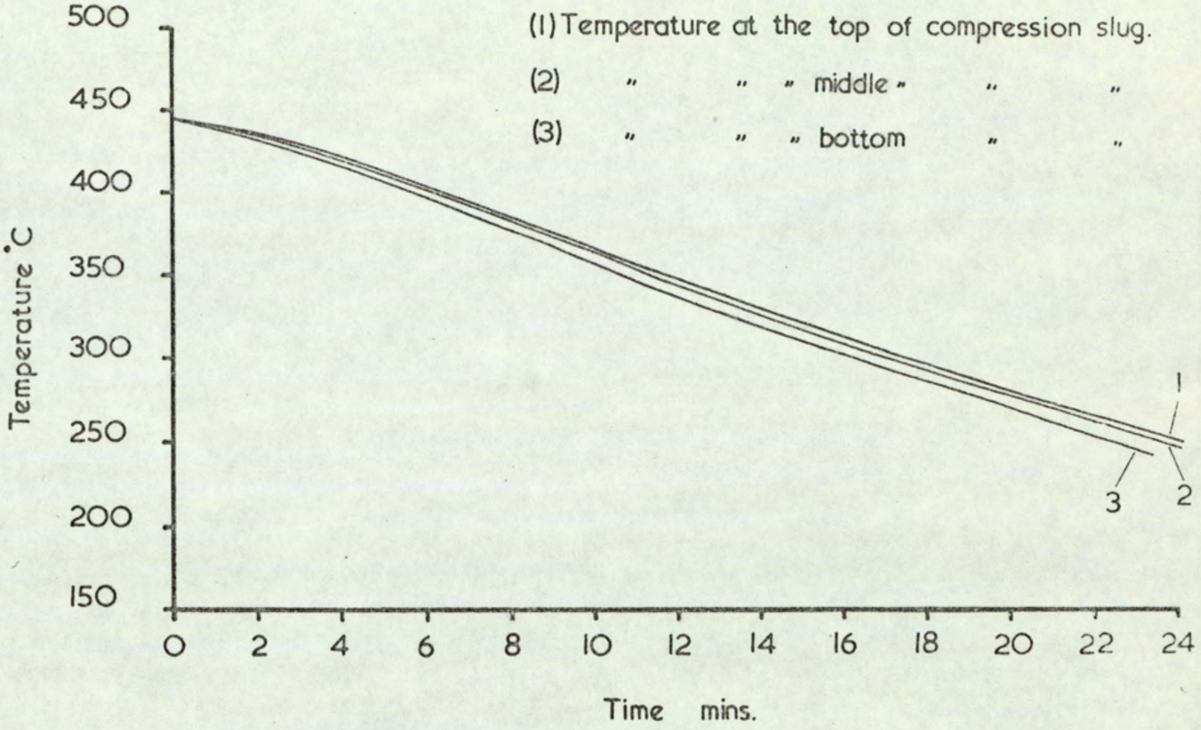

Fig, 89. Cooling curve for a compression slug contained in the die-set. The cooling curve is plotted from measured values of temperature as the heated die-set assembly cools from an initial pre-heat temperature of 450°C. whilst inposition on the press.

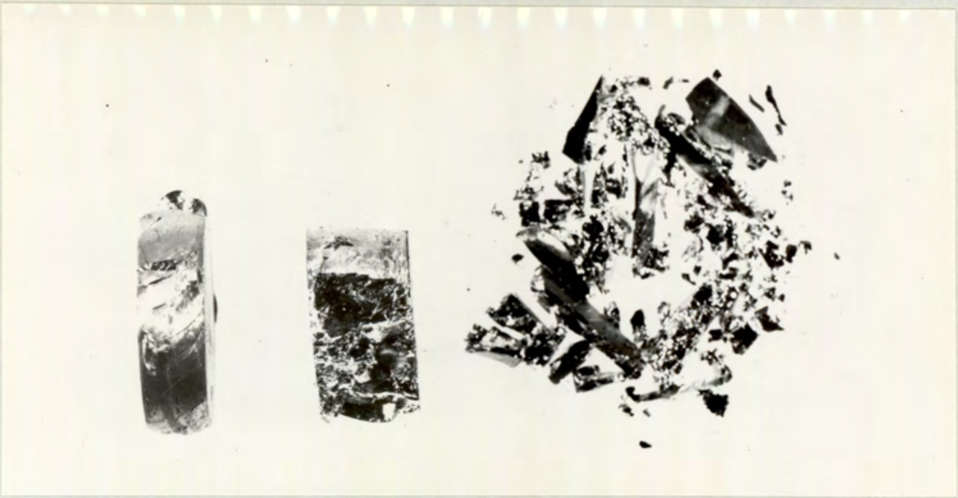

(a) (b)

Fig. 90. The effect of compression on samples of pure $CuAl_2$. (a) 57% reduction at 540°C. (b) 37% reduction at 460°C. Approx. 1.3 x actual size.

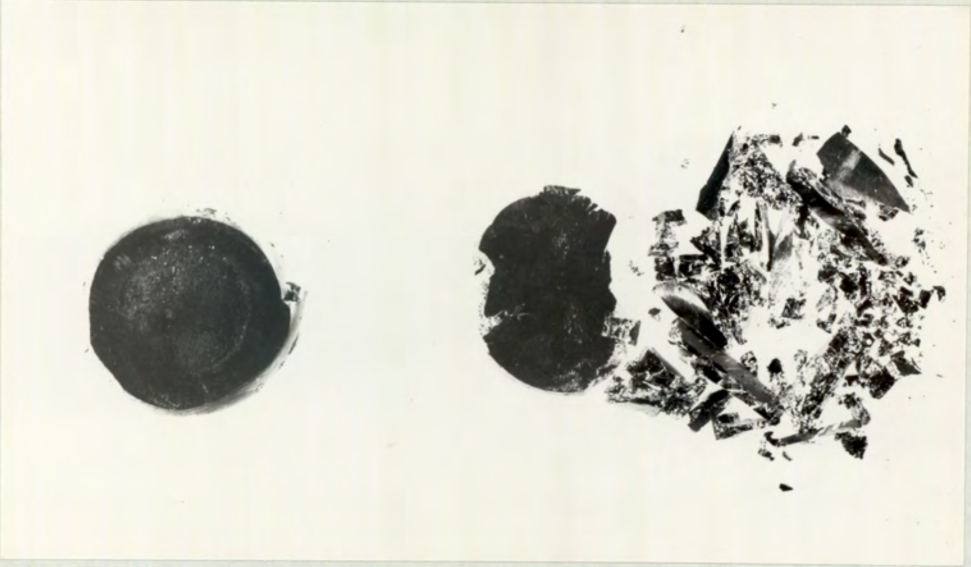

(a) (b)

Fig. 91. The effect of hot compression on samples of pure $CuAl_2$. (a) 57% reduction at 540°C. (b) 37% reduction at 460°C. The photograph shows splintering which results from the presence of cracks produced by contraction stresses during solidification. Approx. 1.3 x actual size.

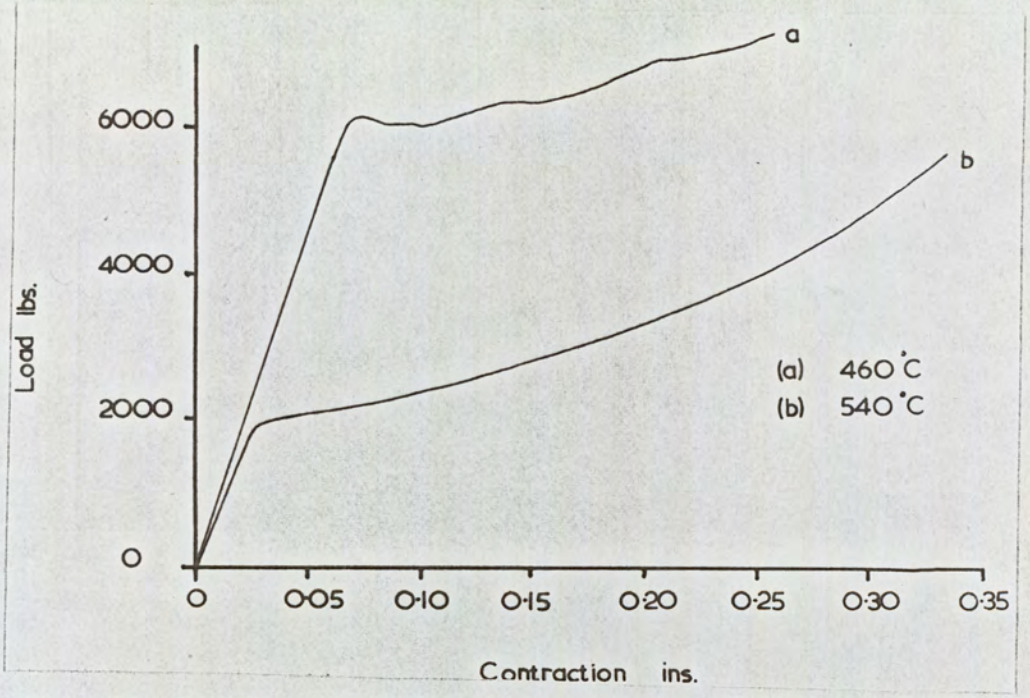

Fig. 92. Load-contraction diagrams for the hot compression of pure $CuAl_2$.

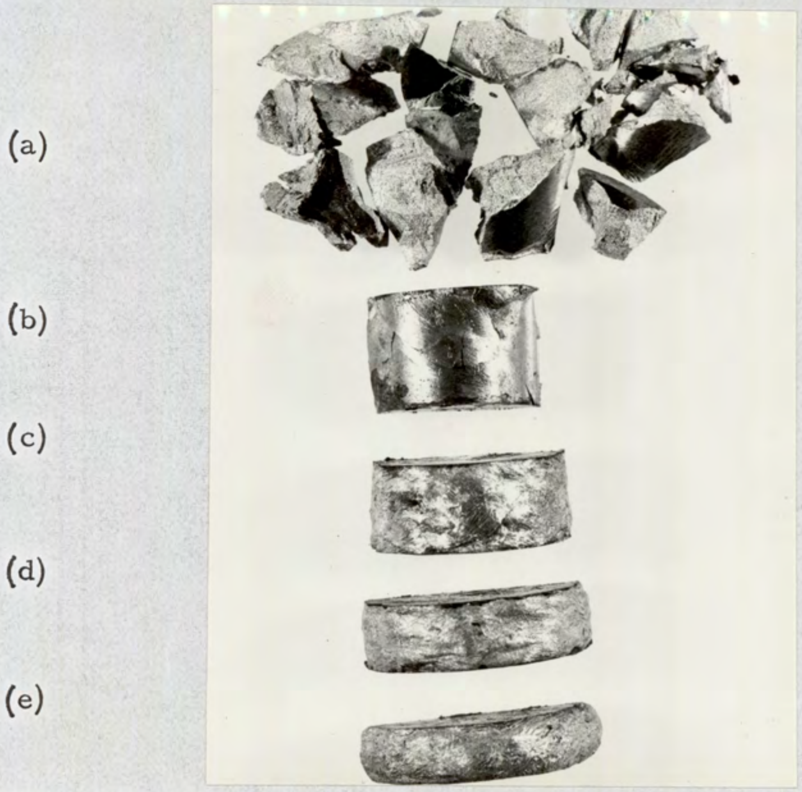

Fig. 93. The effect of hot compression on samples of aluminium 40% copper alloy. Tests were conducted at the following temperatures. (a) 20°C. (b) 250°C. (c) 350°C. (d) 450°C. (e) 500°C. Approx. 1.3 x actual size.

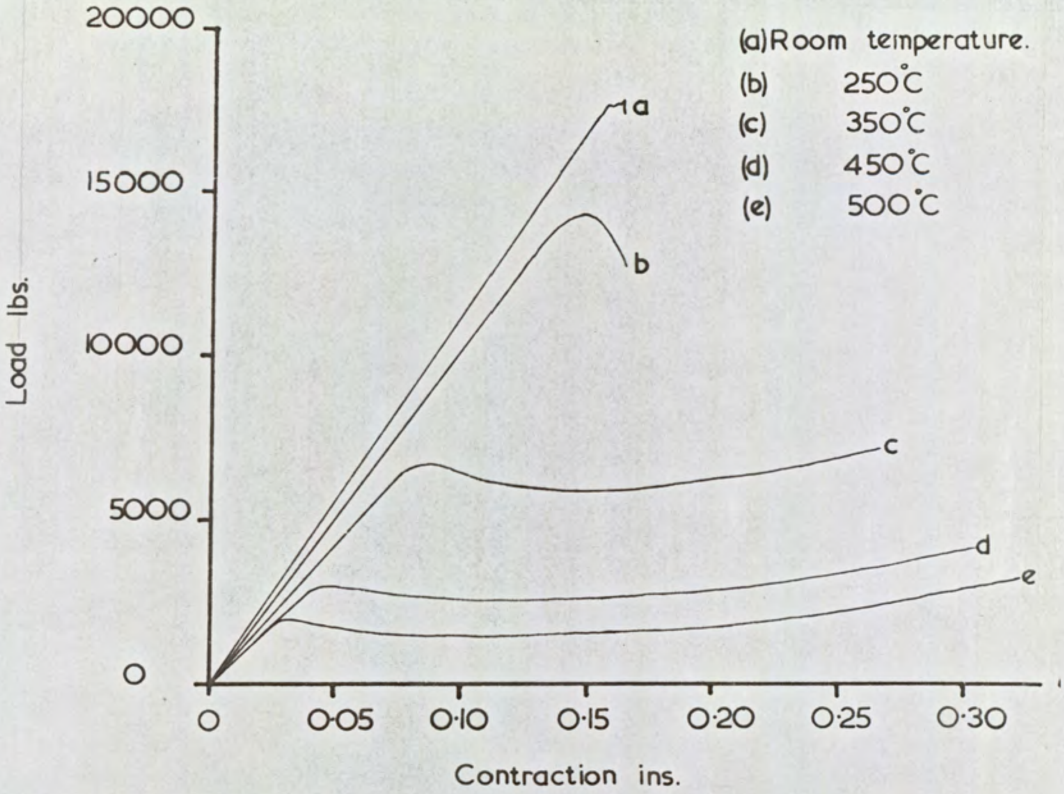

Fig. 94. Load-contraction diagrams for the aluminium 40% copper alloy over the temperature range 20-500°C.

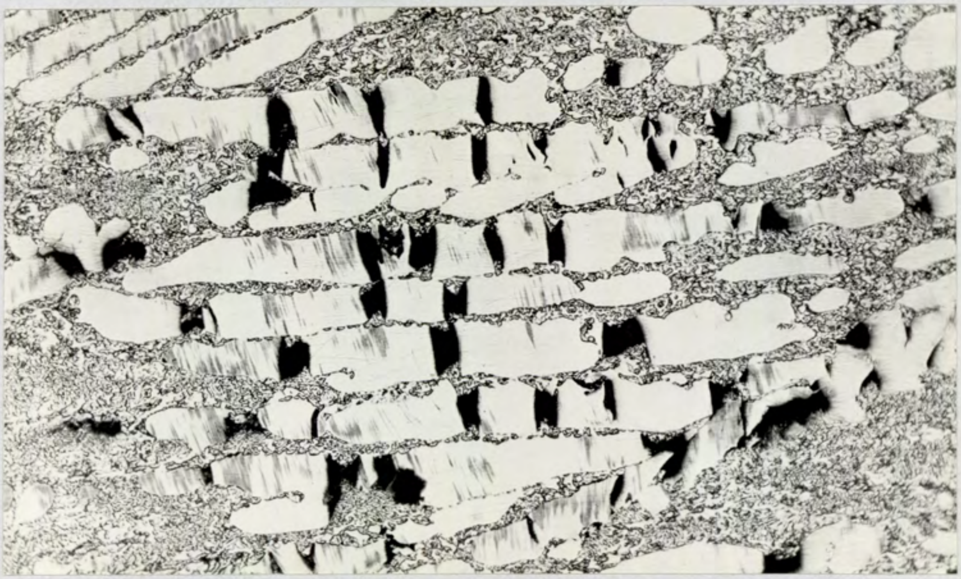

Fig. 95. The fracture of $CuAl_2$ plates during hot compression at 250°C. Mag. x150 Etch - ½% HF.

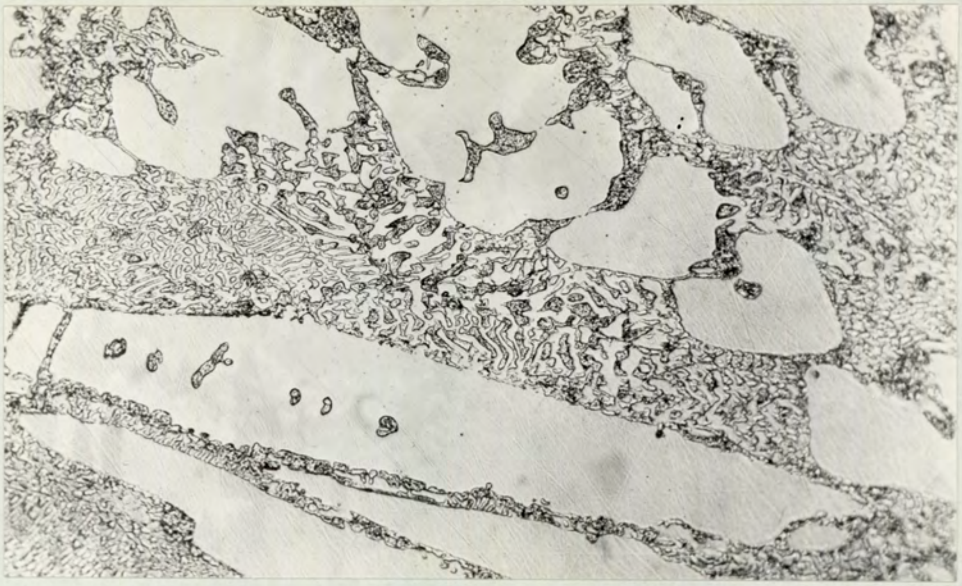

Fig. 96. Plates of $CuAl_2$ unfractured by hot compression at 500°C. Mag. x150. Etch -½% HF.

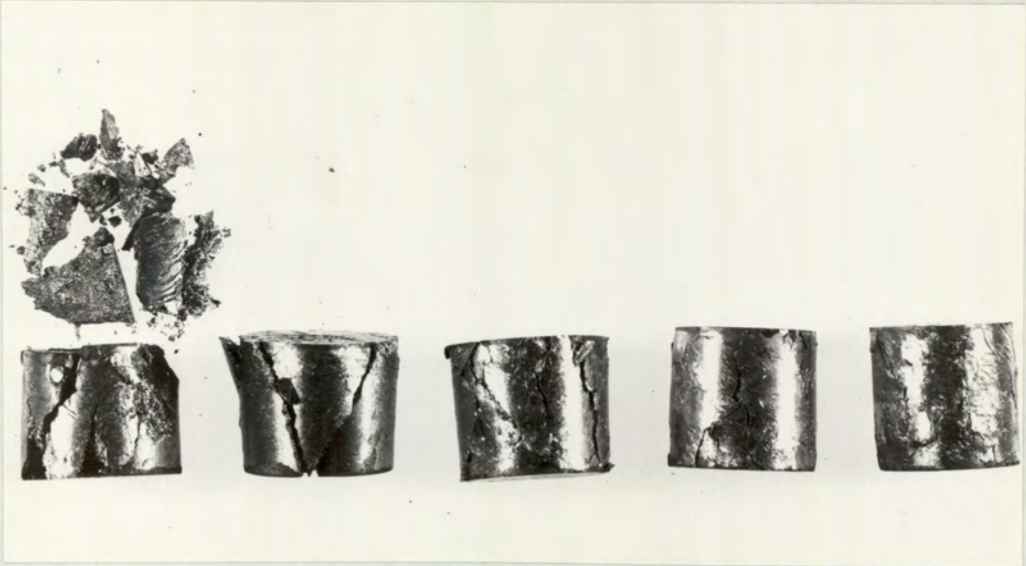

(a) (b) (c) (d) (e)

Fig. 97. The effect of hot compression on samples of aluminion 32% iron. The compression tests were carried out at the following temperatures. (a) 20°C. (b) 250°C. (c) 350°C. (d) 450°C. (e) 500°C.

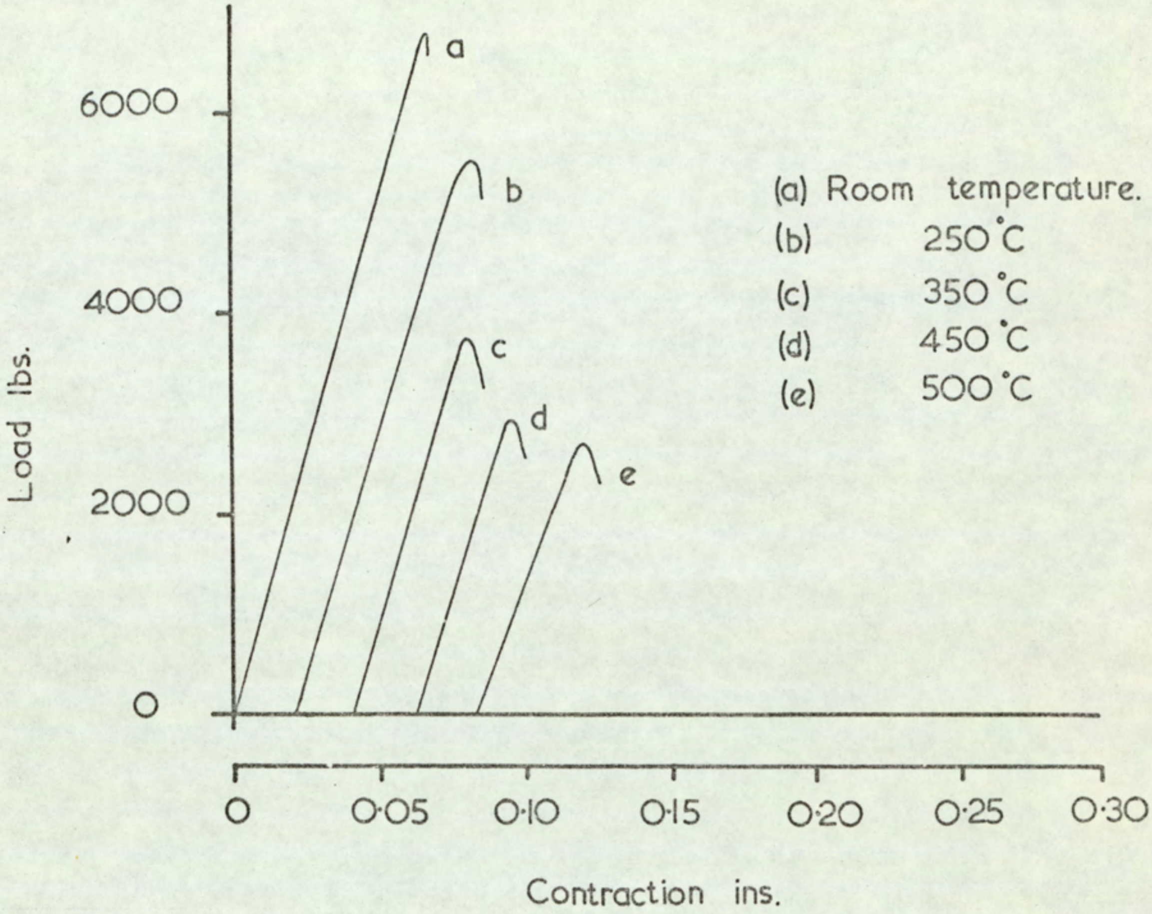

Fig. 98. Load-contraction diagrams for the aluminium 32% iron alloy. The contraction scale is displaced to avoid the confusion of using a common origin for all the curves plotted.

(a) (b) (c)

Fig. 99. The effect of hot compression on samples of pure $MgZn_2$. Compression tests were carried out at the following temperatures. (a) 20°C. (b) 420°C. (c) 500°C.

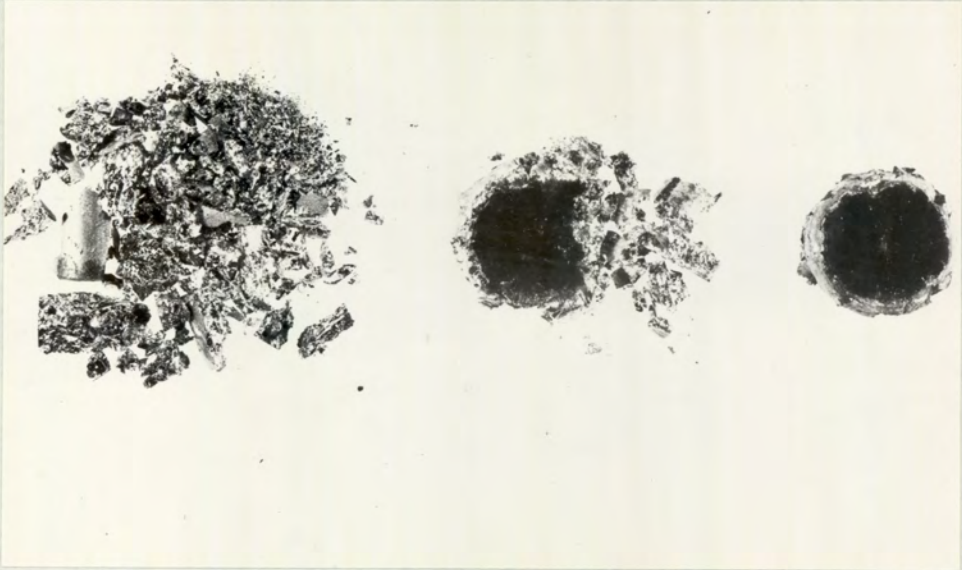

(a) (b) (c)

Fig. 100. The effects of hot compression on samples of pure $MgZn_2$. Compression tests were carried out at the following temperatures. (a) 20°C. (b) 420°C. (c) 500°C.

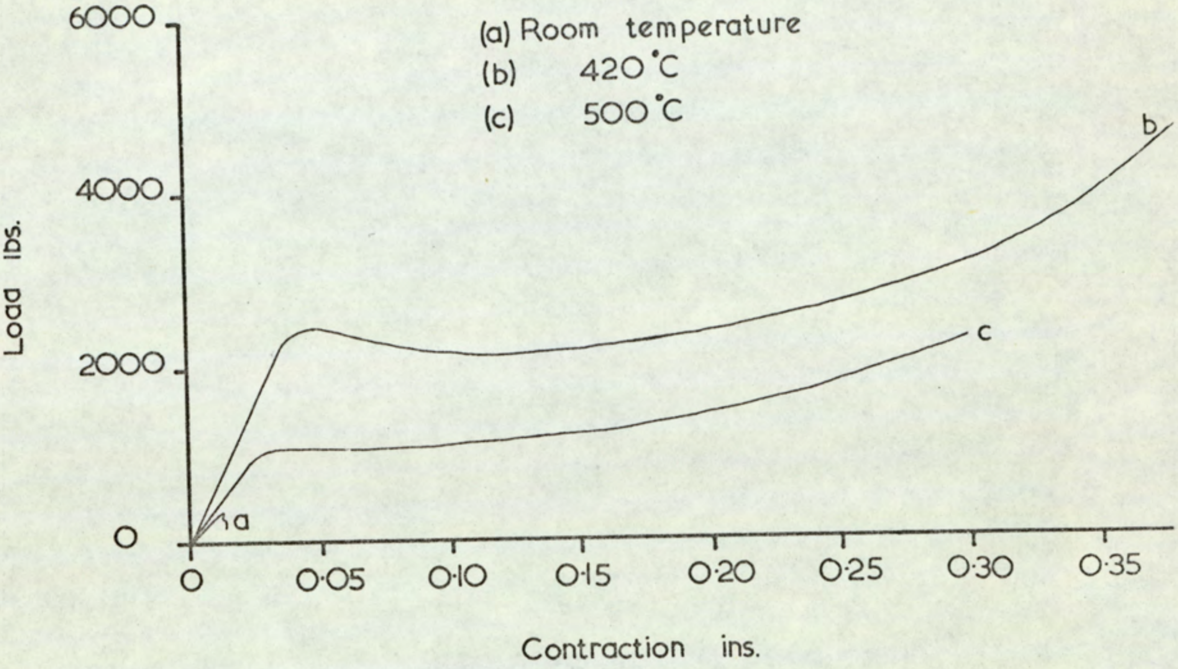

Fig. 101. Load-contraction diagrams for the hot compression of pure $MgZn_2$.

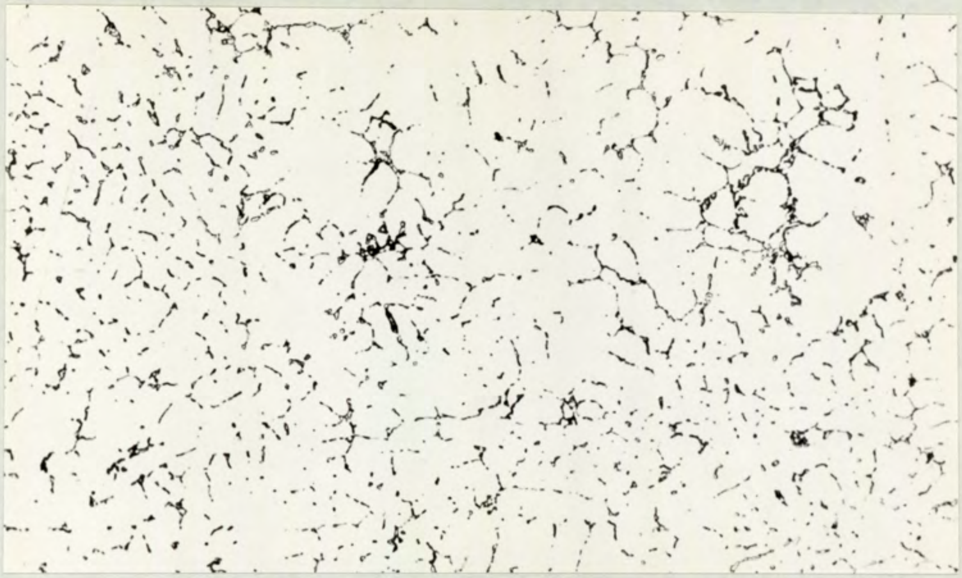

Fig. 102. Microstructure of aluminium 8% copper alloy chill cast. Mag. x250. Etch - 25% ferric nitrate.

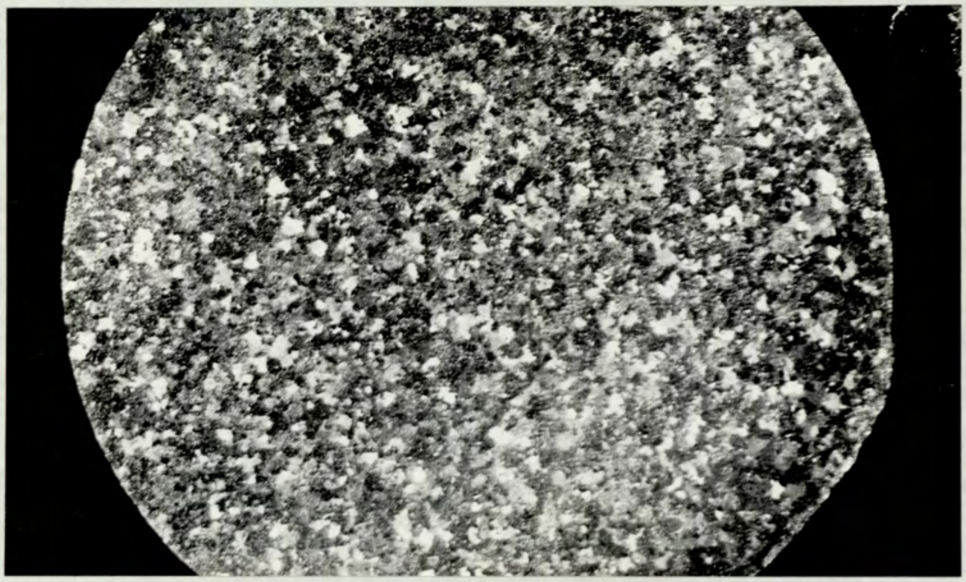

Fig. 103. Macrostructure of aluminium 8% copper alloy chill cast. Mag. x8, Etch -15% phosphoric acid.

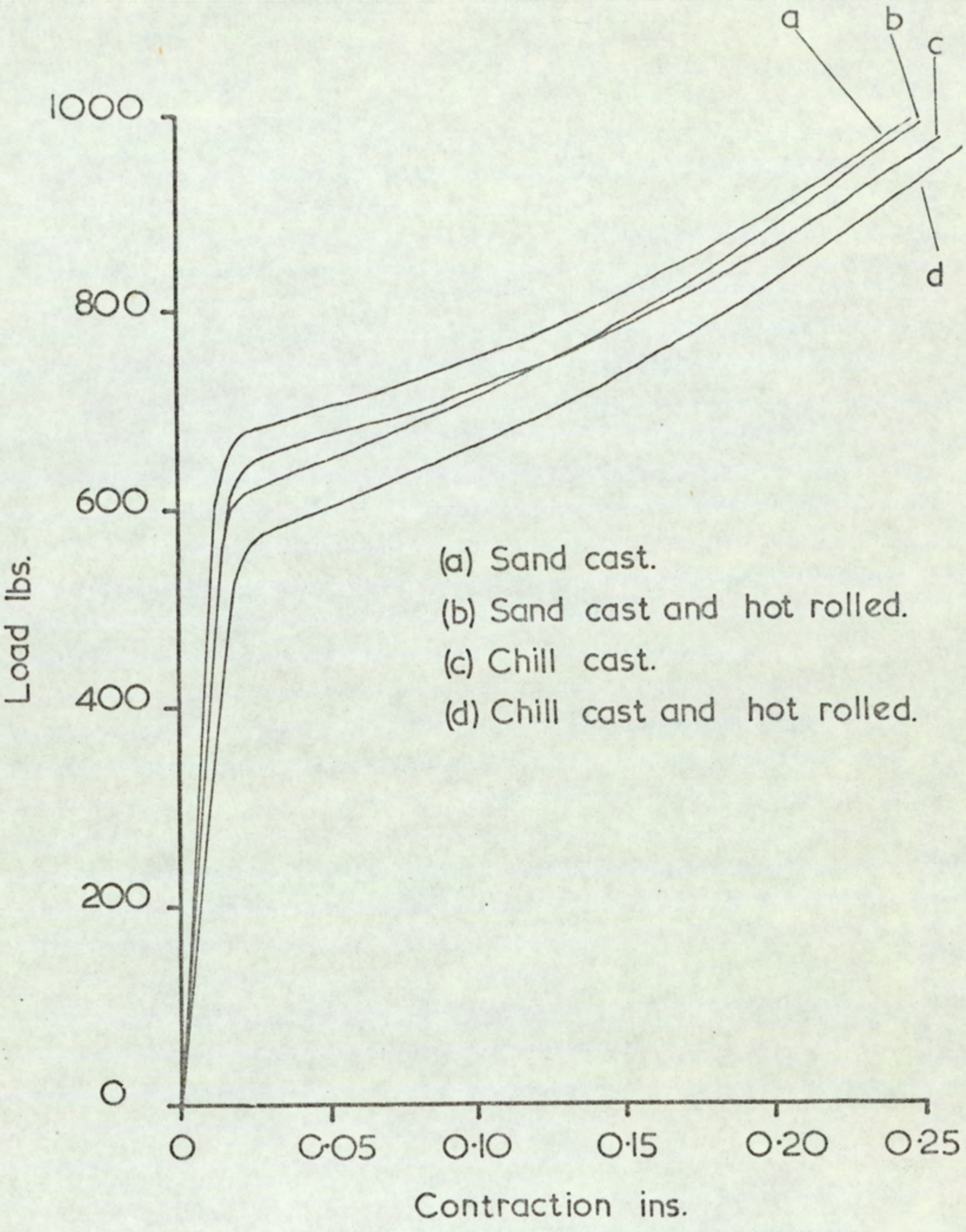

Fig. 104. Load contraction diagrams for aluminium 8% copper in both the sand and chill cast conditions.

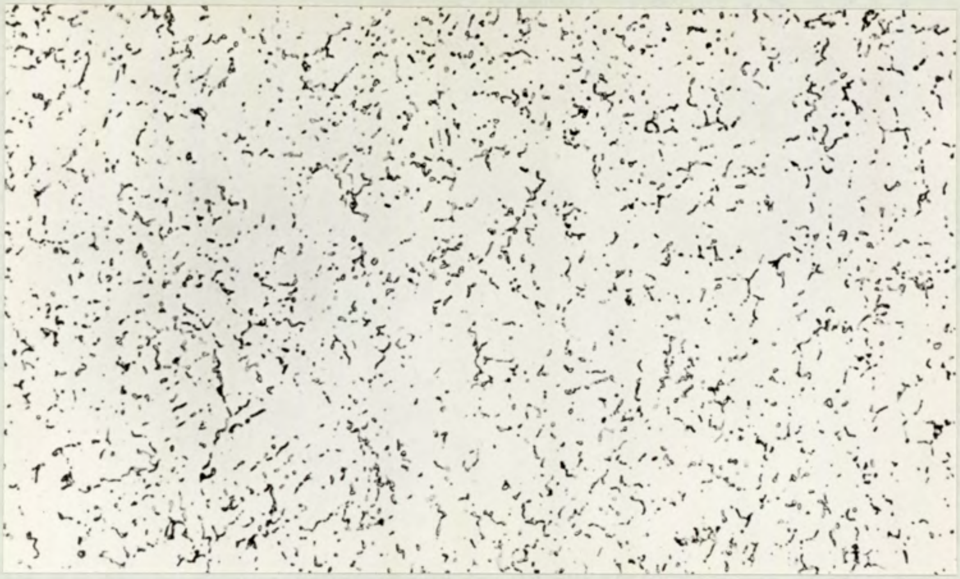

Fig. 105. Microstructure of aluminium 8% copper alloy chill cast and hot rolled 60%. Mag. x250, Etch -25% ferric nitrate.

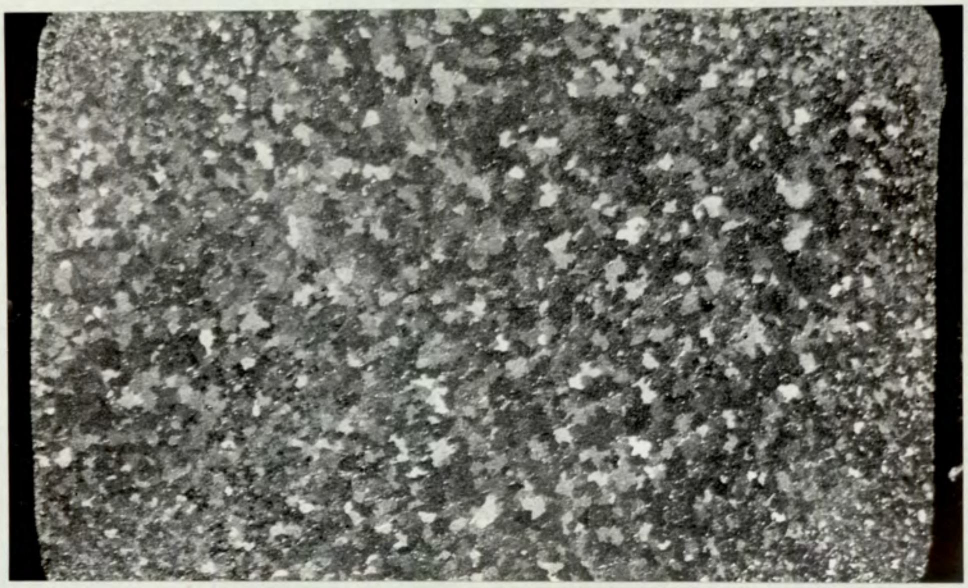

Fig. 106. Macrostructure of aluminium 8% copper alloy chill cast and hot rolled 60%. Mag. x8, Etch -15% Phosphoric acid.

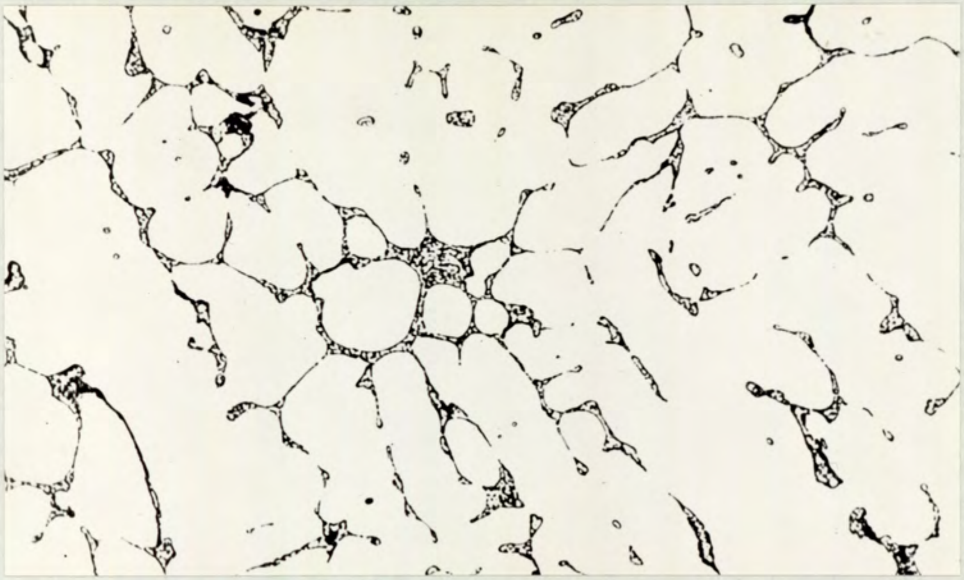

Fig. 107. Microstructure of aluminium 8% copper alloy sand cast.
Mag. x250, Etch -25% ferric nitrate.

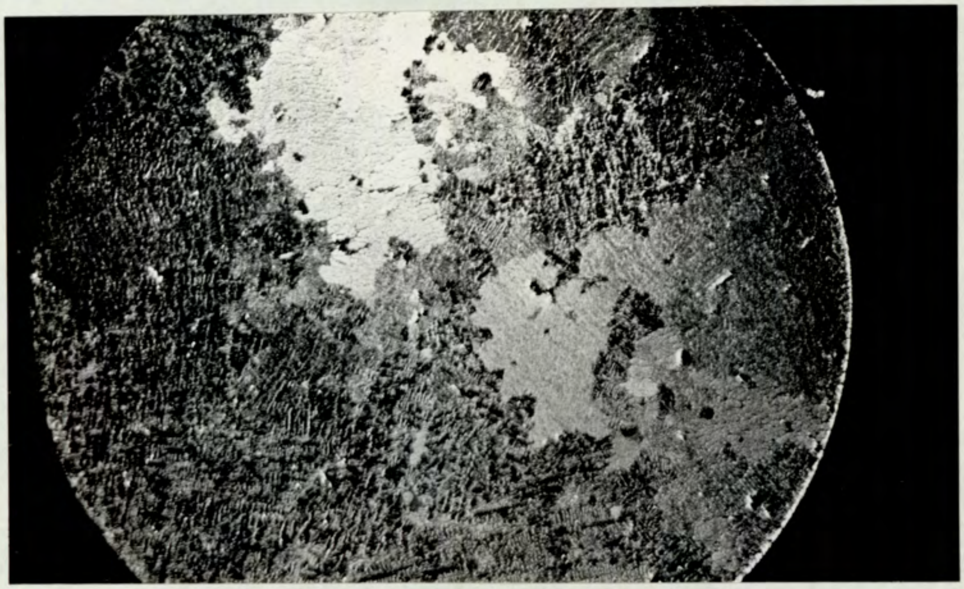

Fig. 108. Macrostructure of aluminium 8% copper alloy sand cast.
Mag. x8, Etch -15% phosphoric acid.

Fig. 109. Microstructure of aluminium 8% copper alloy sand cast and hot rolled 60%. Mag. x250, Etch - 25% ferric nitrate.

Fig. 110. Macrostructure of aluminium 8% copper alloy sand cast and hot rolled 60%, Mag. x8, Etch - 15% phosphoric acid.

Fig. 111. Microstructure of aluminium 8% copper alloy grain refined and sand cast. Mag. x30, Etch- 25% ferric nitrate.

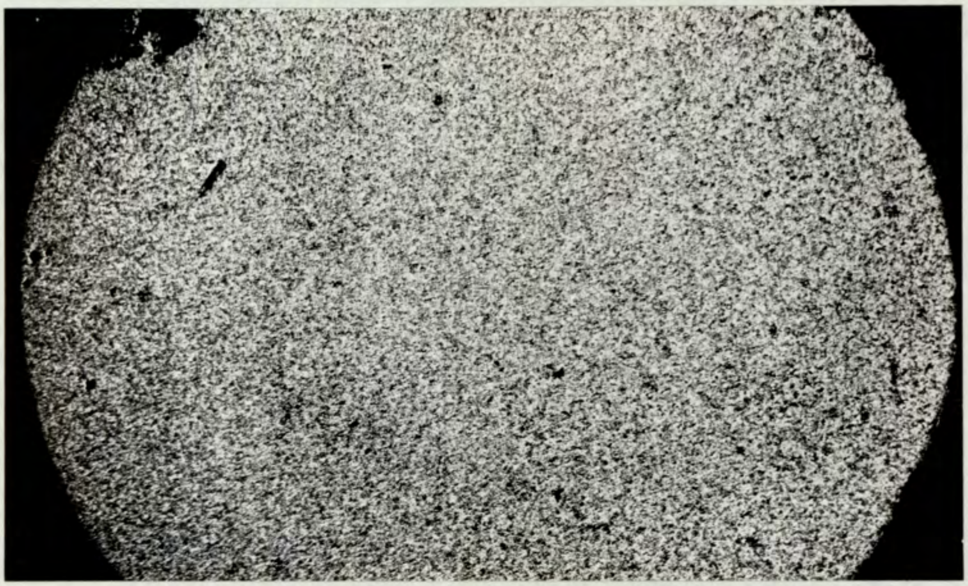

Fig. 112. Macrostructure of aluminium 8% copper alloy grain refined and sand cast. Mag. x3, Etch- 15% phosphoric acid.

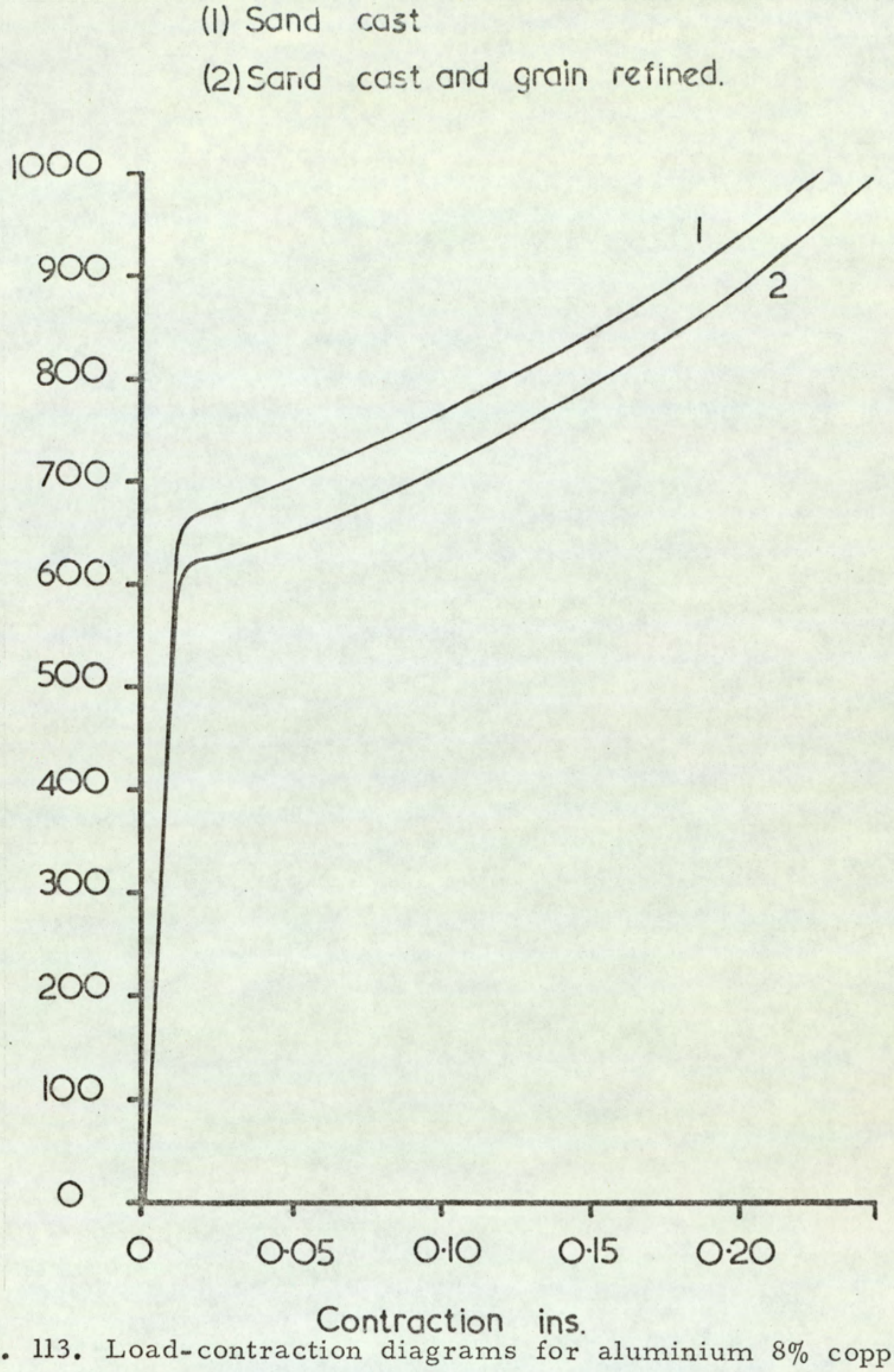

Fig. 113. Load-contraction diagrams for aluminium 8% copper alloy in the sand cast, and sand cast and grain refined conditions.

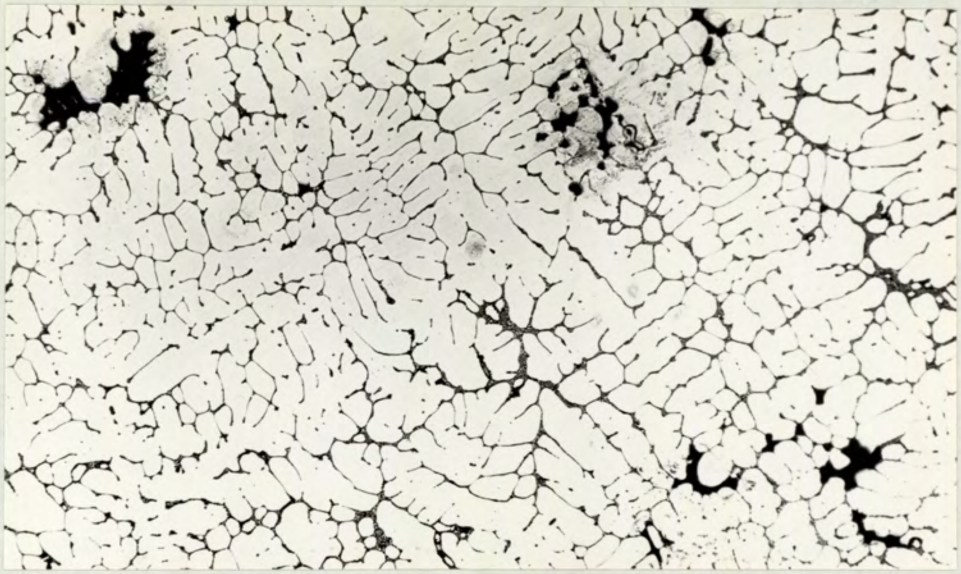

Fig. 114. Microstructure of aluminium 8% copper alloy sand cast. Mag. x30. Etch- 25% ferric nitrate.

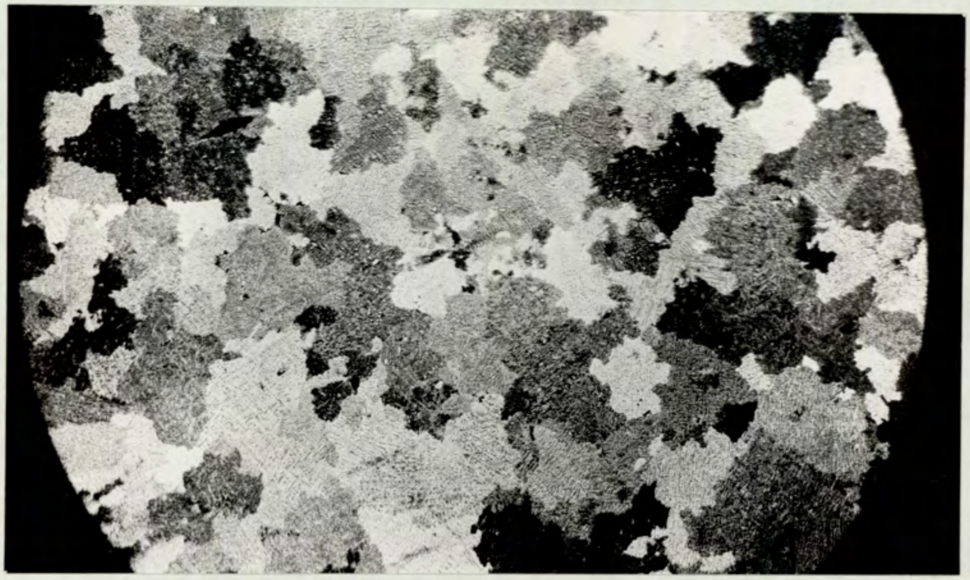

Fig. 115. Macrostructure of aluminium 8% copper alloy sand cast. Mag. x3, Etch - 15% phosphoric acid.

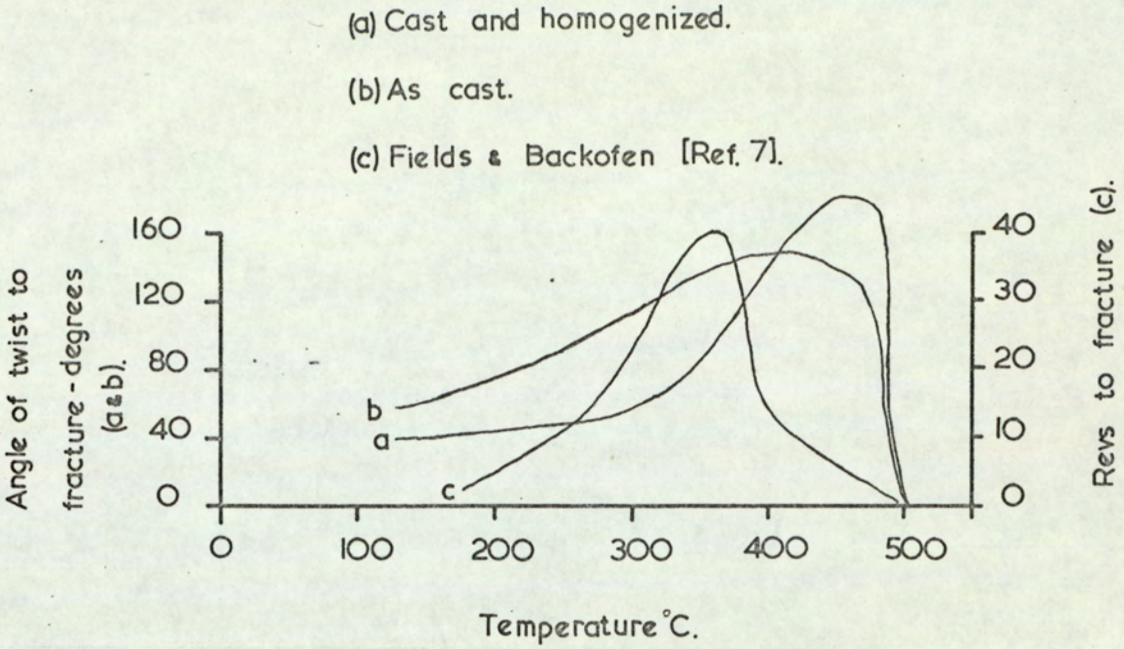

Fig. 116. The effect of temperature on ductility of cast H.15 in hot torsion.

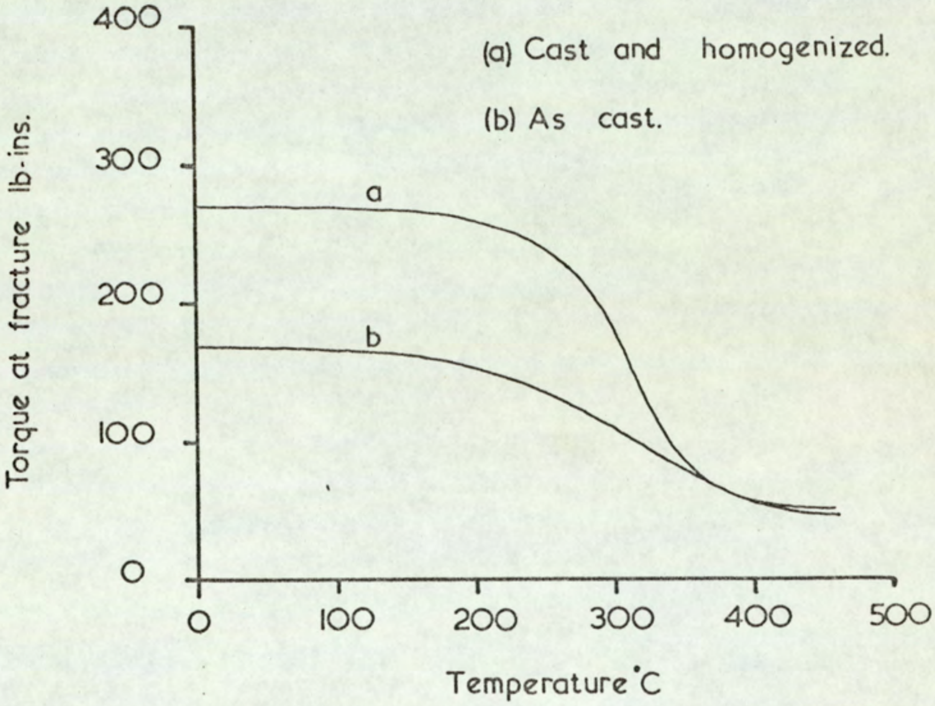

Fig. 117. The effect of temperature on strength of cast H.15 in hot torsion.

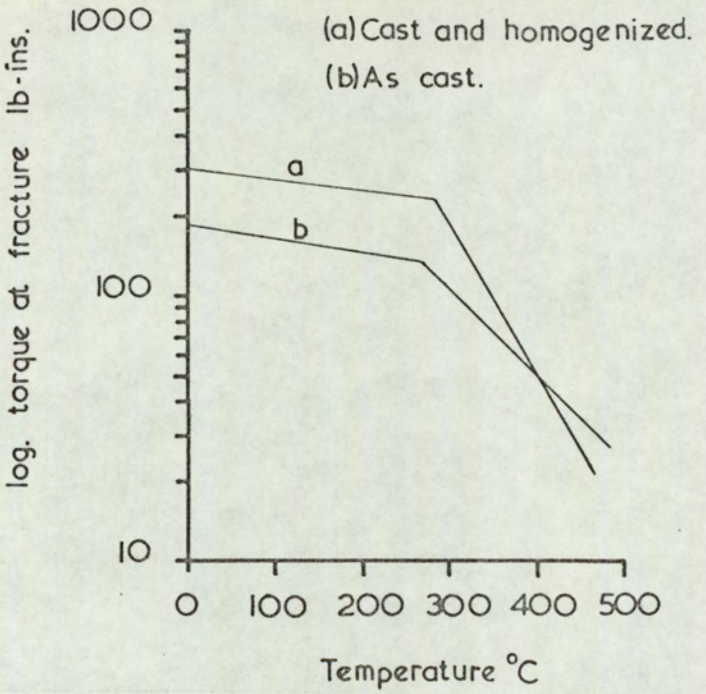

Fig. 118. The relationship between log. ultimate torque at fracture and temperature in hot torsion.

Fig. 119. Fracture of $CuAl_2$ particles during hot torsion below the inflexion temperature for $CuAl_2$. Mag. x 1700. Etch- 0.5% HF.

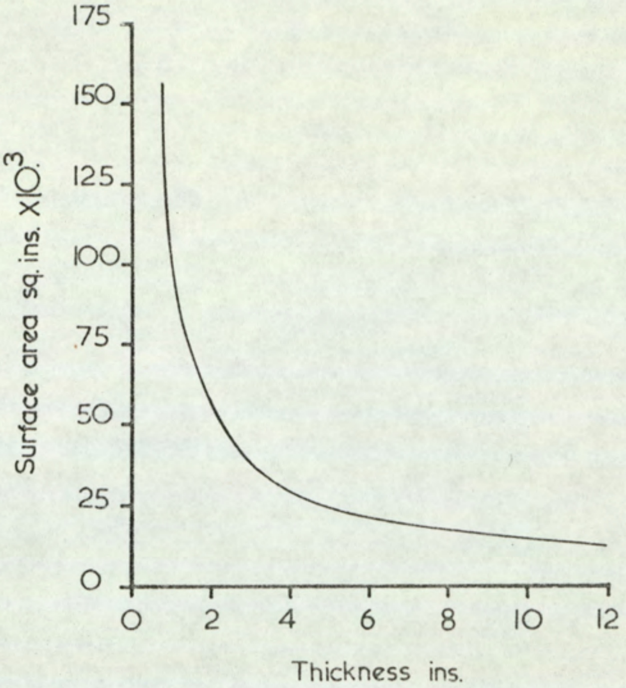

Fig. 120. The increase in surface area of a rolling slab, during hot rolling. Starting dimensions are 12" x 36" x 120".

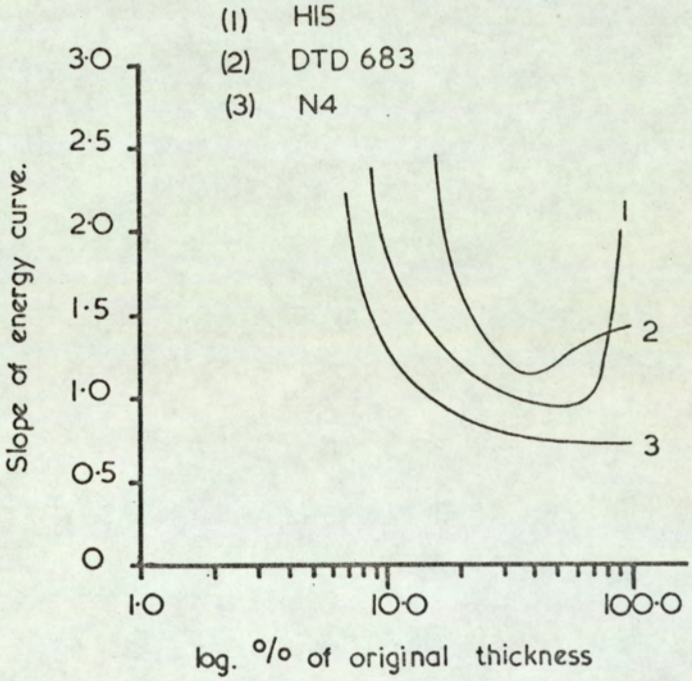

Fig. 121. The relationship between the slope of the energy curve and log.% reduction in hot rolling for some aluminium alloys.

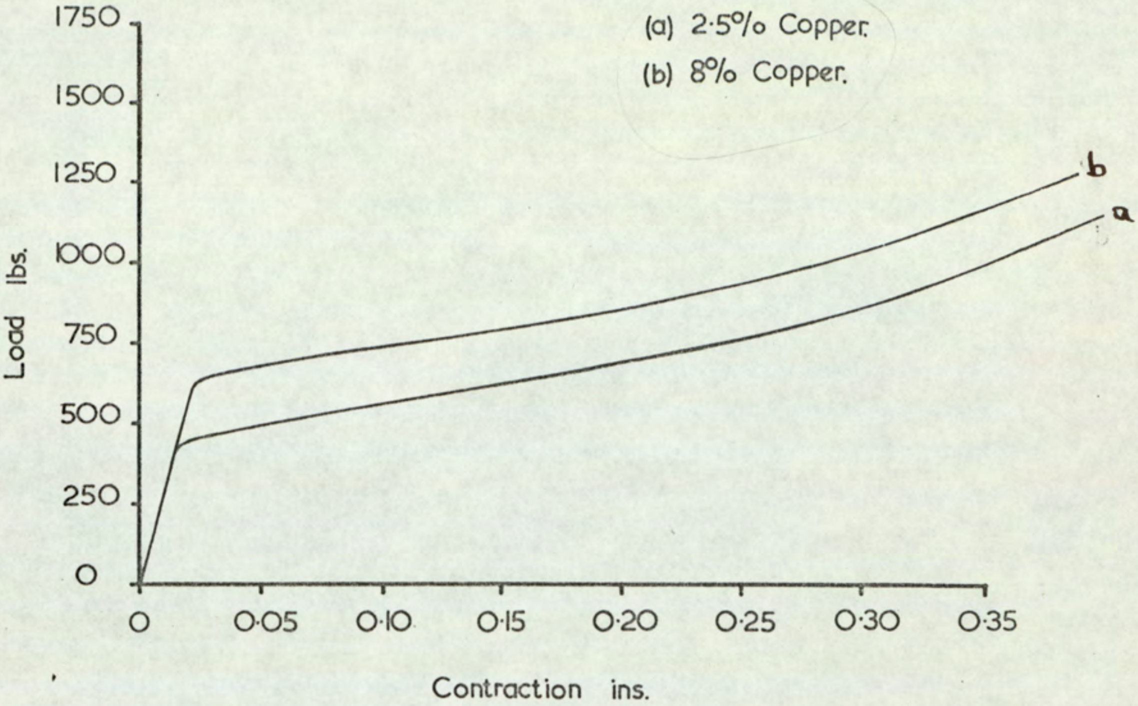

Fig. 122. Load-contraction diagrams for aluminium 2½% copper and aluminium 8% copper alloys showing the strengthening at 460°C. due to the presence of $CuAl_2$ particles.

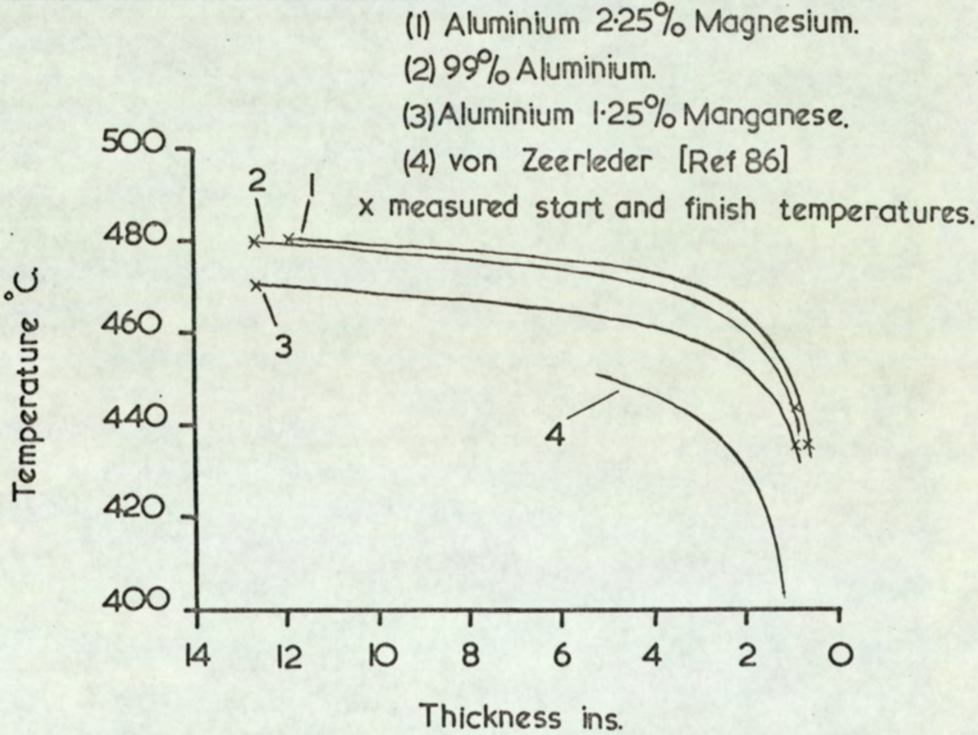

Fig. 123. Calculated temperature variations during the hot rolling of three commercial alloys.

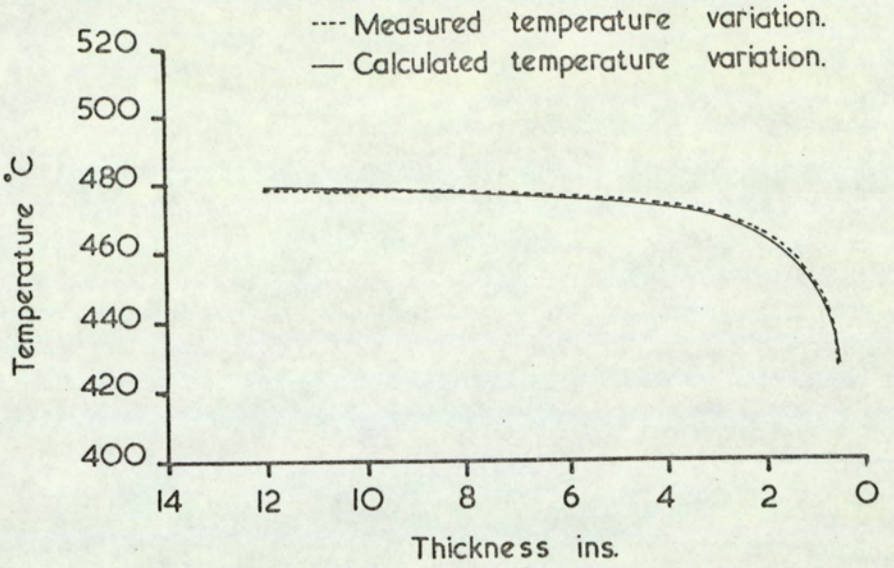

Fig. 124. Comparison of calculated and measured temperature variation during the hot rolling of alloy N4.

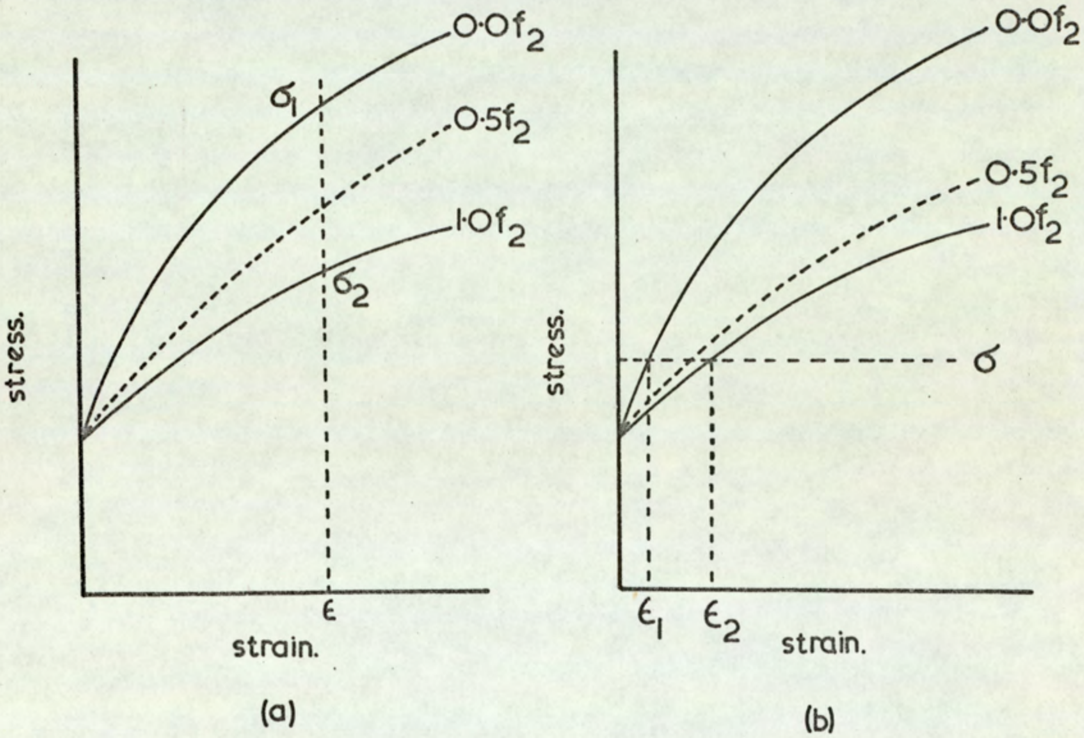

Fig. 125. Calculated flow curves for an alloy containing 0.5 volume fraction of a second hard phase a) calculated from the equal strain hypothesis, (b) calculated from the equal stress hypothesis.[94]

REFERENCE LIST

1. M J Mc. G Tegart "Re-heating for hot working" Iron and Steel Institute Conf. Special Report 111.

2. C Rossard & P Blain "Flat rolled products" (viii) A.S.M. proceedings of the Fourth Technical Conference, Chicago, Illinois, Jan. 17 1962 Publ. Interscience.

3. A Sauveur. Trans. Am. Soc. Steel Treating, 1930, 17, 410.

4. D E R Hughes, J.I.S.I. 1952, 170, 214.

5. H K Ihrig. Trans. A.I.M.M.E. 1946, 167, 749.

6. C L Clark & J J Russ. Trans. A.I.M.M.E. 1946, 167, 736.

7. D S Fields & W A Backofen. Trans. A.S.M. 1959, 51, 946

8. A Guessier & R Castro. Met.Treatment and Drop Forging. 1955, 26, 255, 323, 361.

9 C L Clark. Iron Age. 1944, 153, 11, 52.

10. W A Backofen, A J Shaler & B B Hundy. Trans. A.S.M. 1954, 46, 655.

11. J L Robbins, O Shepard & O D Sherby. J.I.S.I. 1961, 199, 175.

12. R D Olleman, E T Wessel & F C Hull. Trans. A.S.M. 1954, 46, 87.

13. E Orowan. B.I.S.R.A Report MW/F/22/50. 1950.

14. D S Fields & W A Backofen. Proc. A.S.T.M. 1957, 57, 1259.

15. H J Henning & F W Boulger. J. of M. 1963, 15, 361.

16. H K Ihrig. Iron Age, 1944, 153, 86.

17. H Ormerod & W J Mc.G. Tegart. J.I.M. 1960/61, 89, 94.

18. R A Reynolds & W J Mc.G. Tegart, J.I.S.I. 1962, 200, 1044.

19. J Dauvergne, M Pelabon & J Ivernel. Rev. met. mem. 1954, 51, 254.

20. A Nicholson. Iron & Steel. 1964, 37, 260.

21. ibid. 363.

22 F K Bloom, W C Clarke & P A Jenning. Met. Prog. 1951, 59, 250.

23. O W Ellis, Trans. Am. Soc. Treating Steel, 1933, 21, 673.

24. W L Kent. J.I.M. 1928 (No. 1) 209.

25. A Morris. Trans. A.I.M.M.E. 1931, 92, 336.

26. E F Nippes, W F Savage et al. Weld. Journ. Weld. Res. Supp. 1955, 34, 183.

27. M Cooke & E C Larke, J.I.M., 1945, 71, 371.

28. W Loizou & R B Sims. J.Mechs. & Phys. of Solids. 1953, 1, 334.

29. A Pottevin & P G Bastein. J.I.M. 1963, 59, 83.

30. J A Bailey & A R E Singer. J.I.M. 1963/64, 92, 288.

31. F A Hodierne. J.I.M. 1962/63, 91, 267.

32. A B Watts & H Ford. Proc.Inst.Mech. Eng. 1955, 169, 1141.

33. H Takahashi & J M Alexander. J.I.M. 1961/2, 90, 72.

34. N H Polakowski. J.I.S.I. 1949, 163, 250.

35. Private communication R. Grimes.

36. J A Bailey & A R E Singer. J.I.M. 1963/64, 92, 404.

37. J F Alder & V A Phillips. J.I.M. 1954/55, 83, 80.

38. R J Parker & R R Arnold. J.I.M. 1959/60, 88, 255.

39. P M Cooke. Inst. Mech. Eng. Conf. (London) on High Strain Rates. 1957, 86.

40. W A Wood & W A Rachinger. J.I.M. 1949/50, 76, 237.

41. C Rossard. Metaux. 1960. (Corrosion Industry), 35, 190.

42. C Rossard. Ecrouissage, restauration, recristallisation (Presses Universitaires de France, Paris) 111.

43. H J McQueen, W A Wong & J J Jonas. Canada. J. Phys. 1967, 45, 1225.

44. H P Stuwe. Acta. Met. 1965, 13, 1337.

45. D Hardwick & W J Mc.G. Tegart. J.I.M. 1961/62, 90, 17.

46. J J Jonas, H J McQueen, W A Wong & D W Demianczek. "Deformation under Hot Working Conditions" Iron & Steel Institute special report No. 108, 1967.

47. C M Sellars & W J Mc.G. Tegart. Mem. Sci. Rev. Met. 1966, 63, 731.

48. H. Conrad. "Mechanical Behaviour of Materials at Elevated Temperatures". McGraw-Hill. N.Y. 1961. 149.

49. T B Vaughan. "Deformation Under Hot Working Conditions" Iron & Steel Institute special report 108, 1967. 68.

50. B I Edelson & W M Baldwin. Trans. A.S.M. 1962, 55, 230.

51. H C Choa & L H von Vlack. Mats. Res. & Stds. 1965, 5, 611.

52. I L Mogford. Met. Review. 114, "The Deformation and Fracture of Two-Phase Materials". Metals and Materials 1967, 1, No. 3.

53. D Dew-Hughes & W D Robertson. Acta. Met. 1960, 8, 147.

54. G Thomas & J Nutting. J.I.M. 1957/58, 86, 7.

55. G Gurland. Trans. A.I.M.M.E. 1961, 221, 407.

56. F B Pickering. J.I.S.I. 1958, 189, 148.

57. H Unckel. J.I.M. 1937, 61, 171.

58. E R Petty. J.I.M. 1962/63, 91, 274.

59. E M Savitsky. "Mechanical Properties of Intermetallic Compounds". Symposium held during 115th meeting of the Electrochemical Soc. of Philadelphia, 1959, Edited by J H Westbrook. Publ. John Wiley & Sons, N.Y. Chp.3. 87.

60. E MSavitsky "The Influence of Temperature on the Mechanical Properties of Metals and Alloys". Stanford Univ. Press 1962. Chp.6, 169.

61. R B Sims. Iron & Steel Eng. 1960, 37, 69.

62. P W Lee, J.I.S.I. 1963, 201, 270.

63. W C F Hessenberg & R B Sims. J.I.S.I. 1951, 168, 155.

64. R B Sims & H Wright. J.I.S.I. 1963, 201, 261.

65. Private communication D J Arrowsmith.

66. A G Stukach. Stal. 1955, No. 7, 626.

67. D R Howard. The Engineer. 1963, 215, 475.

68. H J Stoever "Applied Heat Transfer" McGraw-Hill, N.Y. 1941, 231.

69. The efficient use of fuel. H.M.S.O. 1958, Ch. 9, 157.

70. H J Stoever. "Applied Heat Transfer" McGraw-Hill, N.Y. 1941, Chp. iv. 54-112.

71. S S Kutateladze & V M Borishanski. "A Concise Encyclopedia of Heat Transfer" by J.B.Arthur, Pergamon,1966.

72. W S Farren & G I Taylor. Proc. Roy. Soc. 1925, 107, 422.

73. A Cibula & R W Ruddle. J.I.M. 1949-50, 76, 361.

74. Private communication R. Grimes.

75. Private communication N Conacher.

76. G Phragmen, J.I.M. 1950, 77, 489.

77. Private communication B Harrison.

78. M von Lancker. "Metallurgy of aluminium alloys" Chapman & Hall, London, 1967. Chp. X. 266.

79. E R Petty. J.I.M. 1960/61, 89, 343.

80. J Philbert. Proc. 3rd Inst. Symp. on X-ray Optics and X-ray Microanalysis, Stanford, 1962, Academic, 1963.

81. H W L Phillips. "Annotated Equilibrium Diagrams of some Aluminium Alloy Systems" Inst. of Metals monograph No. 25, 1959, 7.

82. F Keller & G W Wilcox. Met. Prog. 1933, 23, (2)44, (4)45, (5)38.

83. A Schrader. "atzhef" Berlin 1939, 15.

84. D E R Hughes. J.I.S.I. 1952, 170, 214.

85. F Kasz & P C Varley. J.I.M. 1949/50, 76, 407.

86. A Von Zeerleder. "The Technology of Aluminium and its Alloys", Crosby & Lockwood, London, 1936, 145, 147.

87. E C Larke. "The Rolling of Strip Sheet and Plate", Chapman & Hall, London, 1963, Chp. 13, 385.

88. M Fishenden & O A Saunders. "An Introduction to Heat Transfer," Oxford Univ. Press. 1957, 90.

89. E C Larke. "The Rolling of Strip Sheet and Plate", Chapman & Hall, London, 1963. Chp. 13, 387.

90. B Drury. MSc. Thesis. Univ. of Aston, 1966.

91. P M Slate & M Whitaker. J.I.M. 1963-64, 92, 70.

92. A B Michael & M B Beever. Trans. A.I.M.M.E. 1954, 200, 47.

93. W B Pearson, A Handbook of Lattice Spacings and Structures of Metals and Alloys. Pergamon Press, 1967. 2.

94. J E Dorn, C D Starr, "Relation of Properties to Microstructure" 71-94. American Society for Metals, Metals Park, Ohio, 1954.

95. J Smithells Metals Reference Book 3, Butterworths, London 1967.

96. C S Smith, Trans. A.I.M.M.E. 1948, 175, 15.

97. M F Jordan, G D Denyer, A N Turner, J.I.M. 1962, 91, 48.

98. A H Cottrell "Theoretical Structural Metallurgy" Edward Arnold, London 1960.

99. W A Rachinger & A H Cottrell. Acta Met. Manch. 1956.

100. G Bassi, J.P. Hugo. J.I.M. 87, 1958/59, 155.

APPENDIX 1

A list is given below, which defines the symbols used in the equations appearing in sections 5.7.1 - 5.7.4. The units of these terms are also given.

a) Convective losses

Grashof number = $\frac{a g \theta D^3}{\nu^2}$ ...no units (dimensionless number)

where a = coefficient of thermal expansion of the fluid
units - cm./cm./°C.

g = the accelerating force of gravity
units - cm./sec./sec.

θ = the gas - solid temperature difference
units - °C.

D = the "characteristic dimension", i.e. the diameter of a tube, the length of a plate etc.
units - cm.

$\nu = \frac{\eta}{\rho}$ = the kinematic viscosity of the convective fluid
units - $\frac{\text{gms/cm/sec.}}{\text{gms./cm}^3}$

Prandtl number = $\frac{C_p \rho \nu}{K}$ ...no units (dimensionless number)

where C_p = specific heat for the fluid at constant pressure
units - cals/gm/°C.

ρ = density of the fluid
units - gms/cm^3

K = thermal conductivity of the fluid
units - cals/sec/cm/°C.

Nusselt number = $\frac{HD}{K\theta}$ ... no units (dimensionless number)

where H = heat flow per unit time
units - cals/cm^2/sec.

b) Radiation heat losses

A = area of radiating surface
units - cms^2

t_p = time interval during which the surface radiates heat in each pass
units - secs.

T_1 = the average temperature of the radiating surface through the rolling schedule
units - ^{o}K.

T_2 = ambient temperature
units - ^{o}K.

C_p = specific heat of the rolling slab
units - clas/gm/^{o}C.

M = mass of the rolling slab
units - gms.

c) Heat conducted into the rolls

R = thermal resistance

π = pi = 3.142

k^o = thermal conductivity of semi-infinite plate cals/cm/sec/^{o}

a = length of hot plate
units - cm.

b = width of hot plate
units - cm.

t_1 = mean rolling temperature
units - ^{o}C.

t_a = ambient temperature
units - ^{o}C.

q = rate of heat transfer from slab to the rolls
units - cals./cm^2/sec.

t = time to complete a roll pass
units - secs.

M = mass of the rolling slab
units - gms.

C_p = specific heat of the slab
units - cals/gm./^{o}C.

d) Heat gained by the slab due to deformation

E = voltage across the mill armature per roll pass
units - volts

I = current through mill motor armature per pass
units - amperes

Q = mill throughput
units - lbs/sec.

F = factor which makes allowance for the energy loss due to frictional effects etc. Value of the factor = 0.6

C_p = specific heat of the slab
units - cals/gm/^{o}C.

ACKNOWLEDGEMENTS

The author would like to express his gratitude to Dr. D J Arrowsmith for his helpful supervision of this research project, and also for his valued advice and discussion. Appreciation is also recorded for the assistance willingly provided by Mr T J Jebbett, and members of the laboratory staff of the Department of Metallurgy, University of Aston in Birmingham.